

THE UNIVERSITY OF CALGARY

NARROWBAND ADAPTIVE BEAMFORMING
WITH A MINIMUM REDUNDANCY ARRAY

by

MARK BRADY JORGENSON

A THESIS

SUBMITTED TO THE FACULTY OF GRADUATE STUDIES
IN PARTIAL FULFILLMENT OF THE REQUIREMENTS FOR THE
DEGREE OF MASTER OF SCIENCE

DEPARTMENT OF ELECTRICAL ENGINEERING

CALGARY, ALBERTA

January, 1989

© Mark B. Jorgenson 1989



National Library
of Canada

Bibliothèque nationale
du Canada

Canadian Theses Service Service des thèses canadiennes

Ottawa, Canada
K1A 0N4

The author has granted an irrevocable non-exclusive licence allowing the National Library of Canada to reproduce, loan, distribute or sell copies of his/her thesis by any means and in any form or format, making this thesis available to interested persons.

The author retains ownership of the copyright in his/her thesis. Neither the thesis nor substantial extracts from it may be printed or otherwise reproduced without his/her permission.

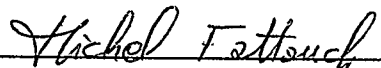
L'auteur a accordé une licence irrévocable et non exclusive permettant à la Bibliothèque nationale du Canada de reproduire, prêter, distribuer ou vendre des copies de sa thèse de quelque manière et sous quelque forme que ce soit pour mettre des exemplaires de cette thèse à la disposition des personnes intéressées.

L'auteur conserve la propriété du droit d'auteur qui protège sa thèse. Ni la thèse ni des extraits substantiels de celle-ci ne doivent être imprimés ou autrement reproduits sans son autorisation.

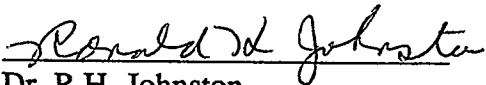
ISBN 0-315-50349-1

THE UNIVERSITY OF CALGARY
FACULTY OF GRADUATE STUDIES

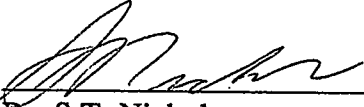
The undersigned certify that they have read, and recommend to the Faculty of Graduate Studies for acceptance, a thesis entitled, "Narrowband Adaptive Beamforming with a Minimum Redundancy Array", submitted by Mark B. Jorgenson in partial fulfillment of the requirements for the degree of Master of Science.



Supervisor, Dr. M. Fattouche
(Dept. of Electrical Engineering)



Dr. R.H. Johnston
(Dept. of Electrical Engineering)



Dr. S.T. Nichols
(Dept. of Electrical Engineering)



Dr. S. Kwok
(Dept. of Physics)

Date: January 18, 1989

ABSTRACT

It is shown, through analysis and simulation, that a constrained adaptive beamformer based on a Minimum Redundancy Array (MRA) outperforms the equivalent system based on a line array with uniformly spaced elements for uncorrelated interferences located in close angular proximity to the look direction.

A thinned suboptimal adaptive array with elements spaced for minimum spatial redundancy is analyzed and compared with a thinned suboptimal adaptive array with uniformly spaced adaptive elements. It is found that the thinned array using adaptive elements chosen for minimum spatial redundancy achieves superior performance against uncorrelated interferences in the main lobe, with no appreciable degradation in the rejection of interferences entering the side lobes. A simulation involving a 37 element thinned adaptive array with 10 adaptive elements confirms the theoretical predictions.

The use of a MRA in conjunction with an adaptive combiner for digital communications is examined. It is shown that the bit error probability achieved by the MRA based system is lower than that achieved by a comparable uniform array based system for interference or multipath components located in close angular proximity to the desired signal. The unconditioned bit error probability achieved by the MRA based system operating in a two ray multipath environment with equal amplitude rays, is shown to be lower than that achieved by a uniform array based system for usable SNR.

ACKNOWLEDGEMENTS

The author is grateful to Dr. Michel Fattouche for his help and guidance throughout the course of this work, and in the preparation of this manuscript. Thanks are also due to Dr. S.T. Nichols for his assistance in technical matters related to this project.

Financial assistance received from the University of Calgary and the Department of Electrical Engineering is gratefully acknowledged.

DEDICATION

To Cecilia

always

TABLE OF CONTENTS

	page
APPROVAL PAGE	ii
ABSTRACT	iii
ACKNOWLEDGEMENTS	iv
DEDICATION	v
TABLE OF CONTENTS	vi
LIST OF TABLES	viii
LIST OF FIGURES	ix
LIST OF SYMBOLS	xiii
1 INTRODUCTION	1
2 A NARROWBAND ADAPTIVE BEAMFORMER BASED ON A MINIMUM REDUNDANCY ARRAY	
2.1 Introduction	6
2.2 Beamforming	6
2.3 Minimum Redundancy Arrays	12
2.4 Eigenvalue Analysis	18
2.5 Adaptive Beamforming	26
2.6 Signal to Noise plus Interference Ratio Calculation	34
2.7 Simulation Results	39
2.8 Conclusion	45
3 A SUBOPTIMAL ARRAY WITH ADAPTIVE ELEMENTS SPACED FOR MINIMUM REDUNDANCY	
3.1 Introduction	46
3.2 The Thinned Adaptive Suboptimal Array	48
3.3 Simulation Results	63
3.4 Conclusion	69
4 AN ADAPTIVE MINIMUM REDUNDANCY ARRAY FOR DIGITAL COMMUNICATIONS	
4.1 Introduction	71

TABLE OF CONTENTS (Continued)

	page
4.2 Complex Envelope Simulation	72
4.3 Uncorrelated Interference	75
4.4 Simulation: Uncorrelated Interference	82
4.5 Multipath	87
4.6 Conclusion	106
5 SUMMARY AND SUGGESTIONS FOR FURTHER RESEARCH	108
REFERENCES	113

LIST OF TABLES

	page
Table 2.1 - Some of the possible MRA configurations for orders 1 through 10.	18
Table 2.2 - Eigenvalue spread ratios for various MRA's.	26
Table 2.3 - Threshold angles for arrays of order 3 to 8.	37
Table 3.1 - SNIR of thinned adaptive arrays relative to the fully adaptive array of the same length; tabulated for interference close to the look direction.	57
Table 4.1 - Probability of error for various interference conditions with unity noise power.	87
Table 4.2 - Error probabilities for equal strength multipath signals with various angular separations and worst case phase.	103

LIST OF FIGURES

	page
Figure 2.1 - Sensor array geometry.	9
Figure 2.2 - (a) Minimum redundancy arrays of orders 1 - 4; (b) Eighth order minimum redundancy arrays.	13
Figure 2.3 - Normalized array patterns for uniform and minimum redundancy arrays of order 4.	15
Figure 2.4 - Normalized unadapted array pattern for 5 element uniform and minimum redundancy arrays.	19
Figure 2.5 - Normalized unadapted array pattern for 6 element uniform and minimum redundancy arrays.	20
Figure 2.6 - Normalized unadapted array pattern for 7 element uniform and minimum redundancy arrays.	21
Figure 2.7 - Normalized unadapted array pattern for 8 element uniform and minimum redundancy arrays.	22
Figure 2.8 - Frost adaptive beamformer structure.	29
Figure 2.9 - SNIR at the output of 4 element converged uniform and minimum redundancy adaptive array systems for various noise magnitudes.	36
Figure 2.10 - SNIR comparison of 3, 5 and 8 element uniform and minimum redundancy adaptive array systems.	38
Figure 2.11 - Directivity patterns for 4 element uniform and minimum redundancy adaptive arrays with additive Gaussian noise.	41

LIST OF FIGURES (Continued)

	page
Figure 2.12 - Directivity patterns for 4 element uniform and minimum redundancy adaptive arrays with -10 dB Gaussian noise and a -3 dB plane wave interference.	42
Figure 2.13 - Directivity patterns for 4 element uniform and minimum redundancy adaptive arrays with 0 dB Gaussian noise and a -3 dB plane wave interference.	44
Figure 3.1 - Thinned adaptive array configurations. (a) Minimum hardware implementation; (b) Null constraint implementation.	49
Figure 3.2 - Output SNIR comparison of a conventionally weighted, a fully adaptive and a thinned uniform adaptive array with 10 adaptive elements, all based on a 37 element array.	59
Figure 3.3 - SNIR at the output of thinned uniform and minimum redundancy converged adaptive arrays with 37 elements, 10 of which are adaptive.	60
Figure 3.4 - Output SNIR comparison for various converged adaptive arrays with a main lobe interference. All arrays employ 37 elements, thinned arrays each employ 10 adaptive elements.	61
Figure 3.5 - 37 element uniform and MRA thinned adaptive array structures with 10 adaptive elements each.	64
Figure 3.6 - Thinned adaptive array directivity pattern obtained with uncorrelated noise and no discrete spatial interference.	65
Figure 3.7 - Converged thinned adaptive array directivity patterns with sidelobe interference.	67

LIST OF FIGURES (Continued)

	page
Figure 3.8 - Converged thinned adaptive array directivity patterns with main lobe interference.	68
Figure 4.1 - Complex envelope equivalent of a narrowband channel; (a) Narrowband channel; (b) Baseband equivalent channel.	73
Figure 4.2 - Signal, interference and array geometry.	76
Figure 4.3 - Uncorrelated interference simulation.	77
Figure 4.4 - Narrowband LMS adaptive combiner.	80
Figure 4.5 - Directivity patterns for 4 element uniform and minimum redundancy adaptive combiners with AWGN.	84
Figure 4.6 - Directivity patterns for 4 element uniform and minimum redundancy array based adaptive combiners with a 10 dB interference located 10 degrees away from the desired signal and AWGN of -40 dB.	86
Figure 4.7 - Directivity patterns for 4 element uniform and minimum redundancy array based adaptive combiners with a 10 dB interference located 10 degrees from the desired signal and AWGN of 0 dB.	88
Figure 4.8 - Directivity patterns for 4 element uniform and minimum redundancy array based adaptive combiners with a 10 dB interference located 16 degrees from the desired signal and AWGN of 0 dB.	89
Figure 4.9 - Directivity patterns for 4 element uniform and minimum redundancy array based adaptive combiners with a 0 dB interference located 22 degrees away from the desired signal and AWGN of 0 dB.	90

LIST OF FIGURES (Continued)

	page
Figure 4.10 - Two ray multipath signal and array geometry.	91
Figure 4.11 - QPSK signals in the two ray multipath environment.	94
Figure 4.12 - Two ray multipath simulation.	102
Figure 4.13 - Bit error probabilities for converged 4 element uniform and minimum redundancy adaptive arrays receiving QPSK signals in a two ray multipath environment with equal amplitude rays.	105

LIST OF SYMBOLS

$\bar{A}(t)$	vector of modulation components
A	QPSK signal amplitude coefficient
a_n	n^{th} complex symbol
\bar{C}	constraint vector
D	unit delay
d	interelement distance
d_k	desired signal at time k
E	energy associated with QPSK signal
\bar{E}'	correction matrix
f	frequency
$g(\alpha)$	array gain as a function of angle of arrival
$H(f)$	frequency response of channel
$\tilde{H}(f)$	baseband equivalent frequency response
$h(t)$	channel impulse response
$\dot{h}(t)$	analytic signal of $h(t)$
$\hat{h}(t)$	Hilbert transform of $h(t)$
$\tilde{h}(t)$	baseband equivalent impulse response

LIST OF SYMBOLS (Continued)

I	identity matrix
k	$=\frac{2\pi}{\lambda}$, the wavenumber
MRA	Minimum Redundancy Array
MVDR	Minimum Variance Distortionless Response
$m_i(t)$	modulation component of i^{th} source
NIP	Noise plus Interference Power
NRA	Non Redundant Array
$\bar{N}(t)$	vector of AWGN inputs
P	projection matrix
P_s	signal power
P_{n+i}	noise plus interference power
$P_b(e)$	bit error probability
$p(t - nT)$	rectangular pulse function
Q	Q function
Q	matrix of space vectors
QPSK	Quadrature Phase Shift Keying
R	spatial correlation matrix
R_i	radial distance from source to i^{th} array element

LIST OF SYMBOLS (Continued)

$r_i(x, t)$	i^{th} signal expressed as a spatially varying function
$\tilde{r}_i(x, t)$	complex envelope of $r_i(x, t)$
SNR	Signal to Noise Ratio
SNR_m	Signal to Noise Ratio achieved by MRA based system
SNR_u	Signal to Noise Ratio achieved by uniform array based system
$SNIR$	Signal to Noise plus Interference Ratio
$SNIR_t$	Signal to Noise plus Interference Ratio of a thinned array
$SNIR_{mt}$	$SNIR$ of a thinned array with MRA spaced adaptive elements
$SNIR_{ut}$	$SNIR$ of a thinned array with uniformly spaced adaptive elements
$\bar{S}(\alpha)$	space vector
$\bar{S}_u(\alpha)$	space vector of nonadaptive subarray
$\bar{S}_v(\alpha)$	space vector of adaptive subarray
$s(t)$	QPSK signal
$\tilde{s}(t)$	baseband equivalent QPSK signal
\bar{U}	conventional subarray weight vector
\bar{V}	adaptive subarray weight vector
\bar{W}_k	weight vector at k^{th} interval

LIST OF SYMBOLS (Continued)

w_i	weight associated with the i^{th} array element
$w_m(di, n)$	weight associated with element at position di of a MRA
$w_u(di, n)$	weight associated with element at position di of a uniform array
\bar{X}_k	observation vector
$\tilde{x}_i(t)$	baseband equivalent signal at i^{th} array element
y_k	beamformer output at k^{th} interval
$y_m(n)$	output of MRA based combiner at n^{th} interval
$y_u(n)$	output of uniform array based combiner at n^{th} interval
$\tilde{z}(x, t)$	complex envelope of signal field
$\tilde{z}(x, n)$	sampled complex envelope of signal field
α	angle of arrival
β_m	eigenvalue spread ratio, MRA
β_u	eigenvalue spread ratio, uniform array
Δ	beamsteering delay
ϵ_k	error at time k
κ	alphabet of MRA element spacings
λ	wavelength

LIST OF SYMBOLS (Continued)

$\lambda_{i,mra}$	i^{th} eigenvalue with MRA
$\lambda_{i,unif}$	i^{th} eigenvalue with uniform array
μ	LMS adaptation factor
$v_i(n)$	AWGN at i^{th} array element at n^{th} interval
ω	radian frequency
ω_0	carrier frequency
Φ_c	normalized array gain for conventional subarray
Φ_m	normalized array gain for MRA
Φ_u	normalized array gain for uniform array
Φ_v	normalized array gain for adaptive subarray
ϕ_i	phase component of i^{th} QPSK signal
π_i	interference power
π_s	signal power
ψ	phase difference between multipath signals
σ^2	noise power
σ_v	standard deviation of AWGN, v
τ_i	multipath time delay of i^{th} path

LIST OF SYMBOLS (Continued)

θ	$kd \sin(\alpha)$
υ	alphabet of uniform array element spacings
ξ_m	spatially variable component of SNR_m
ξ_u	spatially variable component of SNR_u
ζ_e	ratio of MRA and uniform array eigenvalue spreads, equal elements
ζ_l	ratio of MRA and uniform array eigenvalue spreads, equal length
$ \cdot $	magnitude
$\ \cdot\ $	vector norm
\square^T	transposition
\square^*	conjugation
\square^H	Hermitian or conjugate transpose
Re	real part
Im	imaginary part

CHAPTER 1

INTRODUCTION

Beamforming applications are found in many disciplines [1]. A synopsis would include passive and active sonar systems [2-5], seismic signal processing [6], biomedical imaging systems [7], radio astronomical arrays [8-10], phased array radar systems [11,12] and communications applications [13,14]. All of these applications share the common goal of filtering signals with respect to their spatial orientation.

In order to achieve this spatial filtering, it is necessary to obtain information on the spatial makeup of the signals to be considered. This information is obtained by sampling the signal environment at discrete spatial points with an array of sensors. The structure of the array is important in determining the information which can be obtained. The spacing of array elements within a line array can influence the shape of the array pattern. For example, if the elements are located very close to one another, such that the total length of the array is small with respect to the wavelength of the signal, the array pattern will be very broad, having little directivity. Increasing the length of the array increases the directivity. This increase in array length can be accomplished by adding sensor elements while maintaining the same interelement distance, the shortest distance between adjacent

elements within the array, or through increasing the interelement distance. By increasing the interelement distance beyond $\frac{\lambda}{2}$, the main lobe of the array pattern can be made very narrow, but grating lobes begin to appear. Grating lobes may be thought of as a form of ambiguity, in this case, due to a spatial analogue of the well known aliasing phenomenon. Consequently, many array structures formed using isotropic sensor elements employ a $\frac{\lambda}{2}$ interelement distance.

The form of line array which is most commonly employed consists of a row of sensors, each located at a distance, d , from the next. This array structure is known as an equi-spaced or uniform line array and will be hereafter referred to as a uniform array. Another form of line array is one in which the array element spacings are chosen such that the spatial correlations which can be formed using the elements in the array include all integer multiples of the interelement spacing from d to Nd with the fewest possible redundant spatial correlations, where Nd is the length of the array. Such an array is known as a Minimum Redundancy Array (MRA) and is useful for applications requiring high resolution because of the very narrow main lobe associated with this array structure [15]. The large sidelobes which are associated with the array pattern have formed a severe handicap for most applications, but have not prevented the use of MRA's in radio astronomical observations, where post processing of the array output could, to some degree, compensate for known signals entering through the sidelobes.

Adaptive beamforming provides a means by which interferences entering through the large sidelobes of the MRA can be rejected. Chapter 2 begins by introducing the MRA and continues with an introduction to adaptive beamforming [16-18]. The chapter concludes with both calculated and simulated performance measurements of the converged solutions attained by narrowband adaptive beamformers based on both uniform and minimum redundancy array structures in rejecting discrete uncorrelated spatial interferences. The simulations used a Frost adaptive beamformer structure, based on the well known Least-Mean-Squares algorithm, to form converged array patterns for a number of interference conditions [19].

Many of the disciplines which employ beamforming techniques require array structures with large numbers of elements. An adaptive beamformer in which the output of each of these sensors is weighted adaptively, known as a fully adaptive beamformer, would thus employ a very large number of adaptive coefficients, with the attendant misadjustment, slow convergence and large computational burden. To overcome this, a form of adaptive beamformer known as the suboptimal array is sometimes used. In such a system, the number of coefficients which are adjusted by the adaptive algorithm is less than the total number in the weight vector. One specific suboptimal array is the thinned adaptive array [20]. An array of this type consists of two subarrays, one conventionally steered in the look direction, the other weighted adaptively, with the sum of the two subarrays outputs

forming the overall output of the system. In chapter 3, the effect of choosing the adaptive sensor elements in a narrowband thinned adaptive array, on the basis of a minimum spatial redundancy criterion is examined and compared with the performance obtained using the common method of spacing adaptive elements uniformly throughout the array. Again, simulations employing the Frost adaptive beamformer structure to determine the adaptive weight coefficients are undertaken to confirm the results of calculated performance ratios.

Most beamforming applications consider the spatial filtering of an unknown signal from a known direction. In the digital communications case, however, it is quite possible to turn this around. Thus we may desire to observe a known signal originating from an unknown direction or directions. The known signal may be a training signal, such as that employed in setting up the initial convergence of some adaptive equalizers. In this case, the training signal is used to allow the weights of the adaptive beamformer to converge to form the optimum spatial directivity pattern for the given signal environment. Chapter 4 examines such a case. Two signal environments are considered. The first consists of a known digital signal, the desired signal, arriving from an unknown direction, in the presence of an uncorrelated interfering signal arriving from some other direction. The second is based on the two ray multipath model, and postulates two known correlated digital signals, both containing the information of the desired signal, arriving at the array with different spatial orientations. Under these conditions, destructive interference

of the two correlated signals can cause a phenomenon known as fading. The efficacy of adaptive arrays with both uniform and MRA element spacing in reducing fading effects is considered. The performance of the arrays is primarily measured in terms of the predicted and simulated probability of error achieved by the adaptive beamformers after convergence.

A summary of the results obtained is contained in the final chapter. Also included are suggestions for further research in this area.

CHAPTER 2

A NARROWBAND ADAPTIVE BEAMFORMER BASED ON A MINIMUM REDUNDANCY ARRAY

2.1. Introduction

This chapter begins by presenting the background material required for an understanding of adaptive beamforming in general. Following that, the MRA is introduced. A comparison of uniform and MRA based systems in terms of predicted eigenvalues and Signal to Noise and Interference Ratios (SNIR's) is then undertaken. The chapter concludes with the results of a simulation study. Four element adaptive arrays based on both MRA and uniform configurations are simulated to facilitate comparison of the relative merits of the two geometries for the rejection of interfering signals.

2.2. Beamforming

The output signals from an array of sensors may be combined in various ways in order to spatially filter incoming signals in accordance with a particular performance criterion. This combining of signals is generally referred to as beamforming. Beamforming techniques have been used in many varied and

diverse fields; RADAR, SONAR, communications, radio astronomy and seismic exploration to name a few [1,21].

The manner in which the signals are combined may be fixed, as in an optimum beamformer where the signal statistics are assumed to remain constant, or, it may be adaptive, designed to change in response to changes in the signal environment. In either case, a specific performance criterion of one kind or another must be employed. One such possible criterion, for a communications system, might be that the array maximize the signal to noise ratio for a specific known signal, regardless of the direction or directions from which the signal originates. As another example, it may be desired, as in sonar or radar beamforming, to pass signals originating from a given spatial direction and reject all others.

The geometry of the sensor array is also of interest. Perhaps the most commonly treated of all array geometries is the uniformly spaced or uniform linear array. This array consists of a line of equi-spaced sensor elements. Virtually all of the literature dealing with adaptive line arrays focuses upon the uniform linear array. Another form of line array which is used, at least for radio astronomical observations, is the Minimum Redundancy Array (MRA) [15]. This array has certain features which make it desirable for use in a beamforming application [8,22].

The following notation and background follows that given by Hudson (chapter 2 in [16]). The narrowband representation of a signal, travelling in space at a sufficient distance from its source that it may be considered to be composed of plane (as opposed to spherical) waves, is given as follows:

$$\bar{S} \triangleq [e^{-jkR_1} \ e^{-jkR_2} \ \dots \ e^{-jkR_N}]^T \quad (2.1)$$

where

N is the number of spatial samples,

$[\]^T$ denotes a transposition operation,

R_i is the distance from the source to the i^{th} element of the array,

and $k = 2\pi / \lambda$ is the wavenumber.

\bar{S} is known as the space vector and defines the wave's orientation in space with respect to the elements of the array. In most cases, the factor e^{-jkR} , where R is the distance to the center of the array, may be omitted. The signal impinging upon the uniform array shown in figure 2.1 has a space vector of

$$\bar{S}(\alpha) \approx [e^{-j\frac{N-1}{2}kd\sin(\alpha)} \ e^{-j\frac{N-3}{2}kd\sin(\alpha)} \ \dots \ e^{+j\frac{N-1}{2}kd\sin(\alpha)}]^T \quad (2.2)$$

where

α is the angular deviation from a perpendicular to the array

and where the center of the array has been taken as the phase center.

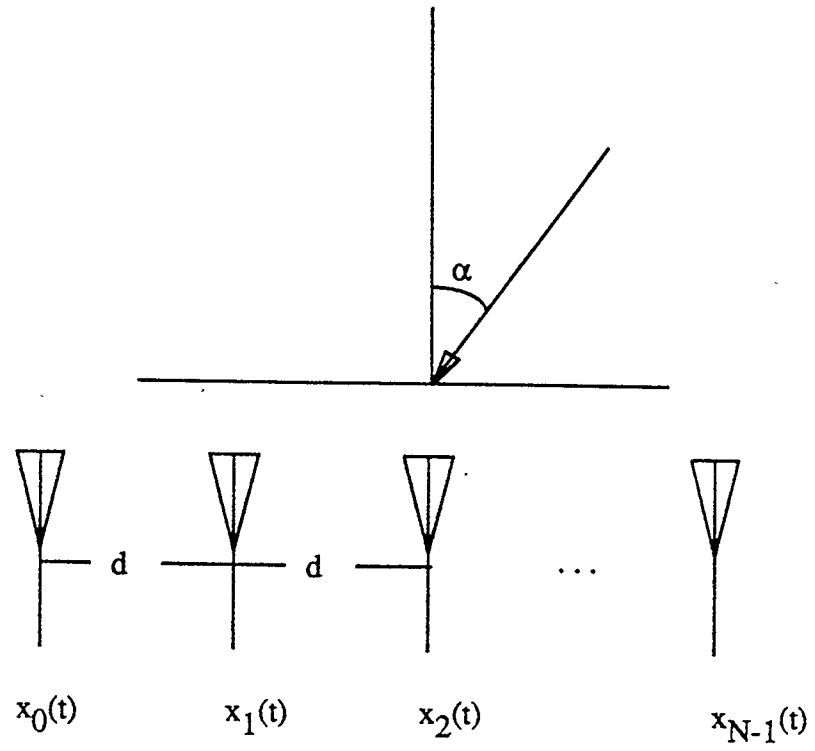


Figure 2.1 - Sensor array geometry.

In the case of multiple sources, the signal $x_i(t)$ at each element of the array is formed as a linear combination of the impinging signals, each individually acted upon by its respective space vector:

$$\bar{X}(t) = m_1(t)\bar{S}_1 + m_2(t)\bar{S}_2 + \cdots + m_M(t)\bar{S}_M \quad (2.3)$$

where

M is the number of signal sources,

$\bar{X}(t) \triangleq [x_1(t) \ x_2(t) \ \cdots \ x_M(t)]$ *is the vector of array element outputs,*

$m_i(t)$ is the modulation component of the i^{th} signal source

and \bar{S}_i is the space vector of the i^{th} signal source.

A compact matrix representation for (2.3) is

$$\bar{X}(t) = \mathbf{Q}\bar{A}(t) \quad (2.4)$$

where

\mathbf{Q} is the $M \times N$ matrix $[\bar{S}_1 \ \bar{S}_2 \ \cdots \ \bar{S}_M]$

and $\bar{A}(t) \triangleq [m_1(t) \ m_2(t) \ \cdots \ m_M(t)]^T$

If we let \bar{W} be the N dimensional weight vector of the beamformer, then the beamformer output $y(t)$ is given as

$$y(t) = \bar{W}^H \bar{X}(t) \quad (2.5)$$

In order to steer a beam in the direction of a source, the weight vector must be such that the antenna amplitude gain, $g(\alpha)$, is maximized in the direction of the source. If we define $g(\alpha)$ as

$$g(\alpha) \triangleq \bar{S}^T(\alpha) \bar{W}^* \quad (2.6)$$

where

$g(\alpha)$ is the antenna gain for signals arriving from angle α ,

it is easy to show that the condition that the gain be maximum in the direction of the source is met by setting [16]

$$\bar{W} = \bar{S}(\alpha_0) \quad (2.7)$$

where

α_0 is the angle of arrival associated with the source,

and $[\]^*$ indicates complex conjugation.

It is often more convenient to deal with normalized beam patterns. These are obtained by dividing the gain, $g(\alpha)$, by the product of the vector norms of $\bar{S}(\alpha_0)$ and \bar{W} . Hence, the normalized unadapted directivity pattern of an array with each element weighted equally is defined as

$$\Phi(\alpha) = \frac{\bar{S}^T(\alpha) \bar{W}^*}{\|\bar{S}(\alpha)\| \cdot \|\bar{W}\|} \quad (2.8)$$

where

all the elements of \bar{W} are equal,

$\Phi(\alpha)$ is the normalized gain, having a maximum amplitude of $1 + j0$

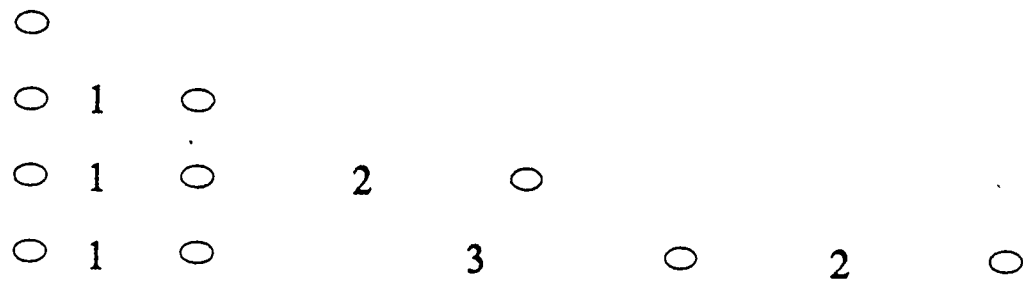
and $\|\bullet\|$ is the Euclidian norm.

2.3. Minimum Redundancy Arrays

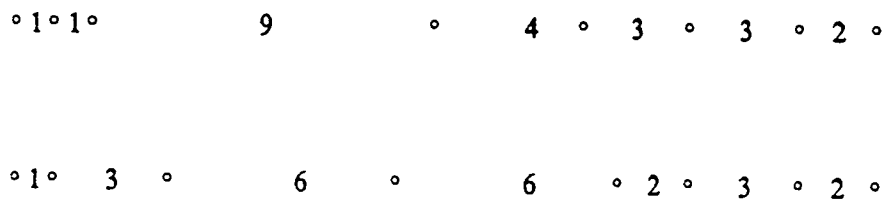
A Minimum Redundancy Array (MRA) of order M , is an array which, using M elements, allows the formation of all integer spatial correlations from 1 to N with the fewest possible elements. A Non-Redundant Array (NRA) is an array which forms all possible integer correlations from 1 to N with no duplications. The MRAs of order 1 to 4, shown in figure 2.2 (a), are NRAs, but it is not possible to form an NRA for arrays with more than four elements. However, for orders greater than four, the MRAs generally have few redundant spacings, and are thus good approximations of the NRA. For example, for order 8, there are two minimum redundancy arrays, shown in figure 2.2 (b), which cover all integer spacings from 1 to 23 with only three redundant spacings [15].

Minimum redundancy arrays have found application in radio astronomy where the characteristically large side lobes did not always pose a problem, and the narrow main beam was necessary to achieve the high spatial resolution required in mapping the night sky. A priori knowledge of that region of the sky could be used to correct for signals entering the system through the side lobes [9]. Obviously, this solution would not be practical for most other disciplines where array processing techniques are used.

We will begin by examining the array patterns of both uniform and minimum redundancy arrays. The normalized array pattern of the uniform array is given by:



(a)



(b)

Figure 2.2 - (a) Minimum redundancy arrays of orders 1 - 4; (b) Eighth order minimum redundancy arrays.

$$|\Phi_u|^2 = \frac{\sin^2(\frac{1}{2}Nkd \sin(\alpha))}{N^2 \sin^2(\frac{1}{2}kd \sin(\alpha))} \quad (2.9)$$

On the other hand, there is no simple, general expression for the array pattern of the MRA. However, if the MRA is approximated by the NRA of equivalent order, a general expression can be derived as follows:

$$|\Phi_m|^2 = \frac{M - 2 + 2\text{Re}[\sum_{n=0}^{N-1} e^{jnkd \sin(\alpha)}]}{M^2} \quad (2.10)$$

$$|\Phi_m|^2 = \frac{M - 2 + 2\cos(\frac{N-1}{2}kd \sin(\alpha)) \frac{\sin(\frac{N}{2}kd \sin(\alpha))}{\sin(\frac{1}{2}kd \sin(\alpha))}}{M^2} \quad (2.11)$$

where

Re indicates taking the real part.

The array patterns of uniform and minimum redundancy arrays of order 4 are shown in figure 2.3.

To understand why the MRA can be useful, it is necessary to consider the relationship between the array directivity pattern and the array spacing employed. For the uniform array, (2.9) is derived from:

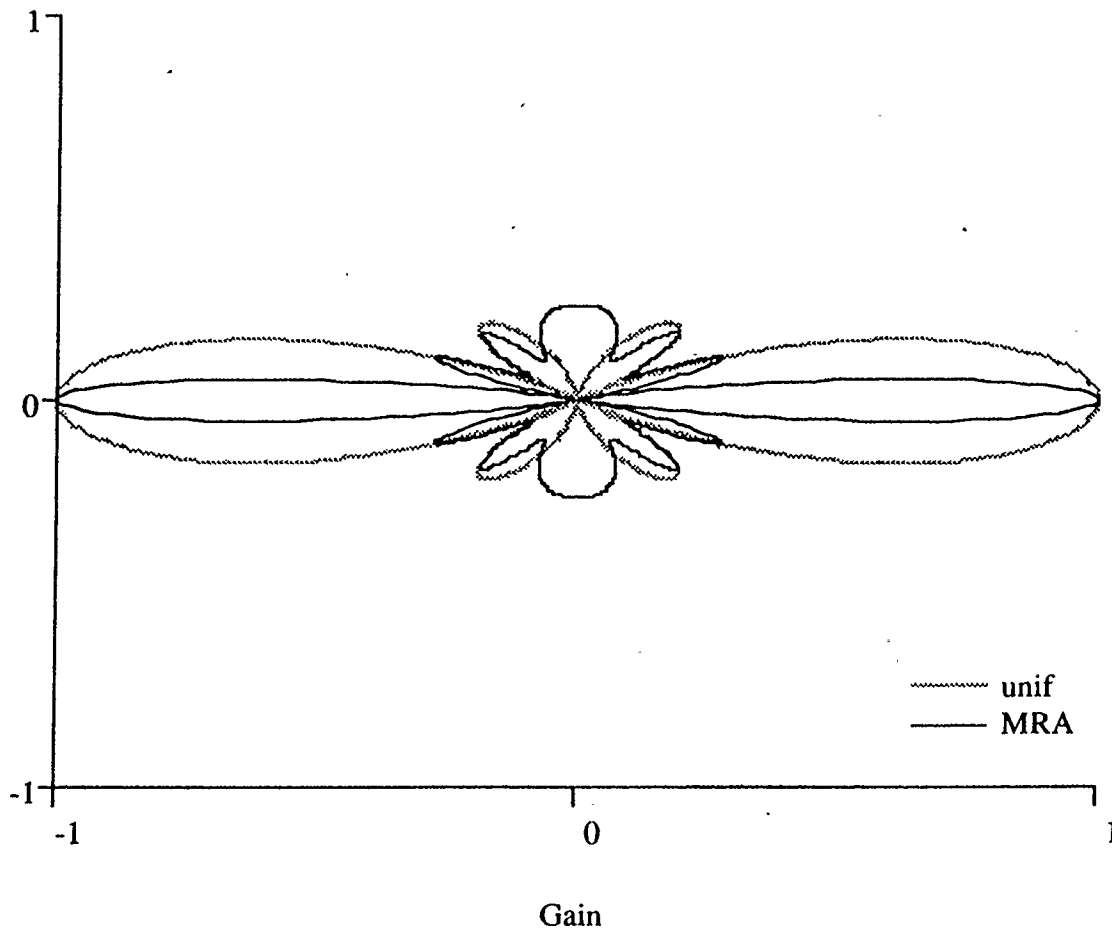


Figure 2.3 - Normalized array patterns for uniform and minimum redundancy arrays of order 4.

$$\Phi_u(\alpha) \doteq \frac{\left| \sum_{n=-\frac{M-1}{2}}^{\frac{M-1}{2}} e^{jnkd \sin(\alpha)} \right|^2}{M} \quad (2.12)$$

where

α is the direction of arrival,

M is the number of elements in the array,

$k = \frac{2\pi}{\lambda}$ is the wavenumber (λ is the wavelength)

and d is the distance between array elements.

From (2.12) the magnitude squared of $\Phi_u(\alpha)$ is

$$|\Phi_u(\alpha)|^2 = \frac{e^{j(-(M-1)\theta)} + 2e^{j(-(M-2)\theta)} + \dots + M + (M-1)e^{j(\theta)} + \dots + 2e^{j((M-2)\theta)} + e^{j((M-1)\theta)}}{M^2} \quad (2.13)$$

where

$$\theta = kd \sin(\alpha).$$

Careful consideration of (2.13) shows that the the power gain of the array is the Fourier transform of the autocorrelation function of the array, with the usual Fourier transform variables of t for time and ω for radian frequency being replaced by x for distance and θ or $kd \sin(\alpha)$ for spatial frequency. In the same manner in which the power spectrum is the Fourier transform of the autocorrelation of a time

domain sequence, we may refer to the spectrum in the spatial frequency domain as the angle spectrum.

Having established this, let us consider what the ideal angle spectrum would be. It is desirable to make it as narrow as possible, accepting only signals which originate from a specified direction; in short it should be an impulse. The transform of an impulse is a flat response in the transform domain. Thus the optimum array should have an autocorrelation which is as close to this ideal as possible.

If the redundant spacings of the MRA are neglected, the angle spectrum of the MRA is given as (2.10). It is instructive to note that the autocorrelation function of the MRA is composed of two components: a uniform grating, and an impulse. Fourier transforming this spectrum results in the uniform grating forming the narrow main lobe of the MRA pattern, while the transform of the impulse makes up the uniform sidelobes.

Note that when used, in conjunction with an adaptive beamformer or combiner, the narrow main lobe of the MRA allows the adaptive algorithm to null interfering signals closer to the direction of the desired signal without adversely affecting the main lobe. Another advantage, in terms of receiving multipath signals, is that the array is more spread out spatially than a uniform array with the same interelement spacing and number of elements and hence there is less chance

that all of the elements of the array will be located in a region of destructive interference. Because of this, the MRA achieves better decorrelation of the received signals for narrow angular separation of the multiple paths.

Table 2.1 details the MRA's of orders 1 through 10 and the unadapted array gains of MRA's containing 5 through 8 elements are compared with their uniform array counterparts in figures 2.4 to 2.7.

Table 2.1. Some of the possible MRA configurations for orders 1 through 10 [15].

MRA Configurations		
Number of Elements	Length	Interelement Spacing
1	-	-
2	1	1
3	3	1,2
4	6	1,3,2
5	9	1,3,3,2
6	13	1,5,3,2,2
7	17	1,3,6,2,3,2
8	23	1,3,6,6,2,3,2
9	29	1,3,6,6,6,2,3,2
10	36	1,2,3,7,7,7,4,4,1

2.4. Eigenvalue Analysis

Following the eigenvalue analysis given by Hudson (chapt. 2 in [16]) consider two signals impinging upon an array:

$$\bar{X}(t) = m_1(t)\bar{S}_1 + m_2(t)\bar{S}_2 \quad (2.14)$$

Array Gain (dB)

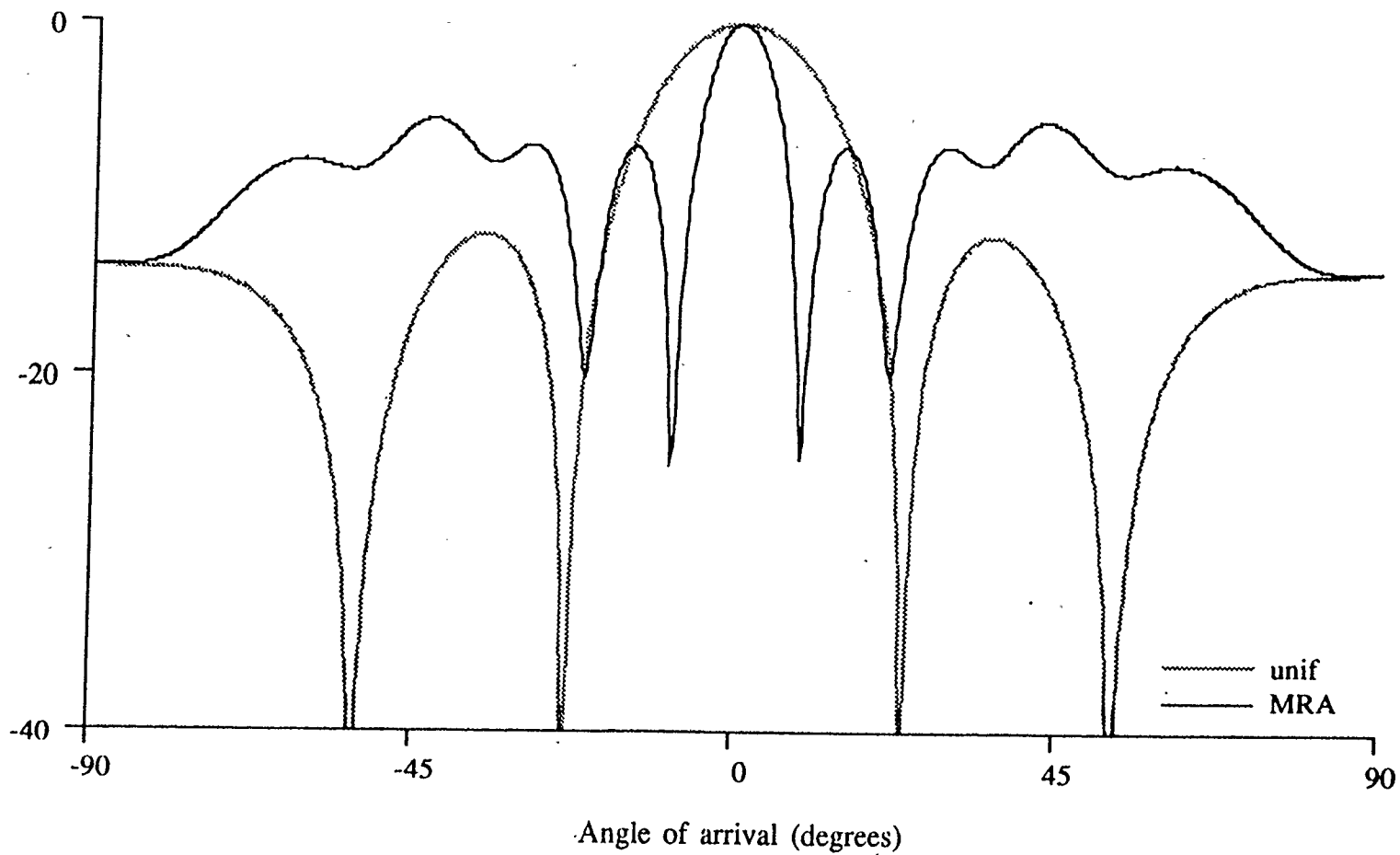
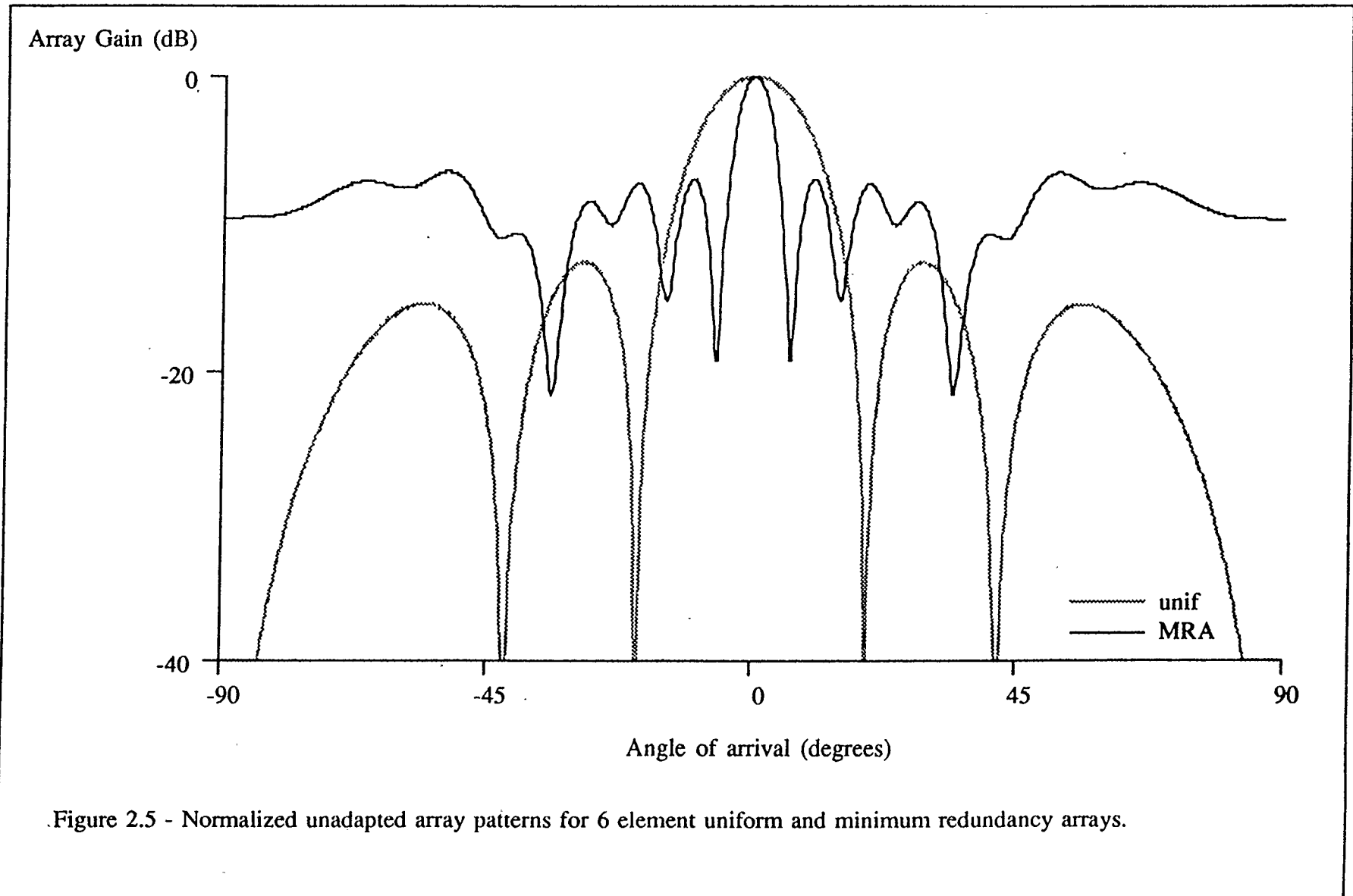


Figure 2.4 - Normalized unadapted array patterns for 5 element uniform and minimum redundancy arrays.



Array Gain (dB)

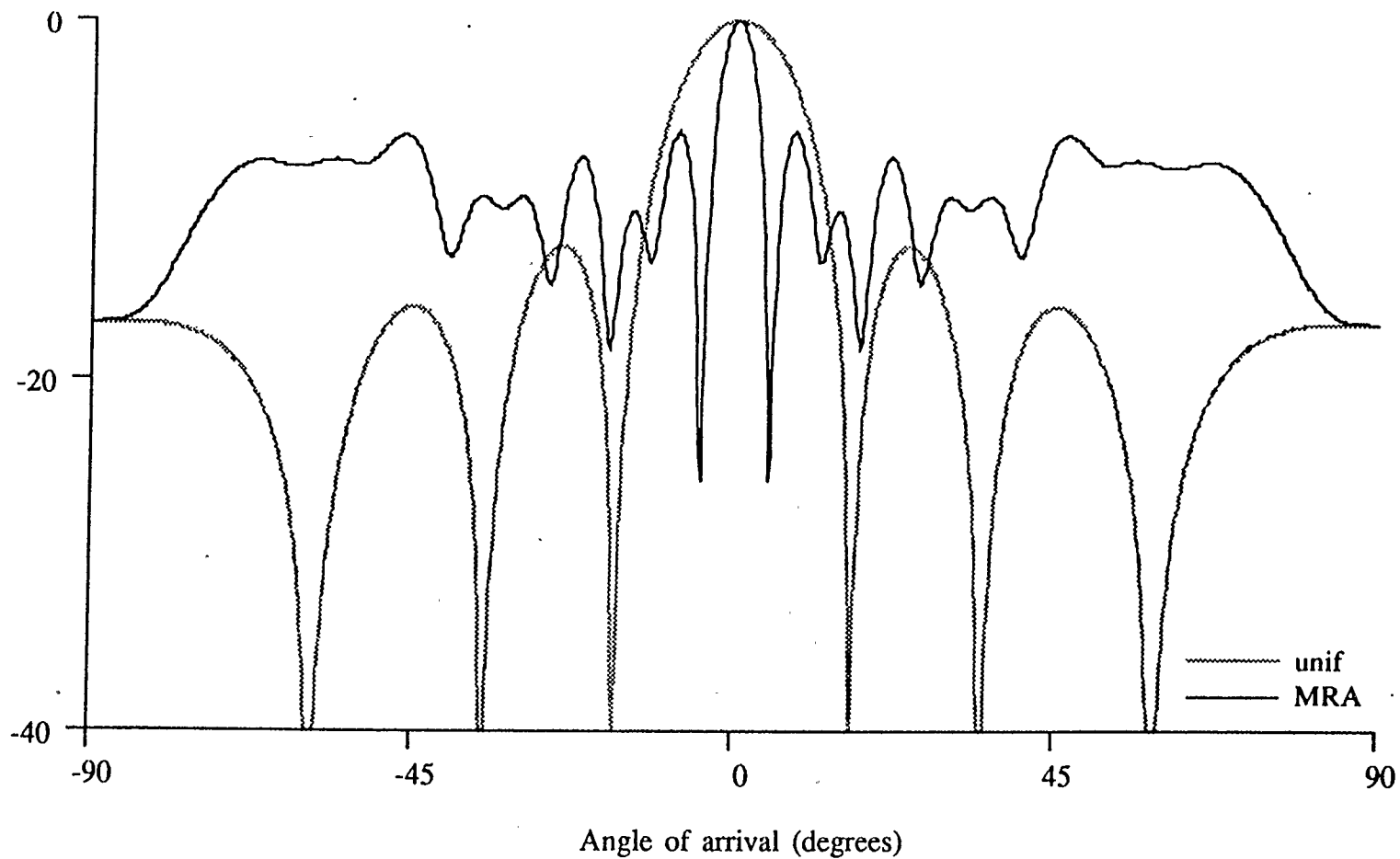
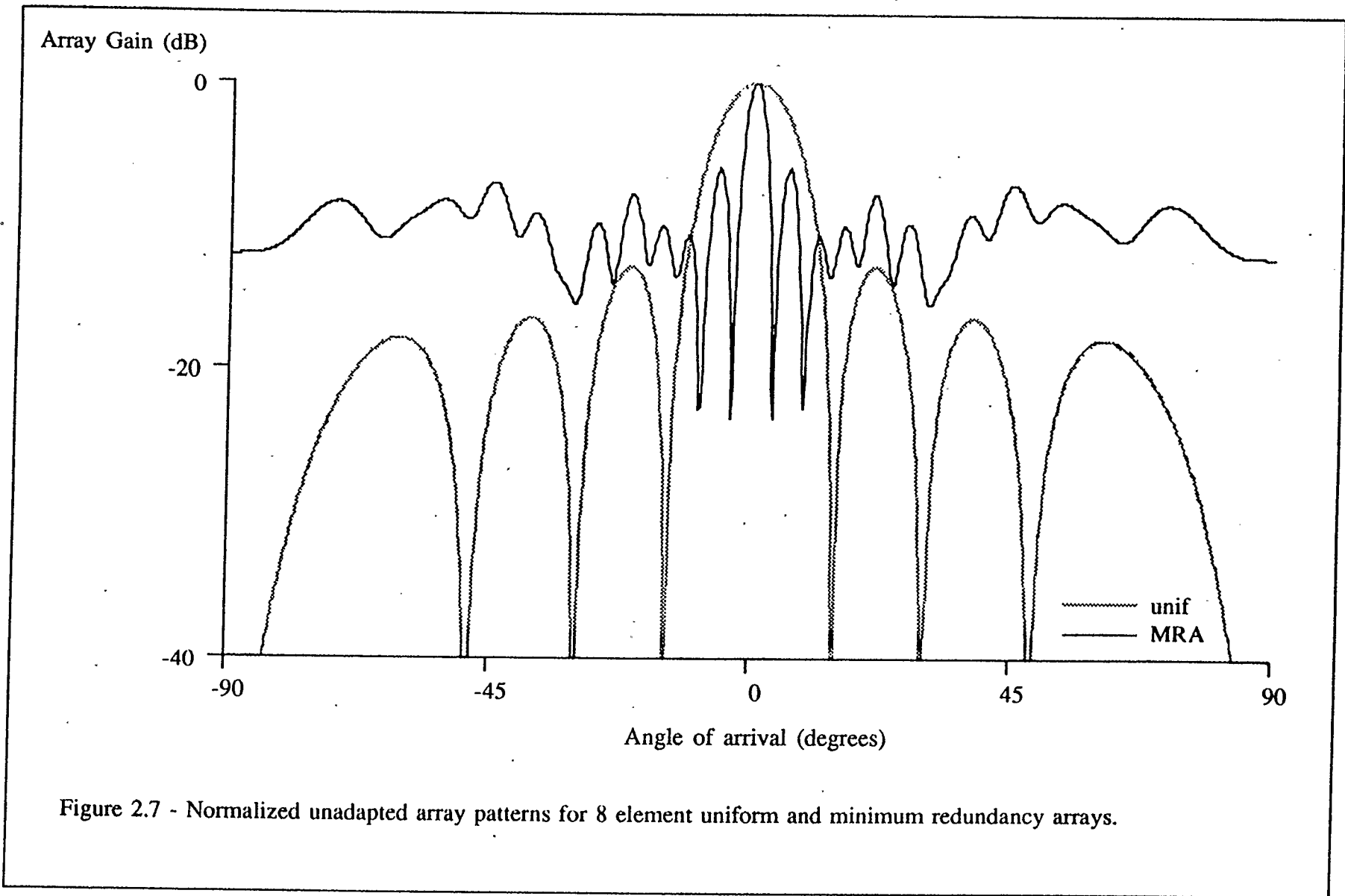


Figure 2.6 - Normalized unadapted array patterns for 7 element uniform and minimum redundancy arrays.



It can be shown that with uncorrelated modulation components and for $|\Phi|^2$ close to 1 [16]:

$$\lambda_1 \approx N(\pi_1 + \pi_2), \quad \lambda_2 \approx N \frac{\pi_1 \pi_2 (1 - |\Phi|^2)}{\pi_1 + \pi_2} \quad (2.15)$$

where

λ_1 and λ_2 are the eigenvalues
and π_i represents the power in the i^{th} signal.

For the uniform array, expanding (2.9) in series, applying long division and truncating the result after 2 terms gives:

$$|\Phi_u|^2 \approx 1 - \frac{1}{12} (kd \sin(\alpha))^2 (N^2 - 1) \quad (2.16)$$

For the NRA, which we use as an approximation to the MRA, $|\Phi_m|^2$ is given by (2.11). Again, expanding sine terms in series, using long division and truncating after the squared terms gives

$$|\Phi_m|^2 \approx \frac{1}{M^2} \left[M - 2 + 2 \cos \left[\frac{N-1}{2} kd \sin(\alpha) \right] \left[1 - \frac{1}{24} (N^2 - 1) (kd \sin(\alpha))^2 N \right] \right] \quad (2.17)$$

Expanding the cosine in a series, multiplying through, again truncating and noting that $(M - 2 + 2N) / M^2 = 1$

$$|\Phi_m|^2 \approx 1 - 2N \frac{4N^2 - 6N + 2}{24M^2} (kd \sin(\alpha))^2 \quad (2.18)$$

Using (2.15) and taking the ratio of λ_1 and λ_2 for the uniform and minimum redundancy arrays yields the eigenvalue spreads for the uniform and minimum redundancy arrays, β_u and β_m respectively.

$$\beta_u = \frac{\lambda_{2,unif}}{\lambda_{1,unif}} = \frac{\pi_1\pi_2(K^2 - 1)(kd \sin(\alpha))^2}{12(\pi_1 + \pi_2)^2} \quad (2.19)$$

where

K is the number of sensors in the array.

$$\beta_m = \frac{\lambda_{2,mra}}{\lambda_{1,mra}} = \frac{\pi_1\pi_2N(2N^2 - 3N + 1)(kd \sin(\alpha))^2}{6M^2(\pi_1 + \pi_2)^2} \quad (2.20)$$

where

M is the number of sensors in the array

and N-1 is the length of the array.

Now comparing the ratios of eigenvalue spreads for arrays of equal length, $N = K$

$$\zeta_l = \frac{\beta_m}{\beta_u} = \frac{2N(2N - 1)}{M^2(N + 1)} \quad (2.21)$$

where

ζ_l is the ratio of eigenvalue spreads for equal length arrays.

and for arrays of equal number of elements, $M = K$

$$\zeta_e = \frac{\beta_m}{\beta_u} = \frac{2N(2N^2 - 3N + 1)}{M^2(M^2 - 1)} \quad (2.22)$$

where

ζ_e is the ratio of eigenvalue spreads for arrays with equal numbers of elements.

Again approximating the MRA with a NRA, we have

$$N = \frac{M^2}{2} - \frac{M}{2} + 1 \quad (2.23)$$

Substituting,

$$\zeta_l \approx \frac{2(M^4 - 2M^3 + 4M^2 - 3M + 2)}{M^2(M^2 - M + 4)} \quad (2.24)$$

$$\zeta_e \approx \frac{M^5 - 3M^4 + 6M^3 - 7M^2 + 5M - 2}{2M(M^2 - 1)} \quad (2.25)$$

This yields two results:

- 1) minimum redundancy and uniform arrays of the same length have eigenvalue spread ratios which are of the same order for narrowly separated signals and
- 2) the MRA exhibits a smaller eigenvalue spread than the uniform array with the same number of elements for closely spaced signals.

Table 2.2 shows some of the ratios obtained for various lengths and element numbers.

Table 2.2. Eigenvalue Spread Ratios for Various MRAs.

Eigenvalue Spread Ratios		
MRA Order (length)	Equal Length ζ_l	Equal No. of Elements ζ_e
4(6)	1.42	4.6
5(9)	1.38	5.7
8(23)	1.41	12.9
∞	2	$M^2/2$

Thus, to resolve signals close together in space, if the number of sensor elements is constrained (perhaps due to the cost of the individual sensor elements) it may be desirable to use a minimum redundancy configuration rather than a uniform array. However, there is a drawback to using the MRA configuration. Because of the large side lobes inherent in the minimum redundancy array configuration, in order to be practical, an array based on this geometry should be adaptive. Hence, if an interference source arises, it can be nulled out by the adaptation process.

2.5. Adaptive Beamforming

Adaptive beamforming allows the weight vector to vary over time to adapt to or to follow changes in the signal environment. This allows beamformers to steer nulls in the direction of interfering signals.

Early adaptive beamformers tended to be useful only when the interfering signals were much greater in magnitude than the desired signal, or when a pilot signal could be provided. Many early beamformers which did not require pilot signals fell into the category of Maximum Entropy (ME) systems in that they attempted to whiten the output of the spatial filter by nulling plane wave sources. If the desired signal were much smaller than the interferences, or were present only a fraction of the time (as might occur in a radar system), the adapted pattern would attenuate the interferences much more than the desired signal and a large improvement in SNIR would result. However, if the interferences were small, or if there were no interferences, the beamformer would attempt to null the desired signal. Obviously this is not acceptable in most cases.

In order to avoid this, it is necessary to impose a constraint upon the gain of the adaptive array for signals arriving from the look direction. A mathematically tractable means of expressing this constraint for the case of a narrowband beamformer where no steering delays have been employed, is to consider the weight vector, \bar{W} as made up of two components, \bar{U} and \bar{V} , with \bar{U} forming the fixed time invariant component required to meet the constraint, and \bar{V} the time varying adaptive component. \bar{V} must be constrained in some fashion so that it does not affect the gain in the look direction. This is achieved by using a projection matrix, \mathbf{P} , to force the adaptive component to have zero gain in the look direction. The projection matrix is of the form

$$\mathbf{P} = \mathbf{I} - \frac{\bar{\mathbf{S}}^*(\alpha_d)\bar{\mathbf{S}}^T(\alpha_d)}{\bar{\mathbf{S}}^T(\alpha_d)\bar{\mathbf{S}}^*(\alpha_d)} \quad (2.26)$$

where

$\bar{\mathbf{S}}(\alpha_d)$ is the space vector of the desired signal,

and \mathbf{I} is the identity matrix.

The overall weight vector then becomes

$$\bar{\mathbf{W}} = \bar{\mathbf{U}} + \mathbf{P}\bar{\mathbf{V}} \quad (2.27)$$

and $\bar{\mathbf{V}}$ can be varied without constraint (chapt 7 in [16]).

One method of achieving this constrained adaptation was developed by O.L. Frost [19]. He devised an adaptive algorithm based on the simple LMS update recursion which allowed the imposition of a linear constraint upon the gain of the system in the look direction. Because of the simple nature of the LMS recursion, the algorithm could be implemented in digital or analog form. The following is the discrete time or digital form of the algorithm.

The structure of the Frost adaptive beamformer is shown in figure 2.8. It may be employed in either narrowband or wideband configurations, the difference being simply the length of the tapped delay lines, with tapped delay lines of length greater than 2 being employed in wideband configurations. The beamformer used in the simulation performed at the end of this chapter was narrowband, so a single delay, D , was chosen to provide a 90 degree phase between the two samples used.

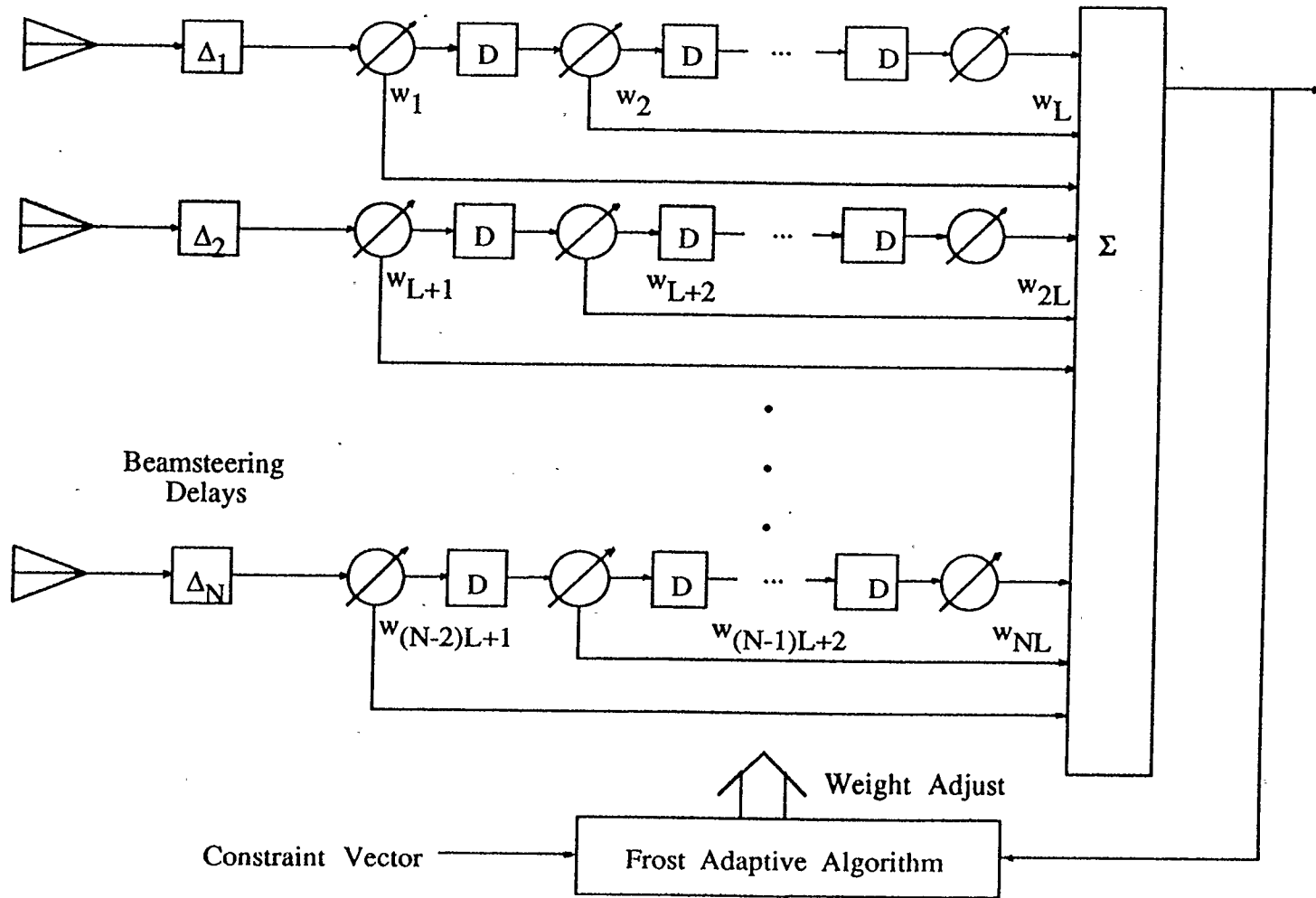


Figure 2.8 - Frost adaptive beamformer structure.

Thus, for a sinusoidal input, this corresponds to quadrature sampling.

In contrast to a Maximum Entropy beamformer, a beamformer which employs a constraint in the look direction cannot simply minimize the output power as is done in Maximum Entropy beamformers. However, no desired signal is generally available, so the common method of minimizing the difference between the output and the desired signal is also not possible. Fortunately, equation (2.27) provides a possibility. By constraining the gain of the beamformer in the look direction in some way, and then minimizing the output power, we achieve the desired result. Thus, the beamformer will maintain the desired gain in the look direction, and will adapt to minimize the total power arriving from all other directions. The constraint vector \bar{C} is used in the adaptation process to maintain a specified response in the desired look direction. This, in conjunction with the beamsteering delays (required to define the look direction) shown in the figure, can be related directly to \bar{U} as \bar{U} also specifies the constant gain in the look direction.

When the constraint used is a unit gain with zero phase, the desired signal will appear at the output undistorted, but with additive noise and interference. This is known as a Minimum Variance Distortionless Response (MVDR) beamformer. It has also been shown that this represents a Maximum Likelihood (ML) estimate of the target signal if all signals involved are Gaussian with zero mean [23].

It should be noted that the beamsteering delays co-phase the desired signal, resulting in the same conditions as would prevail if the look direction was broadside to the array, regardless of the actual look direction. One significant detail which should be made clear, however, is that for two signal - interference configurations to be equivalent, it is not the angular separation which must be equal, but rather the difference in $\sin(\alpha)$. As an example: a look direction of broadside (0 degrees, $\sin(0) = 0.0$) with an interference at 30 degrees ($\sin(30) = 0.5$) would be equivalent to having a look direction of 30 degrees and an interference at 90 degrees ($\sin(90) = 1.0$) as in each case the difference in the sines of the arrival angles of signal and interference are equal. But note that the difference in the angles is 30 degrees in one case and 60 degrees in the other. Since it is possible to treat all cases arising as though the look direction were broadside, from this point forward, the look direction will be implicitly broadside unless otherwise stated. As a final caution on this point, adapted array patterns throughout are plotted with angle of arrival as the horizontal axis. These angles are valid only for the broadside look direction, but the results are still general in that they represent the result for the equivalent case where the differences between the sines of the angles are the same.

The Frost adaptation may be seen as a two step process [17]. The first step is the determination of the unconstrained weight vector. The second step imposes the constraint upon the weight vector, adding correction terms evenly across each

element of the weight vector.

Consider the case where the array has N elements and the tapped delay lines have L taps. Both the weights and observations may be arrayed in rectangular matrices:

$$\bar{W}_k = \begin{bmatrix} w_{1k} & w_{2k} & \cdots & w_{Lk} \\ w_{(L+1)k} & w_{(L+2)k} & \cdots & w_{2Lk} \\ \cdot & \cdot & \cdot & \cdot \\ \cdot & \cdot & \cdot & \cdot \\ \cdot & \cdot & \cdot & \cdot \\ w_{((N-1)L+1)k} & \cdot & \cdots & w_{NLk} \end{bmatrix} \quad (2.28)$$

$$\bar{X}_k = \begin{bmatrix} x_{1k} & x_{2k} & \cdots & x_{Lk} \\ x_{(L+1)k} & x_{(L+2)k} & \cdots & x_{2Lk} \\ \cdot & \cdot & \cdot & \cdot \\ \cdot & \cdot & \cdot & \cdot \\ \cdot & \cdot & \cdot & \cdot \\ x_{((N-1)L+1)k} & \cdot & \cdots & x_{NLk} \end{bmatrix} \quad (2.29)$$

The constraint vector is given as:

$$\bar{C} = [c_0 \ c_1 \ \cdots \ c_{L-1}] \quad (2.30)$$

Because the beamsteering delays shown at the left of the figure have aligned the outputs of the sensors in time such that signals arriving from the desired look direction are in phase, the Frost constraint is implemented by requiring that

$$[1 \ 1 \ 1 \ \cdots \ 1] \bar{W}_k = \bar{C} \quad (2.31)$$

over all time k .

We now briefly examine the Frost algorithm itself.

The first step is the calculation of the unconstrained weight vector:

$$\bar{W}'_{k+1} = \bar{W}_k + 2\mu y_k \bar{X}_k \quad (2.32)$$

where

\bar{W}'_{k+1} is the unconstrained weight vector,

\bar{W}_k is the constrained weight vector obtained from the previous iteration,

μ is the Least Mean Squares (LMS) adaptive gain constant,

y_k is the output of the beamformer at time k ,

and \bar{X}_k is the observation vector at time k .

The constraint error is then calculated and used to form a $N \times L$ correction matrix \bar{E}' .

$$\bar{E}'_{k+1} = [1 \ 1 \ \cdots \ 1]^T \frac{1}{N} \left[\bar{C} - [1 \ 1 \ \cdots \ 1] \bar{W}'_{k+1} \right] \quad (2.33)$$

The second step is then to impose the constraint upon the unconstrained weights so that

$$\bar{W}_{k+1} = \bar{W}'_{k+1} + \bar{E}'_{k+1} \quad (2.34)$$

and this completes the weight update cycle of the Frost algorithm.

Other methods of achieving the Frost constraint have also been devised [24].

2.6. Signal to Noise plus Interference Ratio Calculation

Hudson (chapt. 7 in [16]) has shown that for a single interference and a unity noise variance, the noise plus interference power of a converged linearly constrained adaptive array may be written as

$$P_{n+i}(\alpha) = N + \frac{\pi_i N^2 |\Phi(\alpha)|^2}{1 + \pi_i N (1 - |\Phi(\alpha)|^2)} \quad (2.35)$$

where

$P_{n+i}(\alpha)$ is the total noise plus interference power,

π_i is the interference power,

α is the angle of arrival of the interference signal,

N is the number of elements in the array,

and $\Phi(\alpha)$ is the normalized array gain in the α direction.

Because of the constraint, the signal power, P_s , at the output of the array is fixed at

$$P_s = \pi_s N^2 \quad (2.36)$$

where

π_s is the power in the signal arriving at the array.

From these relations, the *SNIR* can be determined:

$$SNIR = \frac{P_s}{P_{n+i}} \quad (2.37)$$

$$SNIR = N\pi_s \left[1 - \frac{\pi_i N |\Phi(\alpha)|^2}{1 + \pi_i N} \right] \quad (2.38)$$

As mentioned previously, the above relation is based upon a noise variance, σ^2 of 1. Removing this condition, we are left with:

$$SNIR = N \frac{\pi_s}{\sigma^2} \left[1 - \frac{\pi_i N |\Phi(\alpha)|^2}{\sigma^2 + \pi_i N} \right] \quad (2.39)$$

Examining (2.39) we find that the *SNIR* is directly proportional to the power in the signal, thus the overall shape of the *SNIR* function is unaffected by changes in signal power. Closer examination reveals that the shape of the *SNIR* curve is dependent upon the ratio of the interference power and noise power. The best results in terms of *SNIR* occur when α corresponds to a null in the unadapted pattern, giving $|\Phi(\alpha)|^2$ as zero, and the overall *SNIR* then becomes a function of signal power and uncorrelated noise only.

Figure 2.9 shows the *SNIR*'s for various noise and interference power ratios as a function of interference arrival angle for four element adaptive MR and uniform arrays assuming a broadside look direction. The uniform array does achieve a slightly better *SNIR* for interferences which are at some angular distance from the look direction. Note, however, that for interferences located close to the look direction, the MRA far outperforms the uniform array. Because we know the normalized unadapted directivity pattern of the MRA will have a much narrower

SNIR (dB)

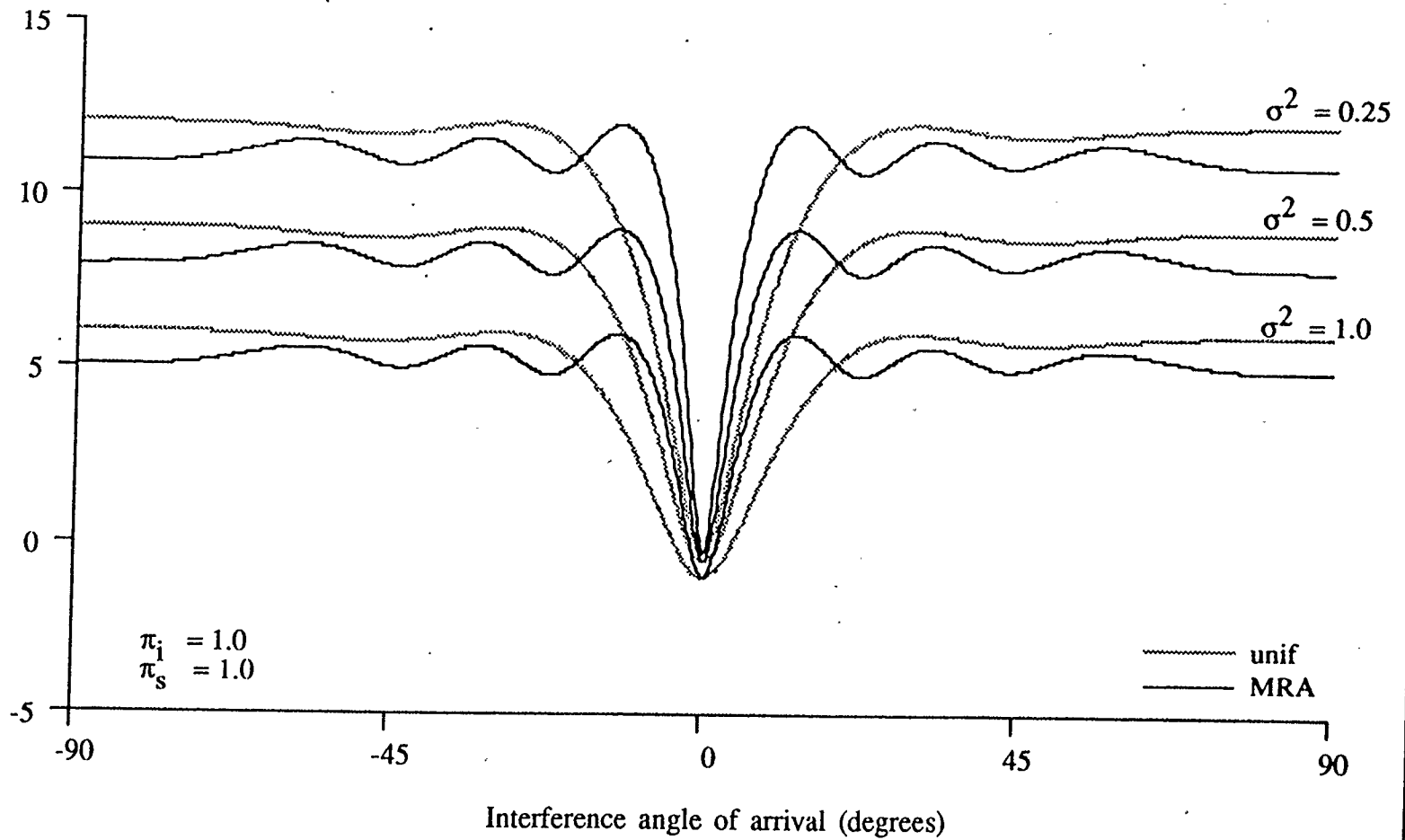


Figure 2.9 - SNIR at the output of 4 element converged uniform and minimum redundancy adaptive array systems for various noise magnitudes.

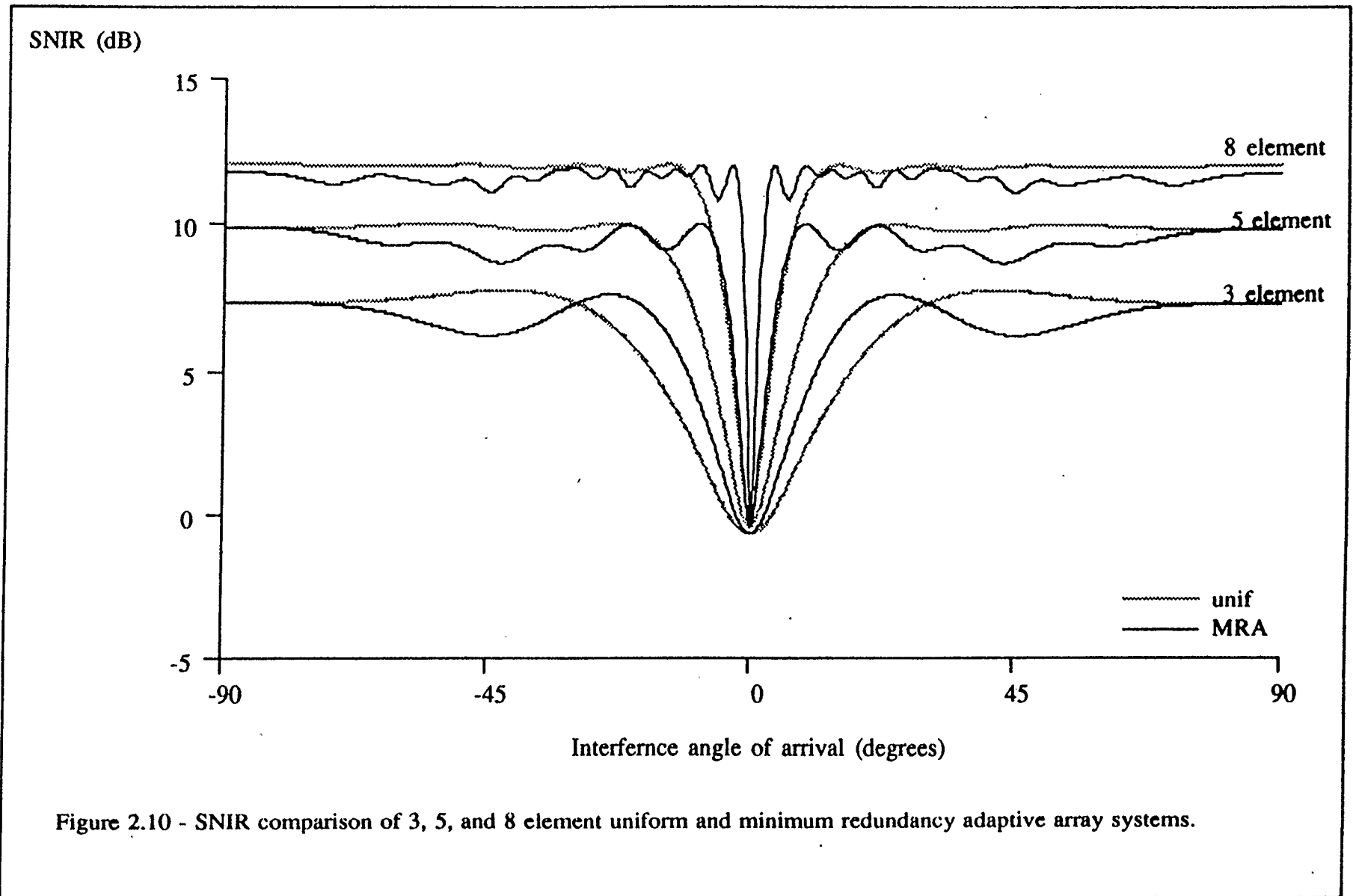
main lobe than the uniform array for any order, it is apparent from (2.39) that MRA's of all orders should offer superior performance for interferences located in close angular proximity to the desired look direction.

From figure 2.9 it is apparent that there is an angle which represents the point at which the MRA based system and the uniform array based system achieve identical performance. In the figure, it is simply the point at which the two curves cross. This angle will be referred to as the threshold angle, α_t . Figure 2.10 indicates the SNIR curves for MRA and uniform arrays containing 3, 5 and 8 elements. Table 2.3 contains the threshold angles, given that the look direction is broadside, for arrays containing 3 to 8 elements.

Table 2.3. Threshold angles for arrays of order 3 to 8.

Threshold Angles for Various Arrays		
Number of Elements	Threshold Angle α_t	$\sin(\alpha_t)$
3	30.0	0.500
4	18.6	0.319
5	15.2	0.262
6	15.8	0.272
7	13.1	0.227
8	10.9	0.189

The numbers in the table may be somewhat misleading. For example, consider the 5 element arrays. The threshold angle is 15.2 degrees, a narrower



angle than that for the 6 element array. An examination of figure 2.10 reveals that the SNIR curves for both the MRA and uniform array are very similar between 15 and 20 degrees.

These results again indicate that MRA based adaptive systems outperform their uniform array based counterparts in the rejection of interferences which are located in close angular proximity to the desired signal. The penalty paid for this, as can be seen in the figure, is a comparatively small degradation in the MRA based systems' ability to reject interferences which are located at some angular distance from the look direction.

2.7. Simulation Results

A Frost beamformer was used in conjunction with both a uniform and a minimum redundancy array with four sensors each to form directivity patterns in response to spatially coherent sinusoidal interferences and Gaussian noise. The noise is modelled as additive noise at the sensor inputs. In all of the following figures, the "look" direction is along the zero axis. Because the constraint selected for the Frost algorithm was the maintenance of a 0 dB gain in the look direction, each pattern exhibits a zero dB gain in this direction. Each directivity pattern was developed by using an LMS adaptation factor, μ , of 0.0005 and allowing the beamformer to adapt for 500000 iterations. The sensor elements were spaced at multiples of $\lambda / 2$. The extremely small value of μ and the long

adaptation time were used to ensure that the beamformers had converged and that the misadjustment of the weight vectors was minimized.

The case of additive noise only with no coherent interference is considered first. In this case the uniform array attenuates the noise by 6.02 dB while the MRA provides 6.00 dB of attenuation. This small difference is probably not significant in most cases, although it does indicate that the uniform array is slightly less sensitive to small weight perturbations. The patterns developed are shown in figure 2.11.

In order to confirm that the MRA geometry is superior for rejecting interferences near the desired signal, a -3 dB sinusoidal interference is established 10 degrees off the "look" direction. Further, additive white noise of -10 dB is included. Figure 2.12 shows the patterns which result for both the MRA and the uniform array for this signal environment. Because the interference at 10 degrees is much larger than the noise background, both patterns show deep nulls in the direction of the interference: 31.6 dB for the MRA based array and 18.6 dB for the uniform array. Note, however, that in order to form the null at 10 degrees and maintain the constraint in the look direction, the main beam of the uniform array pattern has been "pushed" away from the interference. The main lobe is not pointed exactly in the look direction, and consequently the attenuation of the background noise is not as great as would be desirable, only 2.0 dB in this case. The MRA configuration,

Array Gain (dB)

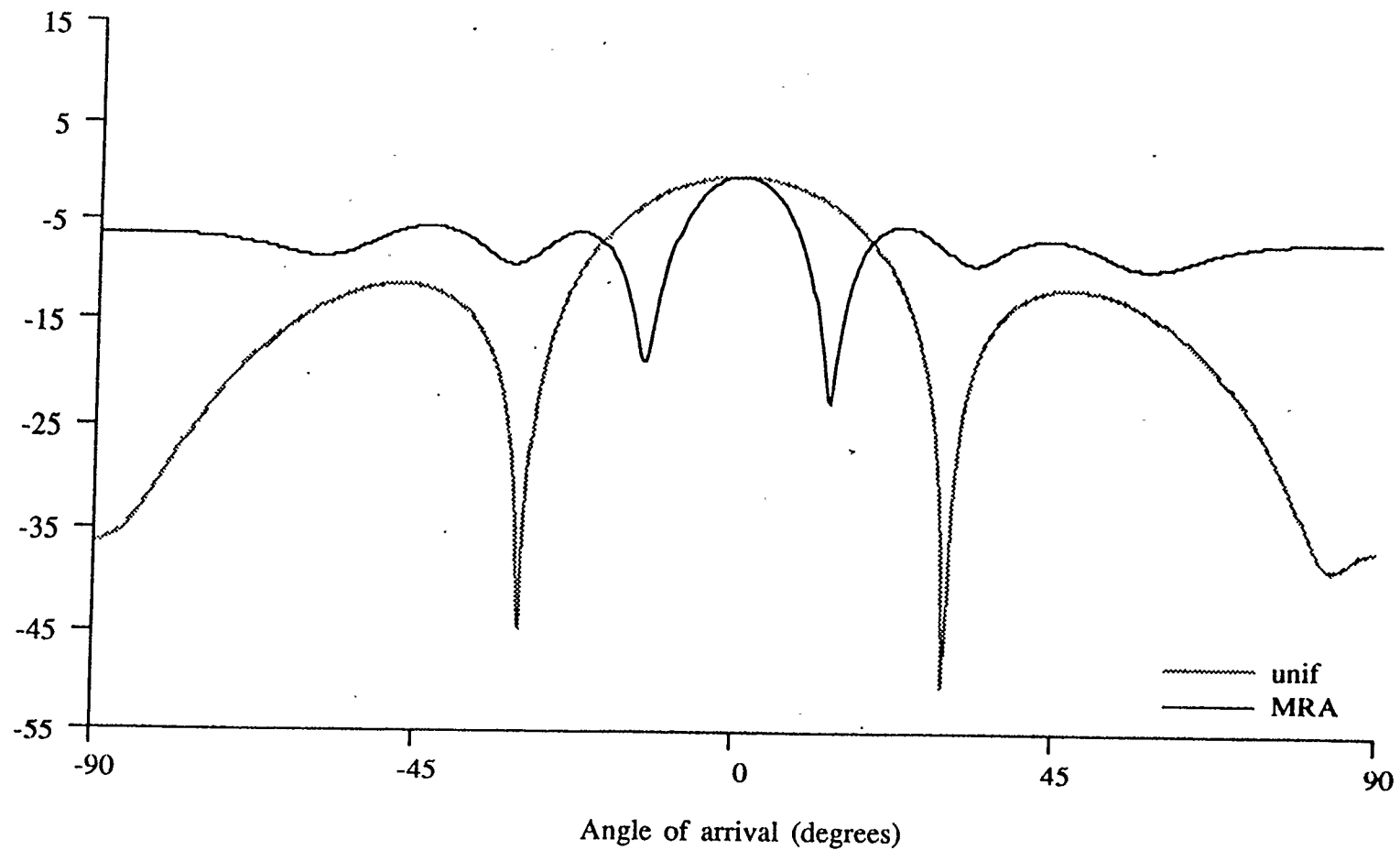


Figure 2.11 - Directivity patterns for 4 element uniform and minimum redundancy adaptive arrays with additive Gaussian noise.

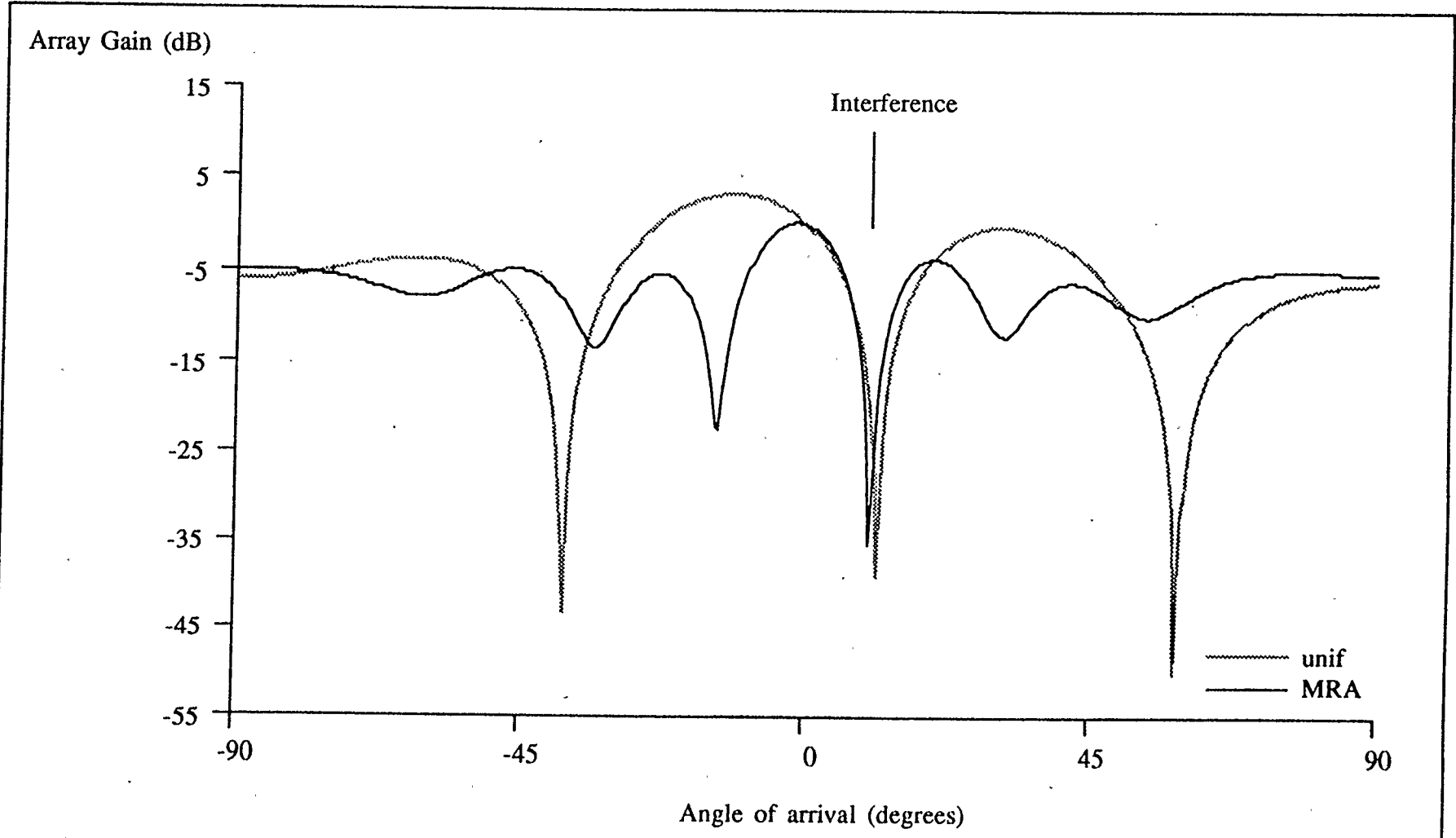


Figure 2.12 - Directivity patterns for 4 element uniform and minimum redundancy adaptive arrays with -10 dB Gaussian noise and a -3 dB plane wave interference.

on the other hand, because of its narrow main lobe, provides both a deep null in the direction of the interference and still maintains a higher degree of attenuation for the additive noise, 5.6 dB in this case. The total Noise plus Interference Power (NIP) is -12.0 dB for the uniform array and -15.6 dB for the MRA. The MRA is thus 3.6 dB superior in performance in this case. This is slightly less than the predicted difference of 4.3 dB from the SNIR calculations of section 2.6.

In the next figure, the same interference is simulated with an increased noise of 0 dB magnitude. Here, the MRA attenuates the noise by 5.9 dB while the uniform array provides 4.8 dB of attenuation. The MRA also forms a deeper null in the interference direction, with the MRA forming a 16.8 dB null and the uniform array forming a 6.2 dB null. The overall NIP is -5.9 dB for the MRA and -4.0 dB for the uniform array. Here, because the noise is more significant than in the previous case, the margin of performance for the MRA is reduced. The predicted superiority of the MRA based system in this case was 2.3 dB which, again, is slightly more than the simulation result of 1.9 dB. As the ratio of noise power to interference power is increased, the uniform array eventually equals the performance of the MRA.

Array Gain (dB)

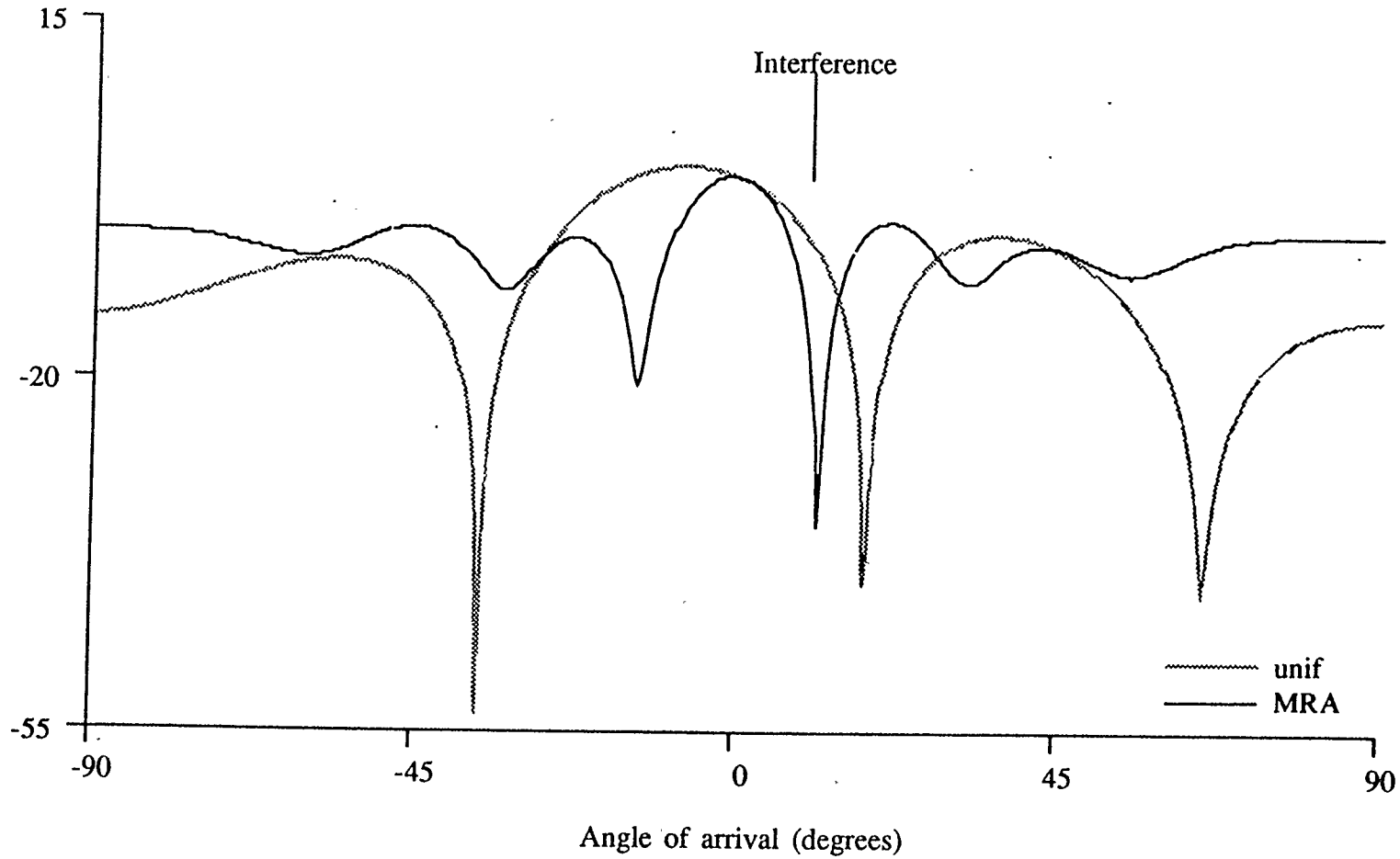


Figure 2.13 - Directivity patterns for 4 element uniform and minimum redundancy adaptive arrays with 0 dB Gaussian noise and a -3dB plane wave interference.

2.8. Conclusion

For four element arrays, an adaptive minimum redundancy array beamformer was shown to achieve superior noise and interference rejection over that achievable with a comparable uniform array based system for cases when spatially coherent interferences of significant strength (with respect to the overall interference and noise power) were present in close angular proximity to the direction of interest. This corresponded to the results predicted from the SNIR analysis. Since the results also seemed to correspond with those expected from the eigenvalue analysis, it would appear likely that the same advantages would also hold for higher order minimum redundancy arrays.

CHAPTER 3

A SUBOPTIMAL ARRAY WITH ADAPTIVE ELEMENTS

SPACED FOR MINIMUM REDUNDANCY

3.1. Introduction

The conclusions drawn in the previous chapter were based on the premise that the outputs of all of the sensors making up the respective arrays were weighted by adaptive coefficients. That is, all of the coefficients in the weight vector were variable over time, with the variation controlled by the adaptive algorithm. However, there are situations in which it may not be desirable to make the weighting coefficient of each and every sensor output adaptive. The greater the number of adaptive elements, the larger the misadjustment associated with the converged solution. Also, with more adaptive elements, the convergence time increases. Finally, the computational burden imposed by requiring that each of a large number of weighting coefficients be adaptive can become prohibitive. Thus, for a large array, there are significant drawbacks associated with using a fully adaptive array.

The suboptimal array seeks to overcome the problems associated with the fully adaptive array by using significantly fewer adaptive coefficients than the total

number of coefficients in the weight vector. It has been shown that for large arrays, the use of suboptimal adaptive systems, with adaptation applied to only a small fraction of the total number of weight coefficients, can achieve results comparable to those attainable with a fully adaptive array so long as sufficient degrees of freedom are provided to cancel all discrete spatial interferences [20,25].

One form of suboptimal array, known as a thinned adaptive array, is an array in which only a portion of the weights applied directly to the output of each sensor are adaptive. There are other means of implementing suboptimal arrays, but only the thinned adaptive array is covered here.

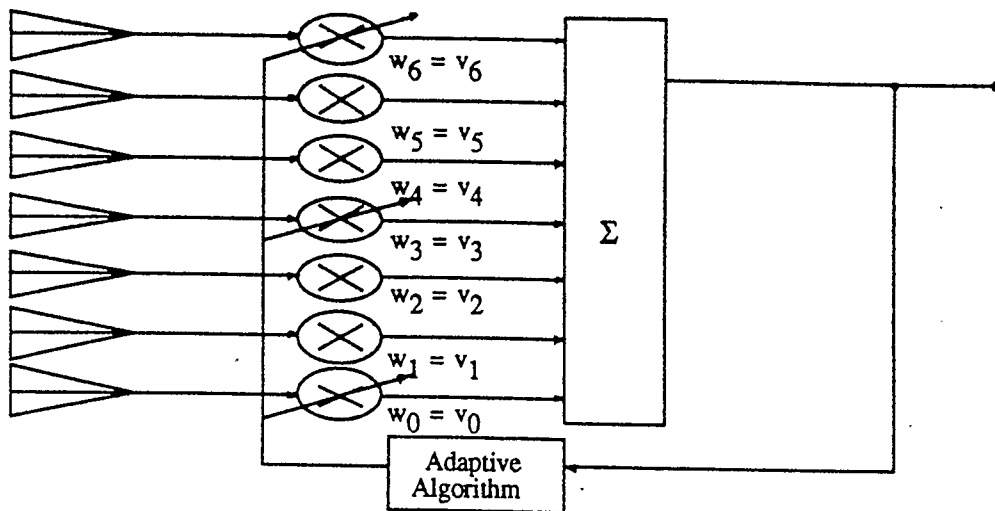
In this chapter, we will study the effects of using adaptive elements spaced for minimum redundancy within a narrowband uniform line array. Such an array belongs to the broad class of suboptimal arrays based on arrays with thinned adaptive elements although the common method of choosing the adaptive elements in a thinned array is to simply space the adaptive elements out equally amongst the nonadaptive elements. Hence, in an array in which one third of the elements were to have adaptive coefficients, every third element would be adaptive. It will be shown that choosing adaptive elements based on a minimum redundancy criterion improves the main lobe interference rejection performance of such an array significantly.

The performance of the different arrays will be compared on the basis of both calculations and simulations undertaken to establish which of the arrays provides the better converged solution in various cases. Because most suboptimal arrays achieve good sidelobe attenuation of interferences, the emphasis will be placed on the ability of each array to reject main lobe interferences.

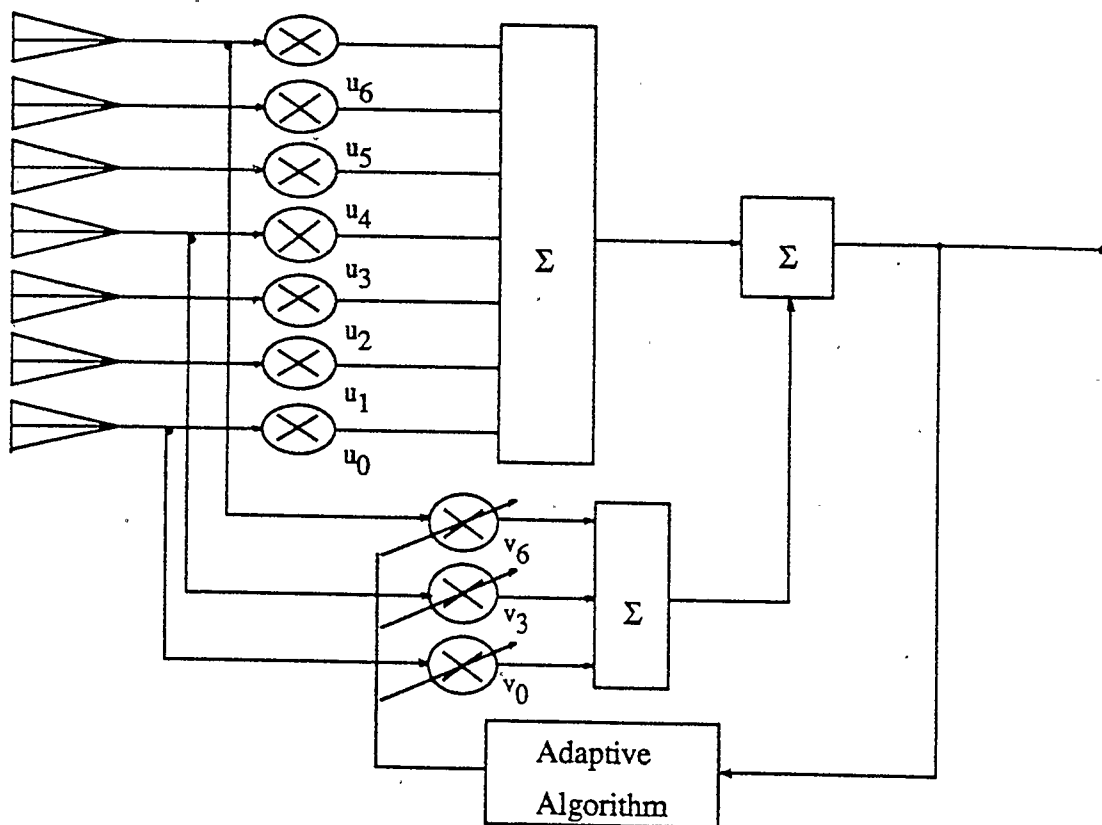
3.2. The Thinned Adaptive Suboptimal Array

In many fields where arrays are used, it is necessary to use arrays with a large number of receiving elements. Consider for example, the passive sonar array, where the number of hydrophones employed in one array can number in the hundreds, and it is desirable to process the data in real time. In cases such as this, it is simply not practical to consider employing a fully adaptive array, weighting each sensor output by a time variable weight, with the value of the weight determined by an adaptive algorithm. The disadvantages associated with such a fully adaptive array were briefly mentioned in the introduction, as was a compromise solution, the suboptimal array.

Figure 3.1 shows two forms of the thinned adaptive suboptimal array. If the null constraint given by (2.27) is employed for the adaptive subarray, these two forms may be equivalent, with 3.1(a) representing the more common implementation, as it requires fewer components. Figure 3.1(b), however, allows a



(a)



(b)

Figure 3.1 - Thinned adaptive array configurations; (a) Minimum hardware implementation; (b) Null constraint implementation

better understanding of the way in which the thinned adaptive array operates. From figure 3.1(b), it can be seen that there are two subarrays; a conventional subarray comprising all the elements which are merely steered in the direction of the desired signal, and an adaptive subarray, the elements of which are weighted by time varying multipliers. In the case of figure 3.1(a), with unity modulus weights employed in the conventional subarray, for a Minimum Variance Distortionless Response (MVDR) beamformer, the adaptive subarray would be constrained to provide a gain in the look direction which was equal to the number of elements in the adaptive subarray. For the configuration shown in figure 3.1(b), the adaptive subarray would be required to have a null in the look direction, with the conventional (fixed) subarray providing all of the gain in the look direction. From this, then, it is apparent that the prime function of the adaptive subarray is to form a beam in the direction of any interfering signals, with the magnitude equal to the magnitude of the conventional array response in that direction, but the phase opposite, producing a null in the direction of the interferences. Using this insight, it becomes clear that the narrowness of the beam formed by the adaptive subarray is of paramount importance, as wider beamwidths would cause more significant distortion of the array pattern of the conventional subarray, with this criterion becoming critical when the interference is within the main lobe of the beam formed by the conventional subarray. This provides the motivation for using adaptive elements spaced for minimum redundancy, as it was shown in the

previous chapter that such a configuration provides the narrowest beamwidth possible without spatial aliasing.

Some simple changes are required to the equations in chapter 2 which describe the weight vector in order to allow for the fact that only some of the weights are adaptive. Once again, (2.27) is used to describe the weight vector, but in this case the form of the projection matrix, \mathbf{P} , previously given by (2.26), is slightly different. Using the structure given by figure 3.1(b), the space vector of the conventional subarray, $\bar{S}_u(\alpha)$ contains N unity modulus coefficients, where N is the number of conventionally weighted elements, which in this case is the same as the number of elements. The space vector of the adaptive subarray, $\bar{S}_v(\alpha)$ contains M unity modulus coefficients, where M is the number of adaptively weighted elements, and $N-M$ zero or null coefficients, with the null coefficients corresponding to those elements which are not adaptively weighted. Hence, for a system with every third element adaptive

$$\bar{S}_u(\alpha) = [s_0 \ s_1 \ s_2 \ s_3 \ \cdots \ s_N]^T \quad (3.1)$$

$$\bar{S}_v(\alpha) = [s_0 \ 0 \ 0 \ s_3 \ 0 \ 0 \ s_6 \ \cdots \ s_{N-2} \ 0 \ 0]^T \quad (3.2)$$

Using $\bar{S}_v(\alpha)$ as given by (3.2), the \mathbf{P} matrix is now

$$\mathbf{P} = \mathbf{I}_v - \frac{\bar{S}_v^*(\alpha_d)\bar{S}_v^T(\alpha_d)}{\bar{S}_v^T(\alpha_d)\bar{S}_v^*(\alpha_d)} \quad (3.3)$$

where

\mathbf{I}_v is a diagonal matrix with zero elements corresponding to nonadaptive elements,

$$\text{i.e. } \text{diag}(1 \ 0 \ 0 \ 1 \ 0 \ 0 \ \dots \ 1 \ 0 \ 0)$$

and α_d is the desired look direction.

From (3.3) it can be seen that the form of \mathbf{P} is such that it is zero over all elements in those rows and columns which do not correspond to adaptive elements, indicating that they are not involved in the adaptation process. Using these relationships, it is possible to derive the noise plus interference power, P_{n+i} , at the output of a converged thinned adaptive array. With a normalized uncorrelated noise power of 1, from Hudson (chap. 7 in [16])

$$P_{n+i} = N + \frac{\pi_i N^2 |\Phi_c|^2}{1 + \pi_i M (1 - |\Phi_v|^2)} \quad (3.4)$$

where

π_i is the interference power,

Φ_c is the normalized array gain of the conventional subarray for the interference arrival angle,

and Φ_v is the normalized unadapted array gain of the adaptive subarray in the direction of the interference.

Equations (2.36) and (2.37) may be applied to find the Signal to Noise plus Interference Ratio (*SNIR*) of the thinned adaptive array;

$$SNIR_t = \frac{N \pi_s (1 + \pi_i M (1 - |\Phi_v|^2))}{1 + \pi_i M (1 - |\Phi_v|^2) + \pi_i N |\Phi_c|^2} \quad (3.5)$$

where

the subscript t is used to indicate that this is the SNIR of a thinned adaptive array.

The case of interferences located at a large angular separation from the signal is considered first. In this case, $|\Phi_v|^2$ is small, allowing $1 - |\Phi_v|^2$ to be approximated by 1. Considering the case of a large interference (π_i large), (3.5) becomes

$$\begin{aligned} SNIR_t &\approx \frac{\pi_s NM}{M + N |\Phi_c|^2} \\ &= \frac{\pi_s}{\frac{1}{N} + \frac{1}{M} |\Phi_c|^2} \end{aligned} \quad (3.6)$$

From (3.6) it can be seen that increasing the number of adaptive elements, M, up to the maximum, N, will provide the best results in terms of SNIR. However, note that if $|\Phi_c|^2$ is very small, as would be expected for interferences located at some distance from the main lobe, then (3.6) is dominated by N, the number of conventional elements. This is the fundamental result which allows the thinned adaptive array to achieve very nearly the same performance as a fully adaptive array for large interferences located in the array sidelobes.

The situation in which the interference is located close to the look direction, within the main lobe of the conventional array beam, is somewhat different. Again considering the case of a large interference, and noting that for interferences close to the look direction, $|\Phi_c|^2$ is close to 1, (3.5) may be approximated by

$$\begin{aligned} SNIR_t &\approx \frac{\pi_s MN(1-|\Phi_v|^2)}{M(1-|\Phi_v|^2) + N} \\ &= \frac{\pi_s}{\frac{1}{M(1-|\Phi_v|^2)} + \frac{1}{N}} \end{aligned} \quad (3.7)$$

A further approximation may be employed. Noting that $1-|\Phi_v|^2$ is a very small quantity, the SNIR may be approximated by

$$SNIR_t \approx \pi_s M(1-|\Phi_v|^2) \quad (3.8)$$

From (3.8) it is apparent that the critical factor for determining SNIR for the main lobe interference case is the factor $1-|\Phi_v|^2$. If $|\Phi_v|^2$ falls off rapidly as the angle α increases, the SNIR in (3.8) increases rapidly. Hence, the ideal $|\Phi_v|^2$ will exhibit a very narrow main lobe.

The approximations developed for $|\Phi_u|^2$ and $|\Phi_m|^2$, (2.16) and (2.18) respectively, can be used to compare the relative performance of thinned adaptive arrays with adaptive elements spaced uniformly and with minimum redundancy. Equation (2.16) must be modified, replacing the interelement spacing d with the spacing between adaptive elements, D , where $D \approx \frac{N}{M}d$, and using M , the number

of adaptive elements, in place of N . This modification to (2.16) yields

$$|\Phi_{ut}|^2 \approx 1 - \frac{1}{12}(kd \sin(\alpha))^2 \frac{N^2}{M^2}(M^2-1) \quad (3.9)$$

Substituting the approximations of (3.9) and (2.18) into (3.8) provides an approximation of the SNIR for main lobe interferences impinging upon thinned adaptive arrays with uniformly spaced ($SNIR_{ut}$) and minimally redundant ($SNIR_{mt}$) adaptive elements respectively;

$$SNIR_{ut} \approx \pi_s \frac{N^2}{12M}(M^2-1)(kd \sin(\alpha))^2 \quad (3.10)$$

$$SNIR_{mt} \approx \pi_s \frac{2N^2-3N+1}{6M} N (kd \sin(\alpha))^2 \quad (3.11)$$

The SNIR approximation of a fully adaptive uniform array is obtained by setting $M=N$ in (3.10) giving

$$SNIR_u \approx \pi_s \frac{N(N^2-1)}{12}(kd \sin(\alpha))^2 \quad (3.12)$$

In order to compare the relative SNIR performances of these arrays, the SNIR of the fully adaptive array will be normalized to 1, and the others will be computed with respect to this. Thus the relative SNIR, $SNIR_{ut}^r$, of the uniformly spaced thinned adaptive array is

$$SNIR_{ut}^r = \frac{NM(M^2-1)}{M^2(N^2-1)} \quad (3.13)$$

which for large N may be approximated by

$$SNIR_{ut}^r \approx \frac{M^2-1}{MN} \quad (3.14)$$

The relative SNIR of the thinned adaptive array with adaptive elements spaced for minimum redundancy is

$$SNIR_{mt}^r = \frac{2(2N-1)}{M(N+1)} \quad (3.15)$$

which for large N may be approximated by

$$SNIR_{mt}^r \approx \frac{4}{M} \quad (3.16)$$

Equation (2.23) relates N and M in an MRA under the assumption that there are no redundant spacings. Using this as an approximation, substituting (2.23) into (3.14) gives an estimate of the performance of a thinned adaptive suboptimal array with equi-spaced adaptive elements, when the same number of adaptive elements as would be found in a thinned array with adaptive elements spaced for minimum redundancy are employed.

$$SNIR_{ut}^r \approx \frac{M^2-1}{\left(\frac{M^2}{2} - \frac{M}{2} + 1\right)M} \quad (3.17)$$

which for $M \gg 1$ is well approximated by

$$SNIR_{ut}^r \approx \frac{2}{M} \quad (3.18)$$

A comparison of (3.18) and (3.16) reveals that a thinned array with adaptive elements spaced for minimum redundancy attains a SNIR performance with main lobe interferences which is approximately twice that attained by a thinned array using the number of equi-spaced adaptive elements. Table 3.1 is a comparison of predicted relative SNIR's for the main lobe interference situation, calculated using (3.13) and (3.15). The array lengths were chosen to correspond to the length of MRA's of order 7 through 10, and the number of adaptive elements employed in each was the same as the number of sensors in a MRA of the same length.

Table 3.1. SNIR of thinned adaptive arrays relative to the fully adaptive array of the same length; tabulated for interference close to the look direction.

Conventional Subarray Length	Number of Adaptive Elements	SNIR Relative to Fully Adaptive	
		Adaptive Element Geometry	
		Uniform	Minimum Redundancy
N	M	$\frac{N(M^2-1)}{M(N^2-1)}$	$\frac{2(2N-1)}{M(N+1)}$
18	7	0.382	0.526
24	8	0.329	0.470
30	9	0.297	0.423
37	10	0.268	0.384

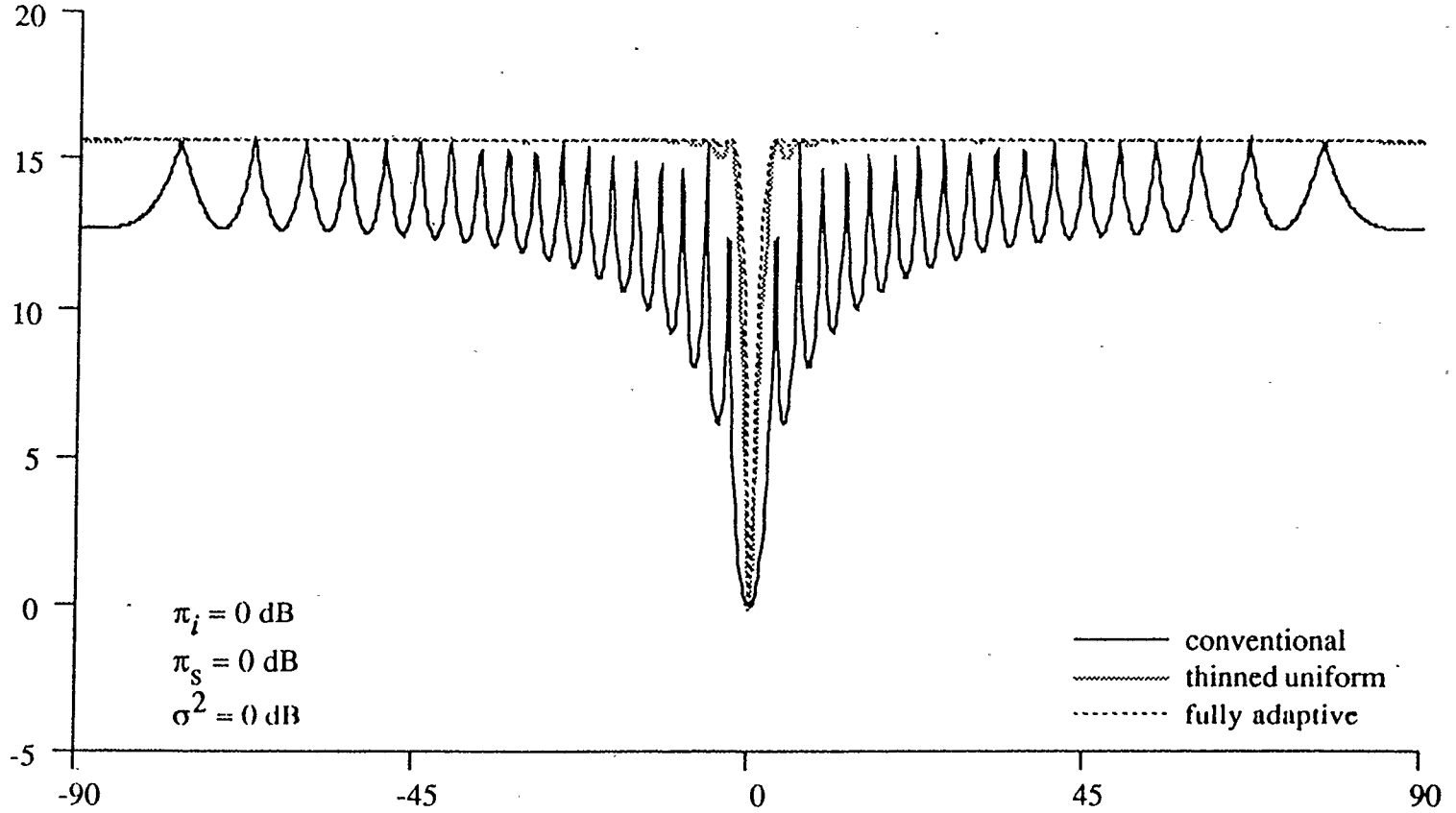
To illustrate the relationships for the SNIR's of each of the arrays, a specific example is now considered. Comparisons are undertaken using the SNIR

relationships given by (2.39) for the fully adaptive array, and (3.5) for the thinned adaptive arrays. A 37 element uniform line array is employed. The thinned adaptive arrays each contained 10 adaptive elements, one array with adaptive elements spaced uniformly throughout the length of the array, the other with adaptive elements spaced for minimum redundancy. For convenience, the look direction is once again chosen as broadside, or zero degrees, again, without loss of generality, and interference angle of arrivals are given with respect to this.

Figure 3.2 relates the SNIR performance calculated for the nonadaptive conventionally weighted array, the fully adaptive array and the thinned adaptive array with equi-spaced adaptive elements. It can be seen from the figure, that the thinned adaptive array with equi-spaced adaptive elements should achieve performance comparable to that of the fully adaptive array for interferences located in the sidelobes.

Figure 3.3 is a comparison of the SNIR performance expected of both forms of thinned adaptive arrays. The performance achieved when the interference is located at a large angular distance from the desired signal, in the sidelobes of the conventional array pattern, is relatively independent of the geometry employed in the adaptive element spacing. However, close observation reveals that the performance of the array using adaptive elements spaced for minimum redundancy is superior for main lobe interferences. This is more apparent in figure 3.4, which is an expanded view of the SNIR curves for interferences located near to the

SNIR (dB)



Interference angle of arrival (degrees)

Figure 3.2 - Output SNIR comparison of a conventionally weighted, a fully adaptive and a thinned uniform adaptive array with 10 adaptive elements, all based on a 37 element array.

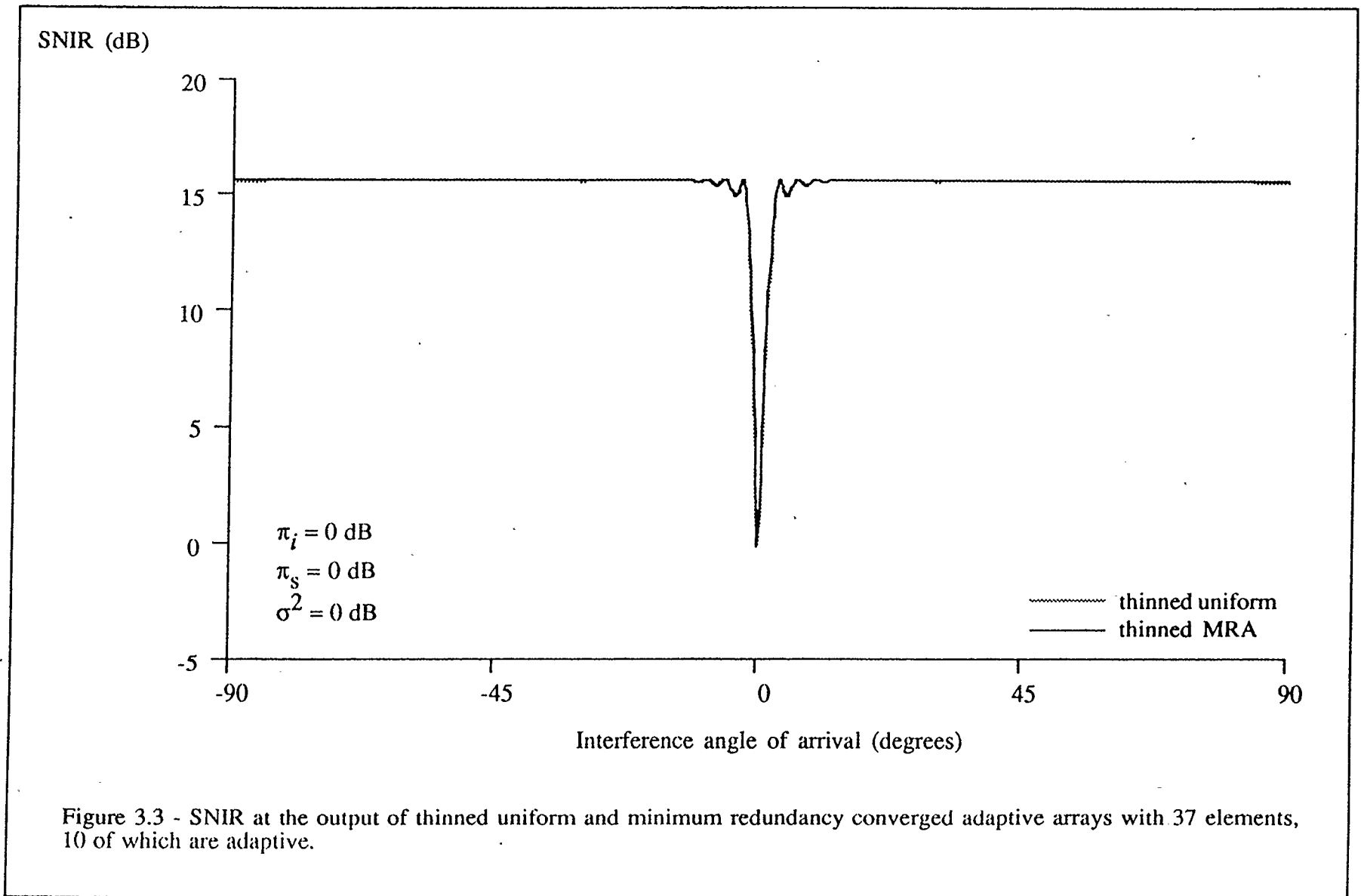
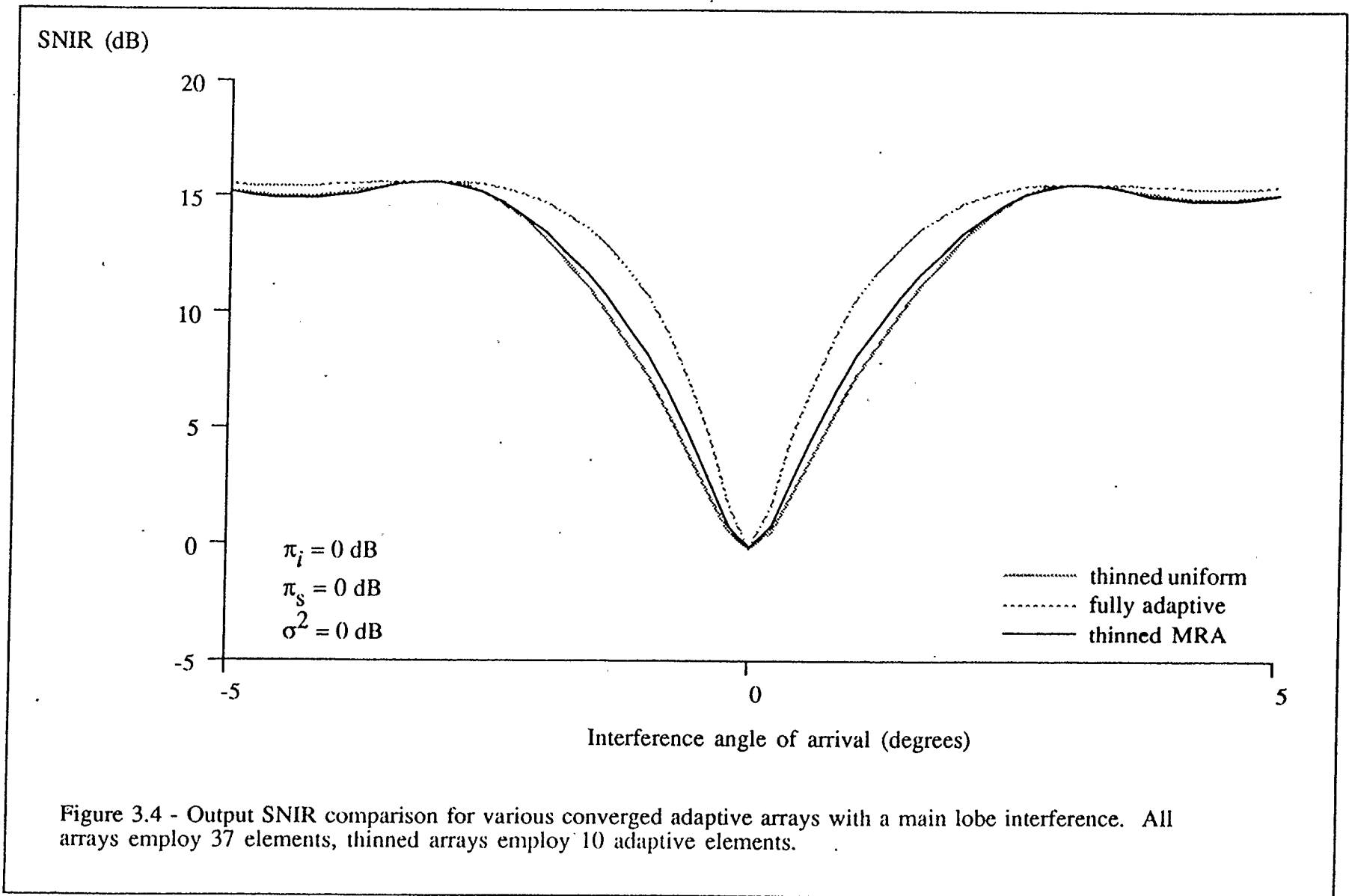


Figure 3.3 - SNIR at the output of thinned uniform and minimum redundancy converged adaptive arrays with 37 elements, 10 of which are adaptive.



desired signal. From figure 3.4, it is clear that the SNIR attained by the thinned adaptive array with adaptive elements spaced for minimum redundancy is superior to that attained by the thinned adaptive array with uniformly spaced adaptive elements. While the difference in the performance of the two systems may not appear to be that significant, the increased SNIR achieved by the thinned adaptive array with adaptive elements spaced for minimum spatial redundancy does not require any increase in the complexity of the system.

It is also seen that the performance attained by both thinned adaptive arrays is significantly inferior to that achieved by the fully adaptive array. Note, however, that the enhanced performance is attained at the expense of employing almost four times as many adaptive elements as are employed in either of the thinned adaptive arrays. It should also be mentioned that the SNIR figures are based on the optimal solutions. If the LMS algorithm is used to determine the weight vectors for both a fully adaptive and a thinned adaptive array, because of the relationship between μ and the number of weight vectors employed, it would be expected that employing 4 times as many weights would result in a convergence time which is approximately 4 times as long or a misadjustment after convergence which is approximately 4 times as large, or some combination of these two factors.

3.3. Simulation Results

A simulation study was undertaken using the example considered in the previous section. That is, suboptimal arrays based on a 37 element line array, with 2 thinned array configurations, one with adaptive elements spaced uniformly throughout the array, the other employing adaptive elements in a minimum redundancy configuration, were simulated. Figure 3.5 shows the simulation model which was employed. Uncorrelated Gaussian noise was added to each of the elements as shown. In the simulations which follow, the noise power, σ^2 , was set to 0 dB. The adaptation was based on the Frost algorithm given in chapter 2, with an LMS adaptation factor, μ of 0.0005. The simulation was permitted to run for 10,000 iterations, allowing the adaptive coefficients to converge, and the resulting converged array patterns for specific interference cases are presented. Due to the constraint employed, the gain in the look direction is always 1 (0 dB) and all null attenuations are given with respect to this.

Figure 3.6 shows the array pattern for the case when only uncorrelated noise, with no interfering spatially discrete signal, is present. Only one pattern is shown, but this represents the converged array pattern of both the uniformly spaced thinned adaptive array and the thinned adaptive array with elements spaced for minimum redundancy. The adaptive weights of both systems have all relaxed, such that the gains of every element are now equal, with the result that the patterns

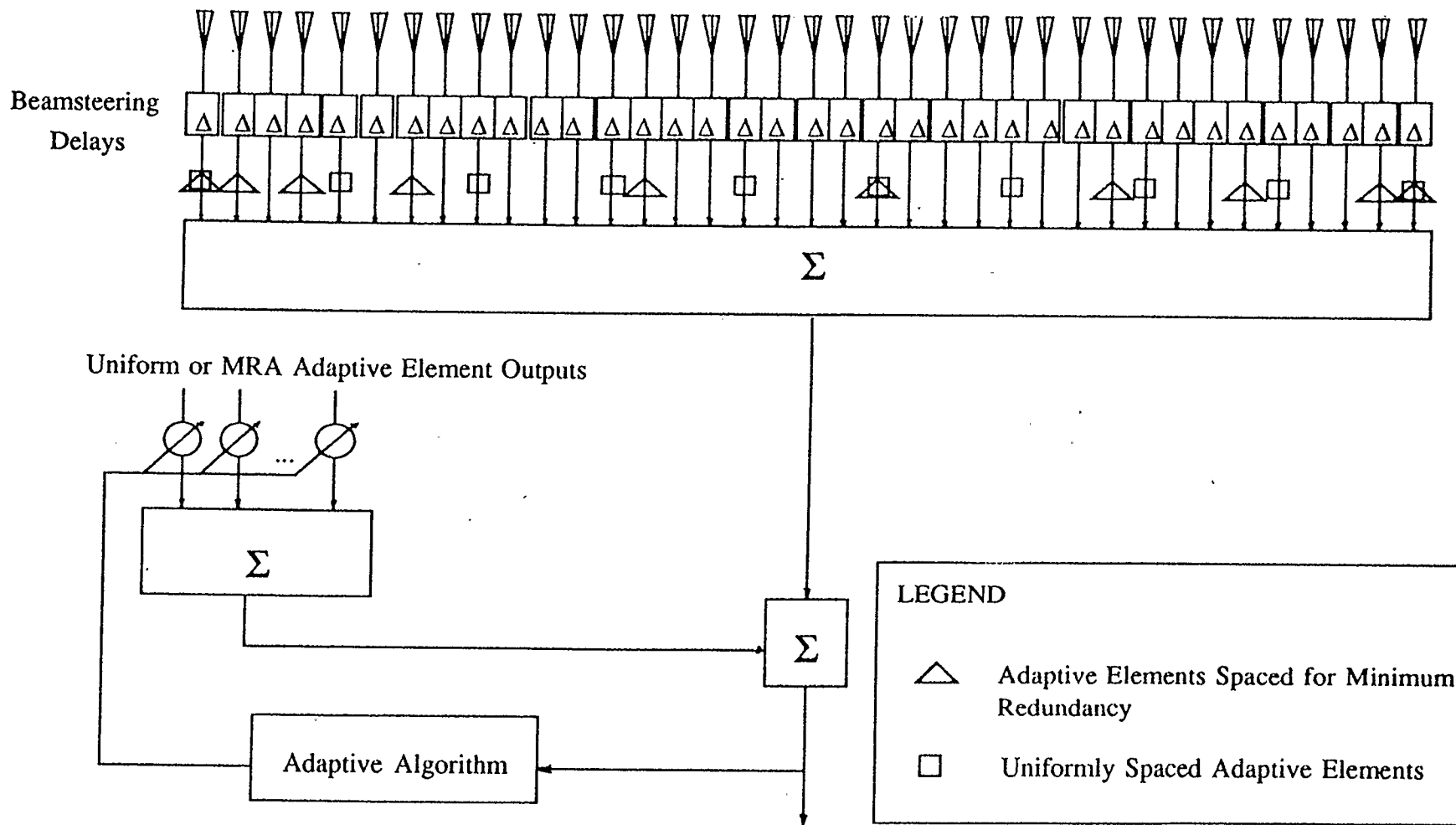


Figure 3.5 - 37 element uniform and MRA thinned adaptive array structures with 10 adaptive elements each.

Array Gain (dB)

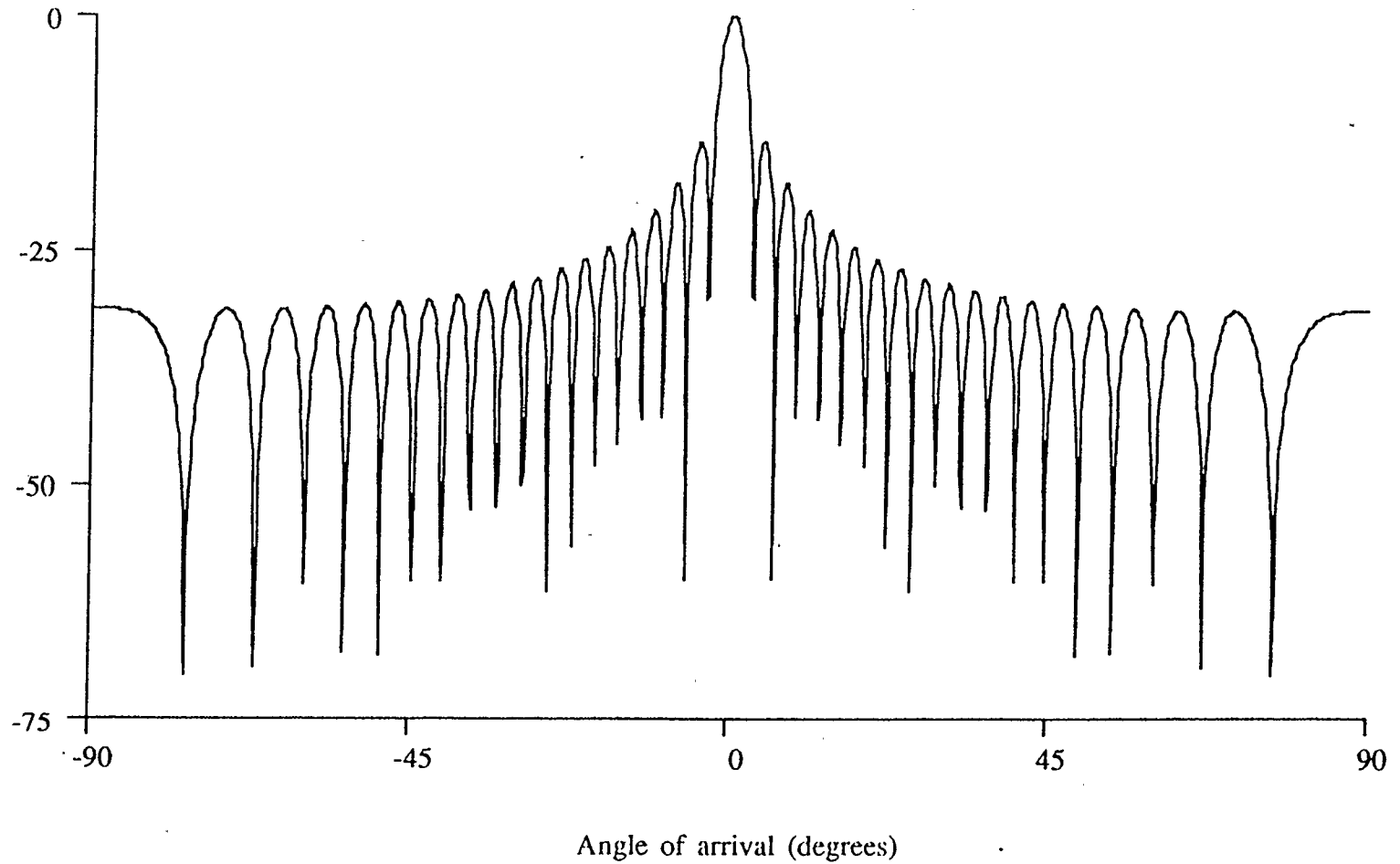


Figure 3.6 - Thinned adaptive array directivity pattern obtained with uncorrelated noise and no discrete spatial interference.

obtained for both thinned adaptive array configurations are equivalent to that of the 37 element conventional beamformer.

Figure 3.7 displays the array patterns obtained for a 20 dB interference located 45 degrees from the look direction, well into the sidelobes of the conventional array pattern. Both thinned adaptive arrays have produced good nulls in the interference direction, with 53.6 dB of attenuation for the thinned MRA configuration, and 53.1 dB of attenuation provided by the thinned array using uniformly spaced adaptive elements. This represents an additional 11.3 dB of attenuation for the MRA configuration, and 10.8 dB for the uniform thinned array, in addition to the 42.3 dB of attenuation provided by a uniformly weighted 37 element conventional array. Hence, both thinned adaptive arrays have succeeded in essentially eliminating the strong 20 dB interference signal in the sidelobes. The uncorrelated 0 dB noise input is attenuated by 15.7 dB by both thinned adaptive array configurations. Thus, in this case, both arrays provide comparable performance, reducing the total Noise plus Interference Power (NIP) to -15.7 dB. It should be noted that this agrees with the results expected from the calculations of the previous section, confirming the conclusion that the thinned adaptive arrays provide performance comparable to that attainable with a fully adaptive array for sidelobe interferences.

Figure 3.8 is the array patterns obtained with a 20 dB interference located only 1 degree from the look direction. This is well within the main lobe of the

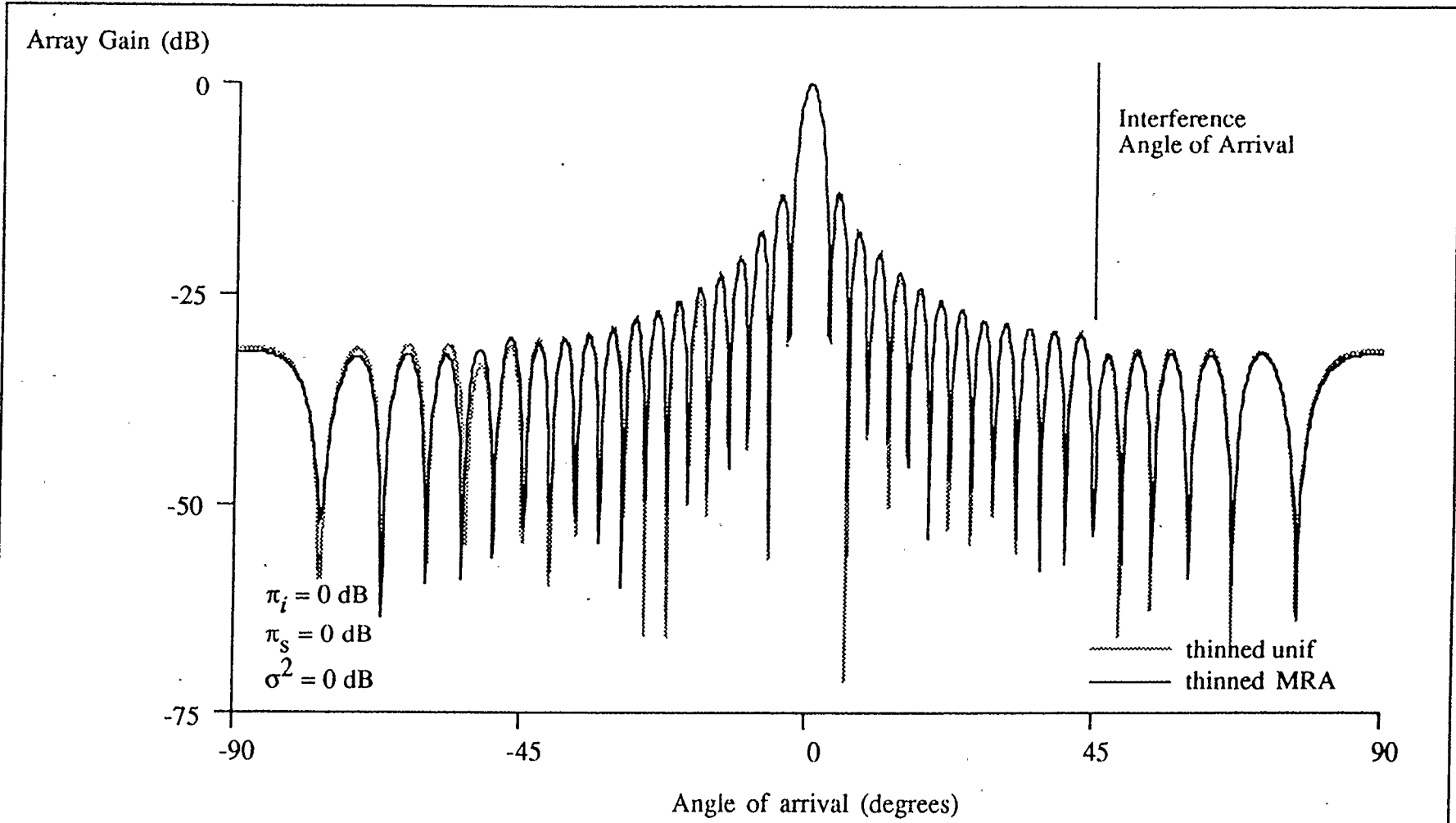


Figure 3.7 - Converged thinned adaptive array directivity patterns with sidelobe interference.

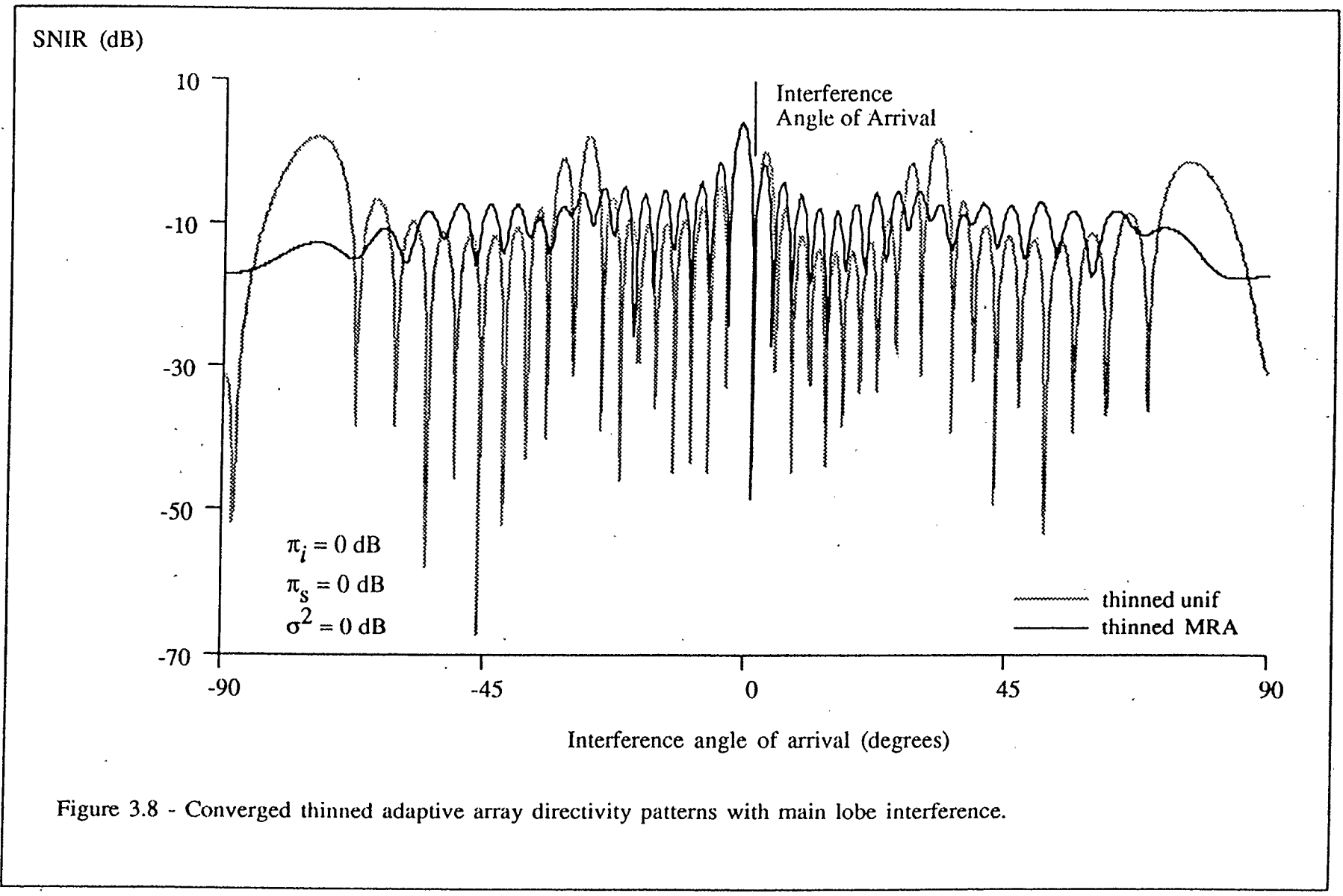


Figure 3.8 - Converged thinned adaptive array directivity patterns with main lobe interference.

conventional array pattern. After convergence, it is seen that both thinned adaptive arrays have formed good nulls in the direction of the interfering signal, 48.7 dB for the MRA configuration and 47.4 dB for the uniform. The attenuation of the uncorrelated noise is much lower in this case; 7.47 dB for the thinned adaptive array with adaptive elements spaced for minimum redundancy, and 6.35 dB for the thinned adaptive array with uniformly spaced adaptive elements. The total NIP is -7.43 dB for the MRA based thinned adaptive array and -6.32 dB for the uniform thinned adaptive array. This compares well with predictions made using (3.5), which show that the thinned adaptive array with adaptive elements spaced for minimum redundancy should reduce the NIP to -7.44 dB, while the thinned adaptive array with uniformly spaced adaptive elements is expected to achieve a NIP of -6.32 dB. Thus, in this case, the overall NIP is reduced by some 1.11 dB by using adaptive elements spaced for minimum redundancy.

3.4. Conclusion

One form of suboptimal array, the thinned adaptive array, was introduced. The common method of choosing the positioning of the adaptive elements in such an array, spacing them uniformly throughout the length of the array, was indicated. It was seen that placing the adaptive elements such that the redundant spacial correlations are minimized by using a MRA geometry for the adaptive elements,

increased the SNIR achieved by the converged array when rejecting interferences located close to the look direction. The increase in SNIR for the main lobe interference case is achieved without a significant increase in SNIR for the side lobe interference case. Further, there is no difference in the complexity of the thinned adaptive array systems.

Since the number of adaptive elements in the thinned adaptive array corresponds directly to the order of the MRA used to provide the spacing of the adaptive elements, the length of the filled array is explicitly specified once the number of adaptive elements is chosen. This is a severe handicap in applying this technique to real world situations. For instance, given an array of length N , more adaptive elements may be required than are found in the MRA of length N . The question then becomes how to allocate the additional adaptive elements. Moffet [15] has addressed a similar problem, that of producing regular array structures which offer reduced redundancy in spatial correlations. Employing such array structures for choosing the adaptive elements in a thinned adaptive array would serve to make the technique more general.

CHAPTER 4
AN ADAPTIVE MINIMUM REDUNDANCY ARRAY
FOR DIGITAL COMMUNICATIONS

4.1. Introduction

In this chapter, a slightly different application of beamforming is considered. Previously, all the cases considered contained the assumption that no prior knowledge of the desired signal other than its direction of arrival was available. Now, the case where the direction of arrival is unknown but the information content of the signal is known is considered. It is therefore necessary to postulate a training sequence, used to allow the weights of the adaptive beamformer to adjust to minimize the mean square error under these conditions. This may be seen as analogous to the case of an adaptive equalizer which relies on a training sequence to provide the initial convergence.

The chapter begins with a look at the complex envelope simulation employed. This includes both the channel simulation and the LMS adaptive combiner used in determining the optimum weight values.

Next, the case of uncorrelated interferences is considered. This situation may occur as a result of co-channel interference or as a result of an intentional attempt to disrupt the communication system in the form of jamming. A comparison of the effectiveness of both uniform array and MRA based adaptive systems under these conditions is then undertaken.

The multipath, or correlated signal, environment is then examined. A simple two ray model is used to allow the calculation of the probability of error under various conditions using both the uniform and MRA based systems. Simulations using the LMS adaptive combiner are undertaken to confirm the results of these calculations. An overall estimate of the total probability of error for each system is also given.

4.2. Complex Envelope Simulation

It is well known that a narrowband bandpass system may be modelled mathematically as a lowpass or baseband system by employing complex demodulation to determine the baseband equivalent of the bandpass system [26]. This property will be used to simplify the analysis of the situation confronting us. Figure 4.1 (a) shows a simplified narrowband communications system, with the channel transfer function indicated. Figure 4.1 (b) shows the baseband equivalent system. The equations which follow indicate the mathematical relationship

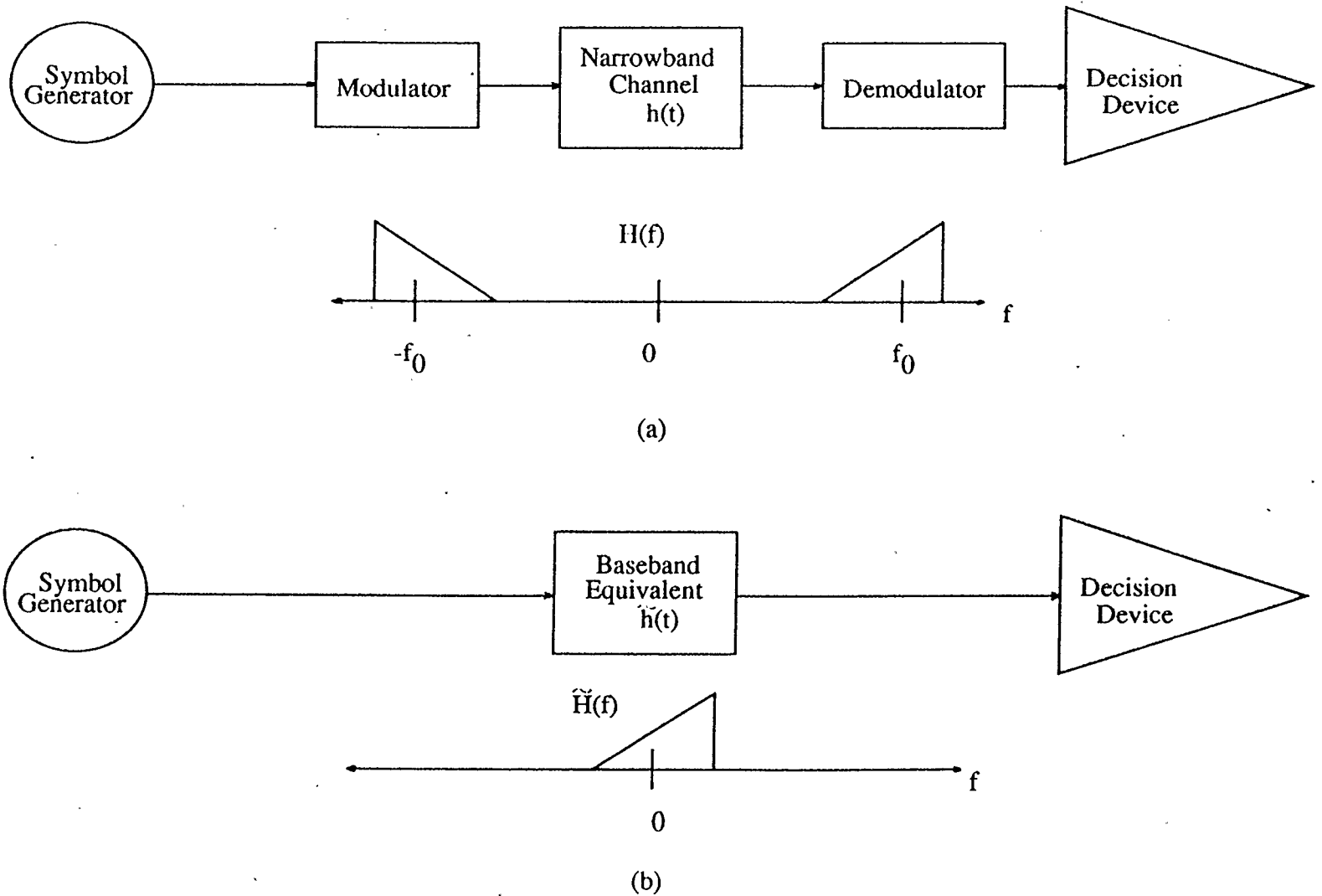


Figure 4.1 - Complex envelope equivalent of a narrowband channel; (a) Narrowband channel; (b) Baseband equivalent channel.

between the narrowband impulse response and its baseband equivalent.

$$\tilde{h}(t) = \dot{h}(t)e^{-j2\pi f_0 t} \quad (4.1)$$

where

$\tilde{h}(t)$ is the baseband equivalent of $h(t)$,

$\dot{h}(t)$ is the analytic signal of $h(t)$,

and f_0 is the center frequency of the narrowband function $H(f)$.

The analytic signal $\dot{h}(t)$ is given by

$$\dot{h}(t) \triangleq h(t) + j\hat{h}(t) \quad (4.2)$$

where

$\hat{h}(t)$ is the Hilbert transform of $h(t)$.

Examination of these equations reveals that, in general, the baseband equivalent representation of the impulse response of a narrowband system will be a complex function. In the simulations which follow, however, in order to reduce the complexity and computational burden imposed by the required convolutions, the complex envelope of the channel impulse response contains only real components. This is equivalent to specifying that $\tilde{H}(f)$, the Fourier transform of $\tilde{h}(t)$, is a Hermite function, implying that $H(f)$ has a passband which is conjugate symmetric about the center frequency, f_0 . While this is clearly an artificial constraint, it does not affect the validity of the results for the more general case where the baseband channel impulse response is complex.

4.3. Uncorrelated Interference

Figure 4.2 indicates the geometry of the situation considered in this section. Two signals are shown impinging upon a receiving array. For convenience, but without loss of generality, in simulations the desired signal always arrives from broadside, that is, with an arrival angle of zero degrees. The second signal is an interfering signal, uncorrelated with the desired signal. The difference in arrival angle between the two signals is given as α .

Figure 4.3 is a block diagram representation of the system used to simulate the conditions of figure 4.2. There are two signal generators, a desired signal generator and an interference signal generator, each generating signals used to simulate Quadrature Phase Shift Keying (QPSK). These signal generators consist of two parts: a symbol source that generates a random sequence with independent real and imaginary components followed by a NRZ rectangular pulse generator. The QPSK signal used, $s(t)$, is written as

$$s(t) = \text{Re}[A \sum_n a_n p(t - nT) e^{j\omega_0 t}] \quad (4.3)$$

where

A is the magnitude of $s(t)$ implying that the energy per bit, $E_b = \frac{A^2 T}{2}$,

a_n is the n^{th} symbol in a sequence of uncorrelated symbols,

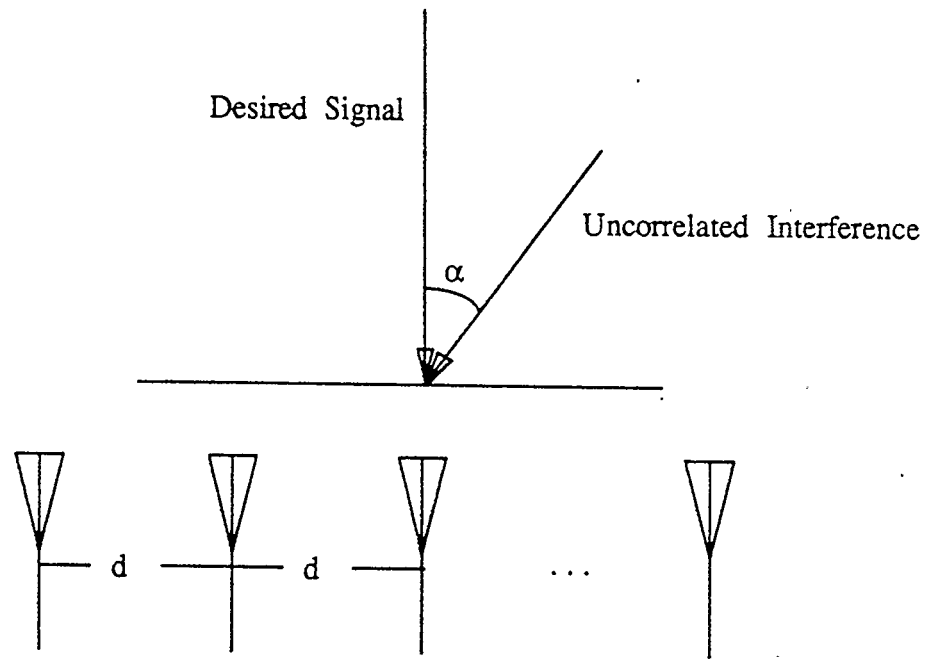


Figure 4.2 - Signal, interference and array geometry.

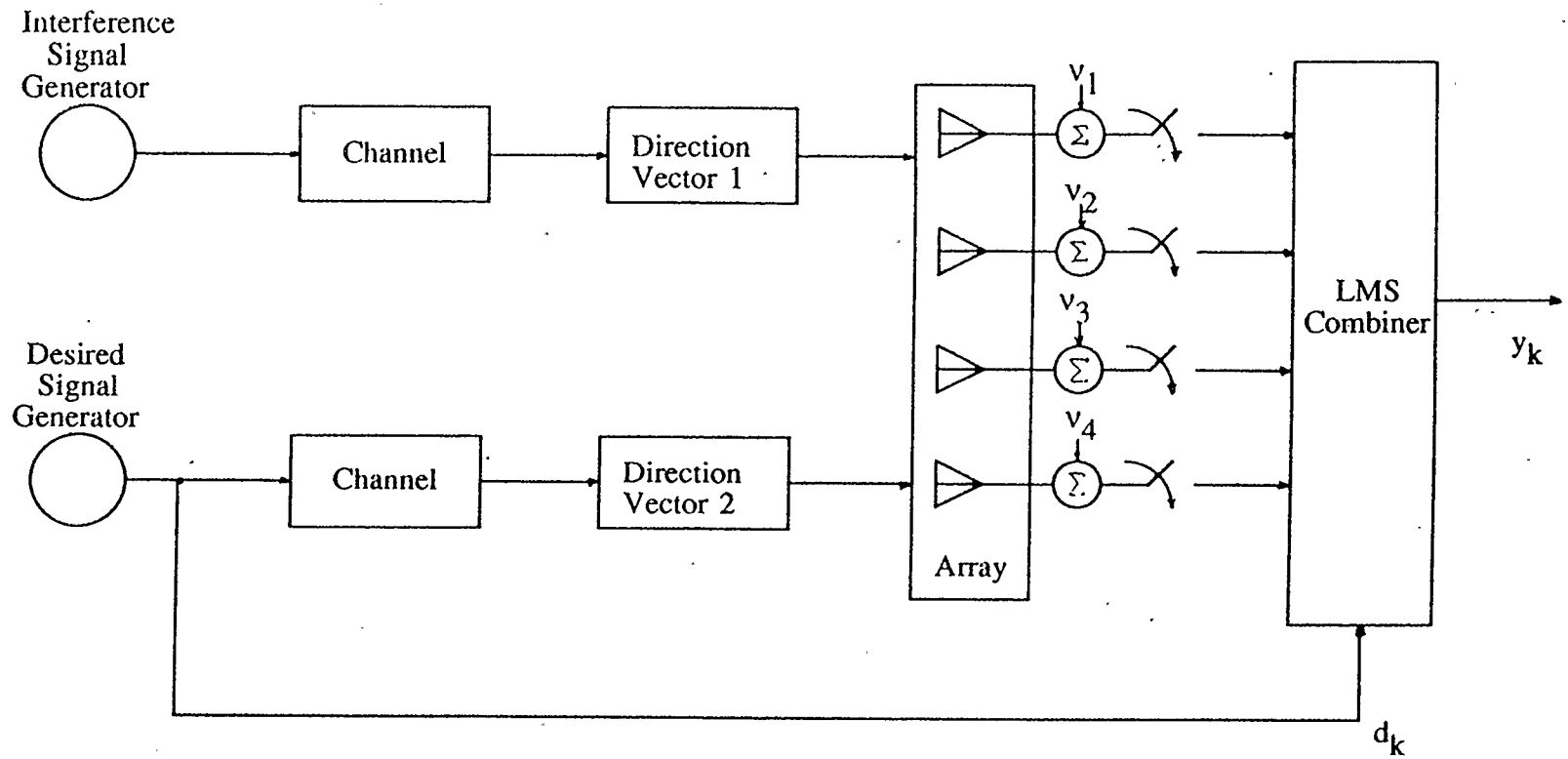


Figure 4.3 - Uncorrelated interference simulation.

$$a_n \in \left\{ \frac{1+j}{\sqrt{2}}, \frac{1-j}{\sqrt{2}}, \frac{-1+j}{\sqrt{2}}, \frac{-1-j}{\sqrt{2}} \right\},$$

$p(t - nT)$ is a rectangular pulse of unity amplitude,

and $e^{j\omega_0 t}$ is a carrier component, with ω_0 the center frequency.

The signals generated in the simulation are the baseband equivalent of $s(t)$ given by

$$\tilde{s}(t) = A \sum_n a_n p(t - nT) \quad (4.4)$$

The generated signals are then convolved with a channel impulse response. In this case, the channel impulse response is a 256 point Hamming window function, providing a basic lowpass characteristic. While the magnitude response of each of the channels is equal, a time delay is introduced into the impulse response, allowing the convolved outputs to differ in phase. It should be noted that in general the channel impulse responses of the interference and desired signals normally differ. However, for simplicity, the same impulse response is employed for each channel. The output of each channel is then multiplied by a direction vector, one for each individual channel, which determines its relative phase at each element of the receiving array. Independent Gaussian noise is then added to the output of each element of the array.

Mathematically, $\bar{X}(t)$, the vector of outputs of the sensors of the array is expressed as:

$$\bar{X}(t) = \tilde{s}_1(t) * \tilde{h}_1(t)\bar{S}_1(\alpha_1) + \tilde{s}_2(t) * \tilde{h}_2(t)\bar{S}_2(\alpha_2) + \bar{N}(t) \quad (4.5)$$

where

$$\bar{X}(t) = [\tilde{x}_0(t) \tilde{x}_1(t) \cdots \tilde{x}_N(t)]^T,$$

$\tilde{x}_i(t)$ is the output of the i^{th} sensor,

$s_1(t)$ is the desired signal,

$s_2(t)$ is an uncorrelated interference,

$\tilde{h}_i(t)$ is the complex envelope representation of the i^{th} channel impulse response,

$\bar{N}(t) = [v_0(t) v_1(t) \cdots v_n(t)]^T$ is a vector of independent, zero mean, AWGN elements

and $\bar{S}_i(\alpha_i)$ is the space vector producing the required phase relationship.

The outputs of the receiving elements are then sampled and input to the LMS adaptive combiner, shown in figure 4.4, which is based upon the following update recursions from chapter 6 in [17]:

$$y_k = \bar{W}_k^H \bar{X}_k \quad (4.6)$$

$$\varepsilon_k = d_k - y_k \quad (4.7)$$

$$\bar{W}_{k+1} = \bar{W}_k + \mu \varepsilon_k^* \bar{X}_k \quad (4.8)$$

where

k is the time index,

μ is the LMS adaptation factor,

$\bar{W}_k = [w_0 \ w_1 \ \cdots \ w_N]_k^T$ is the weight vector at time k ,

$\bar{X}_k = [\tilde{x}_0 \ \tilde{x}_1 \ \cdots \ \tilde{x}_N]_k^T$ is the observation vector at time k ,

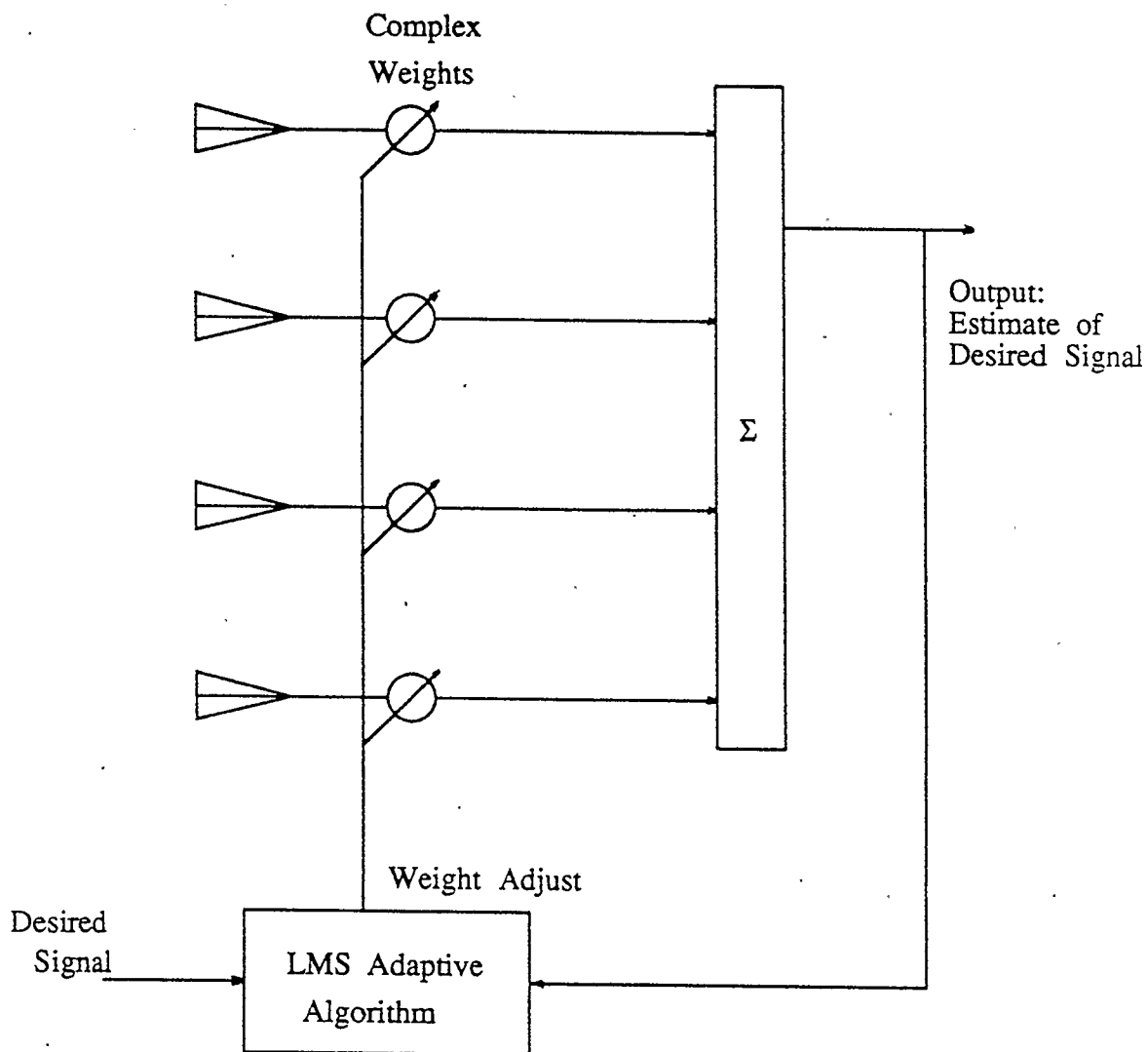


Figure 4.4 - Narrowband LMS adaptive combiner.

d_k is the desired signal at time k ,

y_k is the output of the combiner at time k ,

ε_k is the error at time k ,

$[\]^T$ indicates transposition,

$[\]^*$ indicates conjugation,

and $[\]^H$ indicates the Hermitian or conjugate transpose.

The outputs of the sensor elements form the observation vector, \bar{X}_k , input to the combiner. This vector is multiplied by the Hermitian of the weight vector, \bar{W}_k , to form an estimate of the desired signal, y_k , which is then subtracted from the known value of the desired signal, d_k , to produce the error term. This error term is then used (in (4.6)) to determine the magnitude of the correction applied to the weight vector.

The combiner can be used to receive broadband signals by employing a tapped delay line to maintain a memory of the past observation vectors. If no memory is employed, the system is narrowband as in the case shown. Another important feature is the lack of a constraint on the look direction, found in most beamformers.

The output of the combiner, y_k , is then input to a decision device, which determines which symbol was transmitted. Although it was not examined in this study, it seems probable that decision directed learning, using the output of the

decision device to produce the desired signal, would allow the adaptive combiner to depend upon a training sequence only for initial convergence. Following the initial convergence, obtained with the known desired signal provided by the training sequence, a sufficiently large proportion of the decisions will be correct, allowing the combiner to be switched to decision directed learning. Again, this was not examined in this study, but decision directed learning is employed in FIR based linear adaptive equalizers [27]. There appears to be no reason why the same technique could not be employed in this case.

4.4. Simulation: Uncorrelated Interference

A four element equi-spaced array and a four element MRA, each with $\frac{\lambda}{2}$ interelement spacing were employed in the following simulations. The combiner employed was narrowband, using one complex sample per element from the current symbol interval. In all cases, the LMS combiner employed an LMS adaptation factor, μ , of 0.0005 and the recursion was allowed 1000 iterations to complete its initial convergence. After the initial convergence, the outputs of the combiner were compared with the transmitted symbols and the probability of error under these conditions was determined. Additionally, the weights developed by the combiner could be used to indicate the directivity pattern of the system.

To establish a baseline for the system, a simple test case was employed. Additive White Gaussian Noise (AWGN) of 0 dB was added to each of the four receiving elements while a QPSK signal of 3 dB (corresponding to 0 dB per bit) was transmitted. Because the desired signal is co-phased, or multiplied by complex weights such that the desired signal component of each sensor output is added in phase by the combiner, the SNR is increased by a factor of 4, the number of elements in the array. Employing the relationship for the bit error probability for the QPSK signals of (4.3) with AWGN [28]:

$$P_b(e) = Q \left[\sqrt{\frac{A^2}{\sigma_n^2}} \right] \quad (4.9)$$

where

$$\text{the } Q \text{ function is given by: } Q(x) \triangleq \frac{1}{\sqrt{2\pi}} \int_x^{\infty} e^{-\frac{\lambda^2}{2}} d\lambda$$

and σ_n is the standard deviation of the AWGN,

it is found that the expected bit error probability using the ideal weight vectors for both MRA and equi-spaced systems under these conditions is 0.023. From simulation, the MRA based system achieved a bit error probability of 0.025 while the equi-spaced array system achieved a 0.023 bit error probability over an 18,000 bit (9,000 complex symbol) run. Figure 4.5 shows the directivity pattern of the combiners under these conditions.

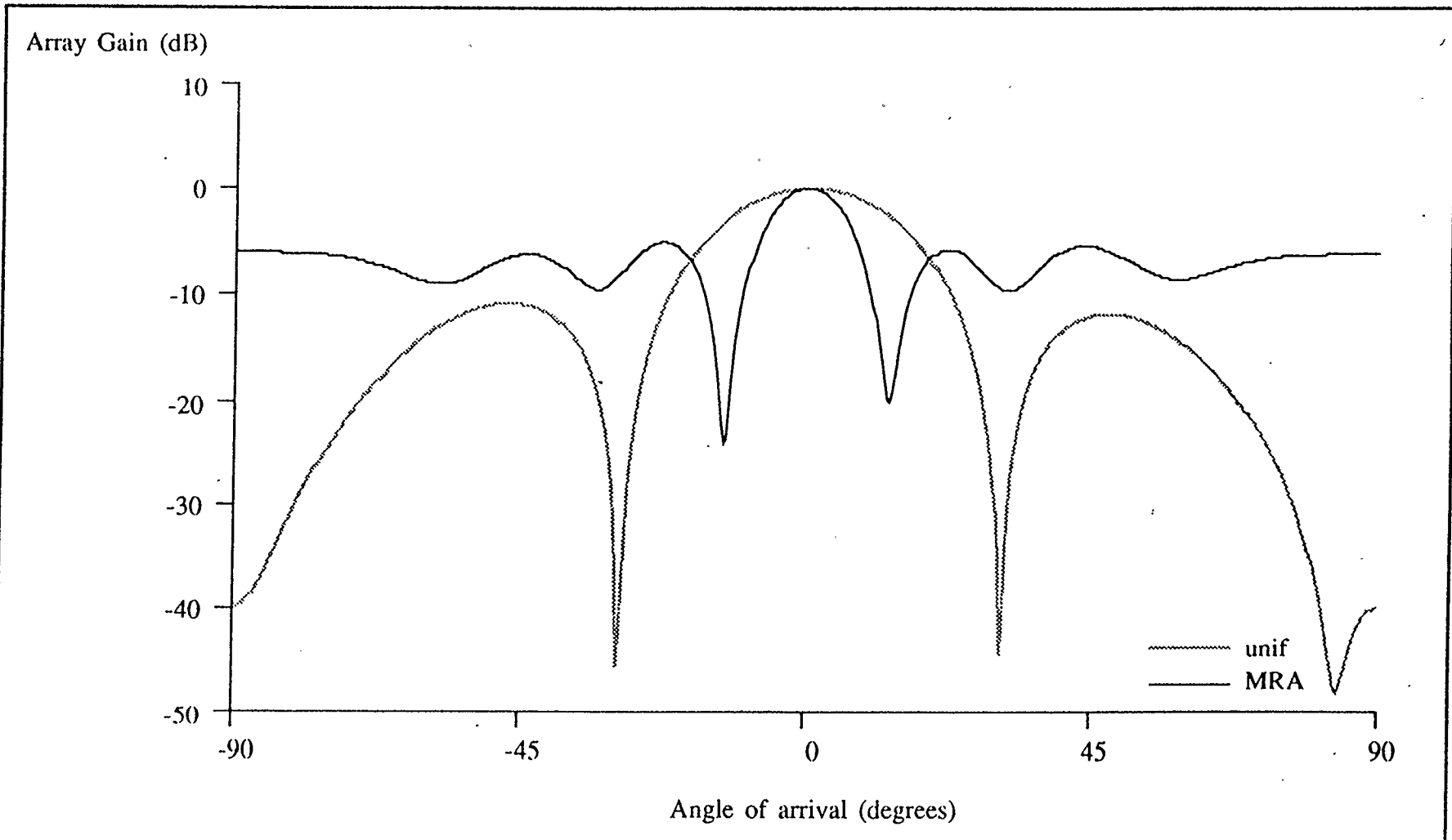


Figure 4.5 - Directivity patterns for 4 element uniform and minimum redundancy adaptive combiners with AWGN.

To further test the working of the combiners, a 10 dB interfering signal, uncorrelated with the desired signal, was placed 10 degrees from the desired signal. The signal power was 3 dB, while the uncorrelated noise employed was -40 dB. Under these conditions, both combiners succeeded in nulling out the interference satisfactorily, completing 18,000 bit runs with no errors. Figure 4.6 shows the resulting directivity pattern. Notice the deep null at 10 degrees in each of the resulting directivity patterns.

Five more simulations were then carried out. Each involved 3 dB desired signals, 0 dB additive Gaussian noise and spatially coherent interferences of 10 dB magnitude. The interferences were placed successively at angles of 10, 12, 14, 16 and 22 degrees away from the desired signal. The 22 degree angle is significant as that represents the peak of the first sidelobe of the MRA pattern. Thus, the performance of the MRA based system with an interference at that angle should be as bad as for any angle outside of the main lobe. The results, based on data samples of 22,000 bits, are tabulated in table 4.1.

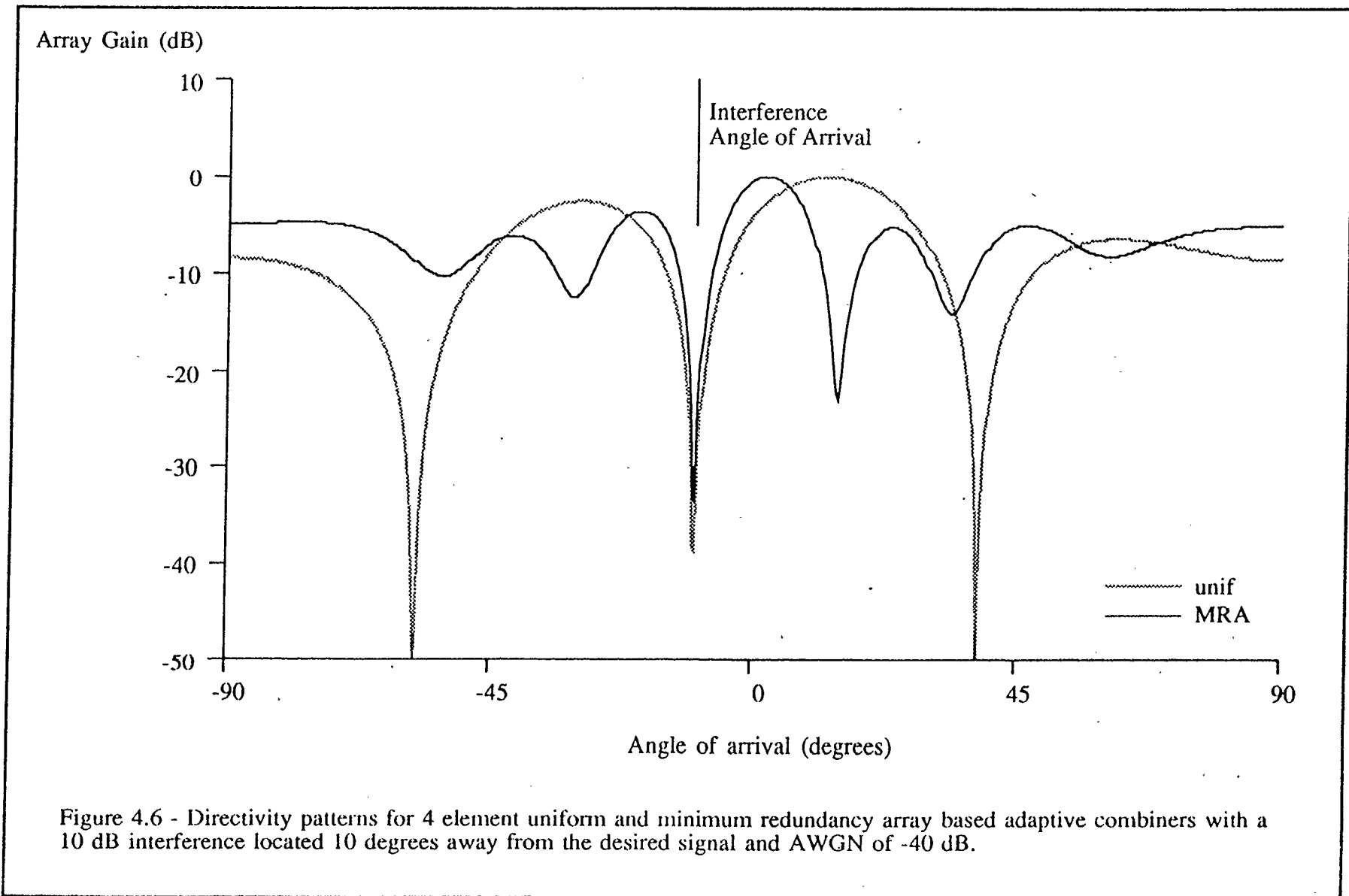


Figure 4.6 - Directivity patterns for 4 element uniform and minimum redundancy array based adaptive combiners with a 10 dB interference located 10 degrees away from the desired signal and AWGN of -40 dB.

Table 4.1. Probability of Error for Various Interference Conditions with Unity Noise Power.

Interference		$P_b(e)$	
Angle (degrees)	Power (dB)	MRA	Equi-Spaced
-	-	0.0248	0.0234
10	10	0.0309	0.1320
12	10	0.0263	0.0980
14	10	0.0265	0.0724
16	10	0.0322	0.0552
22	10	0.0499	0.0317

Figures 4.7 through 4.9 show the directivity patterns developed for the 10, 16 and 22 degree interference conditions.

With these results it is apparent that the MRA based system is better at rejecting uncorrelated interferences which are close in angular proximity to the desired signal, while the uniform geometry achieves superior performance for interferences located far from the desired signal.

4.5. Multipath

If the second signal shown in figure 4.10 is a time delayed version of the desired signal with variable amplitude, a multipath condition occurs. It is necessary to further examine the implications of this two ray multipath model. The examination begins by showing that it is possible to calculate the expected

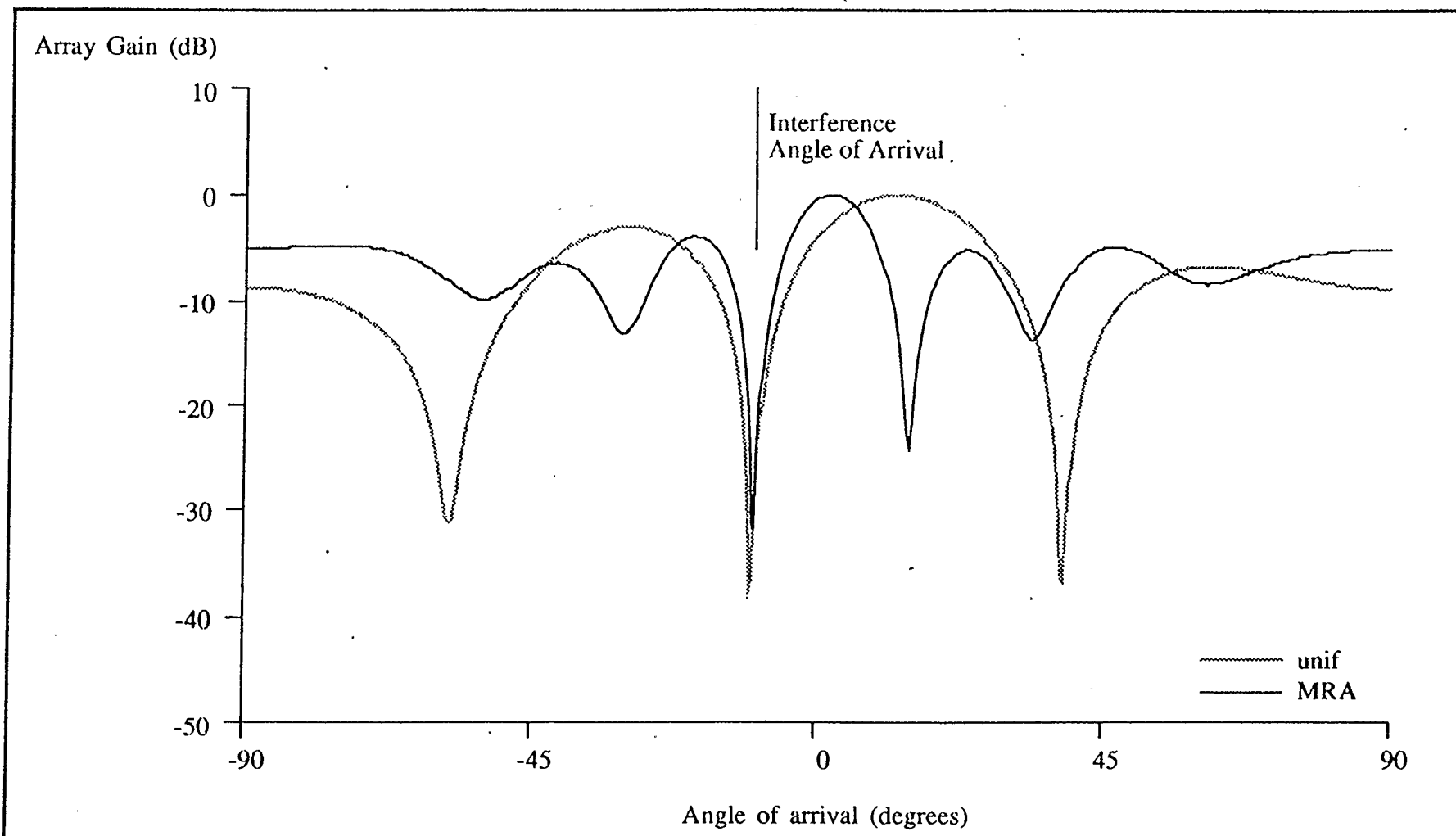


Figure 4.7 - Directivity patterns for 4 element uniform and minimum redundancy array based adaptive combiners with a 10 dB interference located 10 degrees from the desired signal and AWGN of 0 dB.

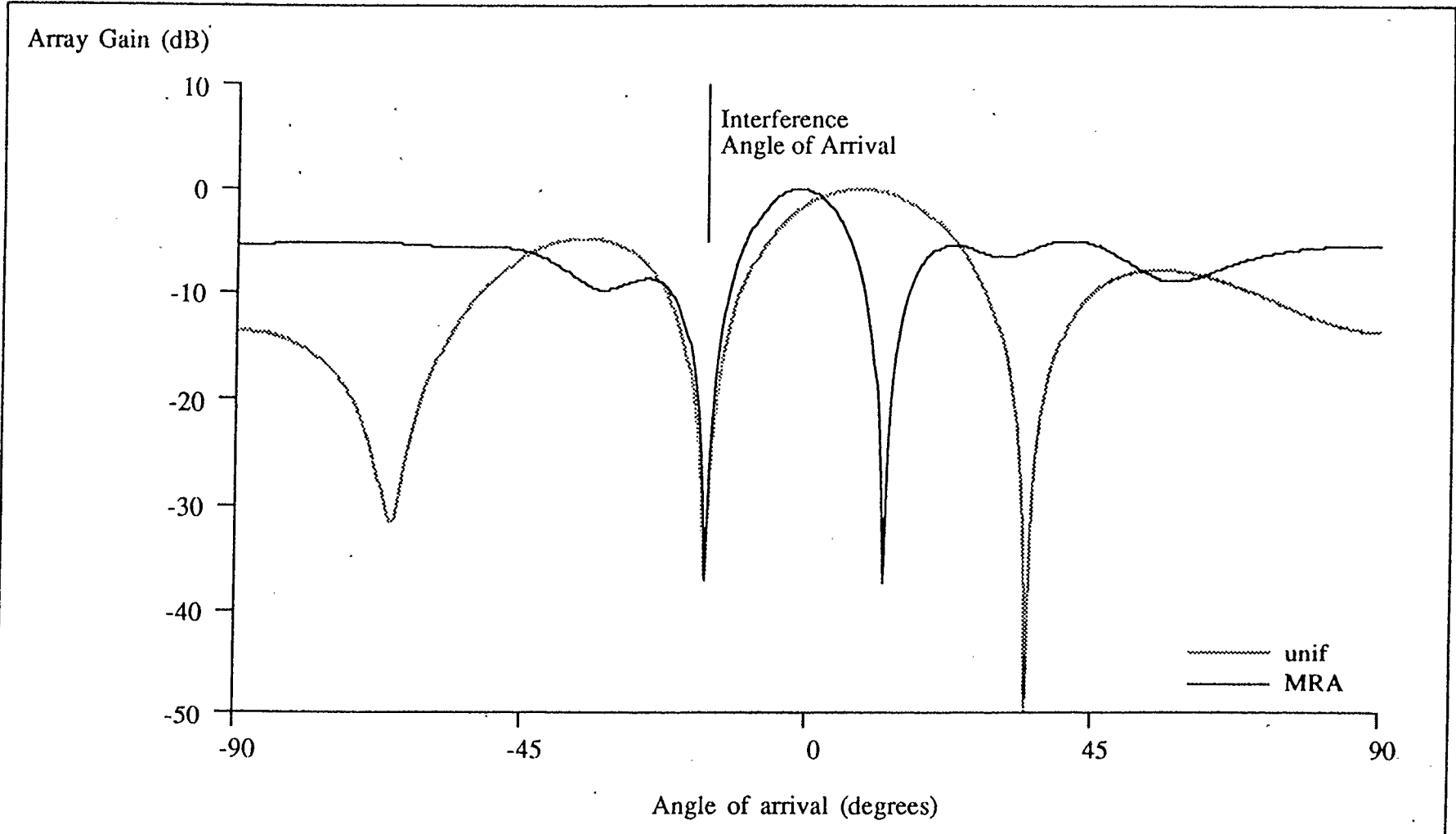


Figure 4.8 - Directivity patterns for 4 element uniform and minimum redundancy array based adaptive combiners with a 10 dB interference located 16 degrees from the desired signal and AWGN of 0 dB.

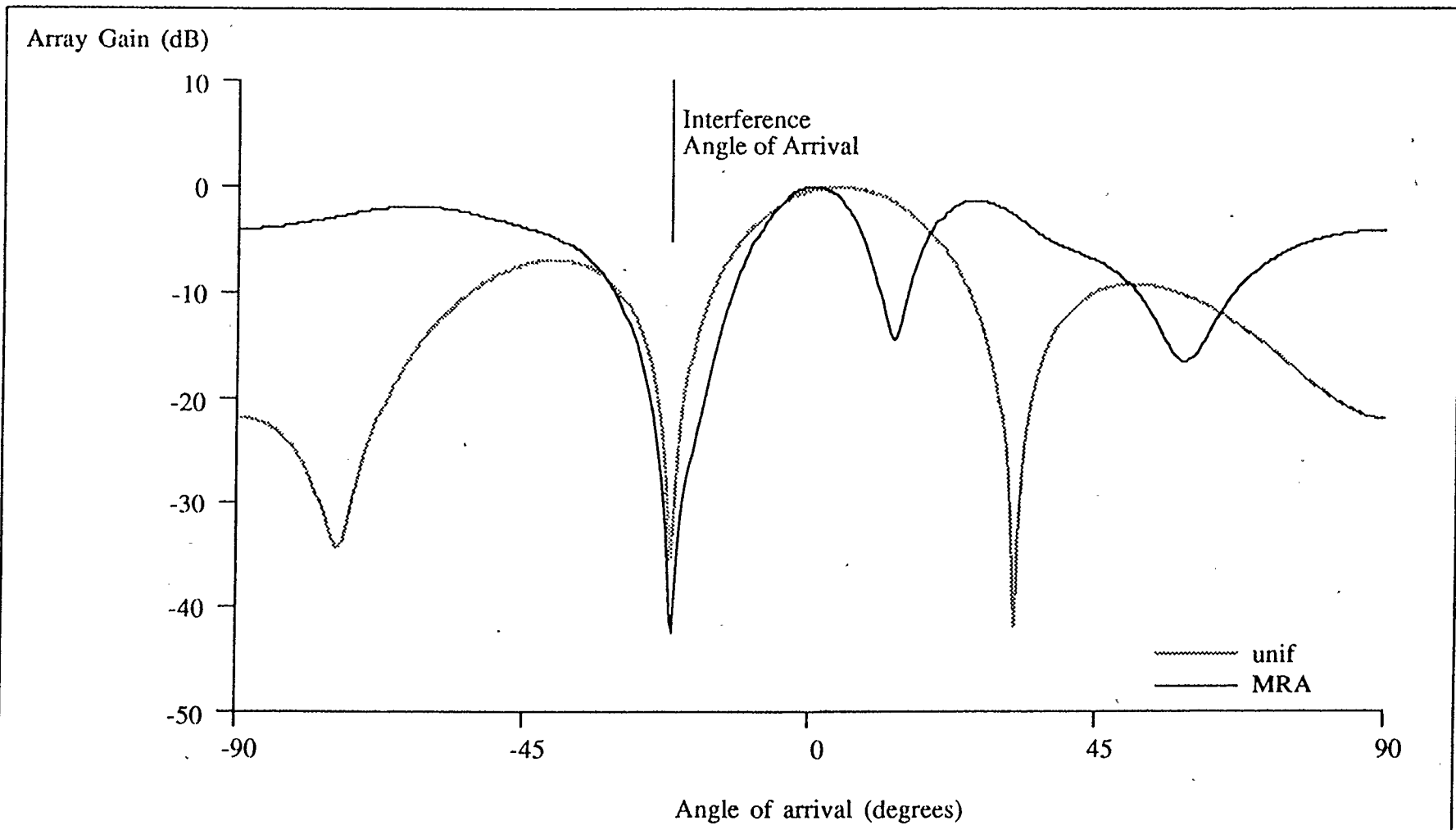


Figure 4.9 - Directivity patterns for 4 element uniform and minimum redundancy array based adaptive combiners with a 10 dB interference located 22 degrees away from the desired signal and AWGN of 0 dB.

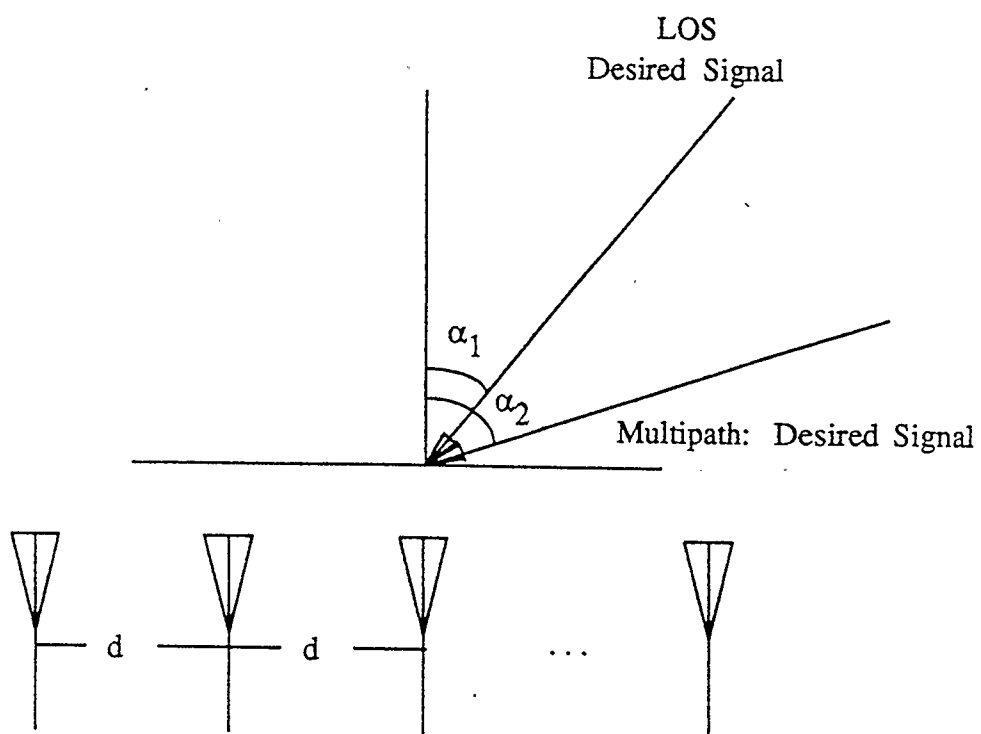


Figure 4.10 - Two ray multipath signal and array geometry.

error probabilities by determining the SNR at the output of an optimal combiner for various multipath conditions using this model.

Because these two rays in the multipath model actually represent continuous plane waves propagating in space, a field is set up which can be expressed as the sum of the two waves at any point in space. Since this thesis deals exclusively with line arrays, the field need only be expressed as a function of one dimension, x , where the x axis is the axis of the array. Using (4.3), the contribution of each signal, $r_i(x, t)$, at a point x along the axis of the array is given as:

$$r_i(x, t) = \text{Re}[A_i \sum_n a_n p(t - \tau_i - nT) e^{jkx \sin(\alpha_i)} e^{j\omega_0 t} e^{j\phi_i}] \quad i = 1, 2 \quad (4.10)$$

where

A_i is the amplitude of the i^{th} signal,

τ_i is the time delay component associated with the i^{th} signal,

$e^{jkx \sin(\alpha_i)}$ represents the spatial variation of the signal along the x axis,

α_i is the direction of arrival of the i^{th} signal,

and $\phi_i \triangleq -j\omega_0 \tau_i$.

Equation (4.10) can be simplified by virtue of the fact that it is not necessary to deal with the carrier component, as only the complex envelope, $\tilde{r}_i(x, t)$, of the signal, $r_i(x, t)$, is of interest, where

$$\tilde{r}_i(x, t) = A_i \sum_n a_n p(t - \tau_i - nT) e^{jkx \sin(\alpha_i)} e^{j\phi_i}$$

At any point along the x axis, we may find the envelope of the field, $\bar{z}(x,t)$ as the sum of the two ray components.

$$\bar{z}(x,t) = \bar{r}_1(x,t) + \bar{r}_2(x,t) \quad (4.11)$$

If $\tau_i \ll T$, the symbols, a_n , in each of the signals ($i = 1, 2$) will be the same over most of each symbol interval. This is illustrated in figure 4.11. This case, with the symbols in each ray correlated with those in the other ray is the multipath case which will be considered. (If the symbols in the two rays are uncorrelated the signal environment becomes identical to that considered previously, that of a desired signal with an uncorrelated interference.) The sampled complex envelope, $\bar{z}(x,n)$, under the two ray multipath model is obtained by sampling the envelope, $\bar{z}(x,t)$. Substituting (4.10) into (4.11) and taking the magnitude squared (with the assumption that the symbols in the two rays are the same) gives

$$|\bar{z}(x,n)|^2 = A_1^2 + A_2^2 + 2A_1A_2\cos(kdi(\sin(\alpha_1) - \sin(\alpha_2)) + \phi_1 - \phi_2) \quad (4.12)$$

From $\bar{z}(x,n)$ in (4.12), the SNR at the output of an optimal combiner can be determined (and hence, employing the assumption that the noise is AWGN, the error probability for a digital communications system can be derived). Let $y_u(n)$ denote the output of a uniform optimal combiner at time nT , while $y_m(n)$ denotes the output of a MRA based optimal combiner at time nT . Sampled outputs of the uniform and MRA based combiners respectively, at the n^{th} interval are:

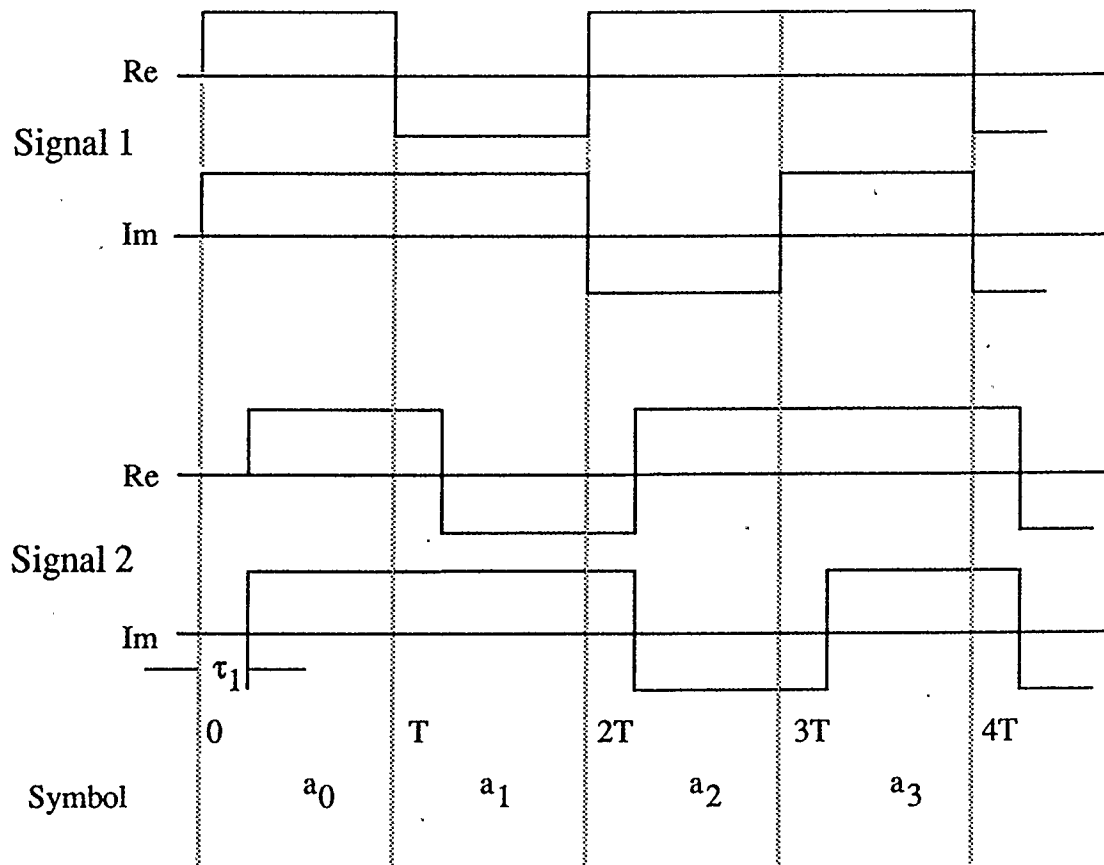


Figure 4.11 - QPSK signals in the two ray multipath environment.

$$y_u(n) = \sum_{i \in \mathfrak{v}} w_u(di, n)(\bar{z}(di, n) + v_i(n)) \quad (4.13)$$

$$y_m(n) = \sum_{i \in \kappa} w_{mi}(di, n)(\bar{z}(di, n) + v_i(n)) \quad (4.14)$$

where

d is the interelement distance,

$\mathfrak{v} = \{\text{alphabet of uniform array element positions}\}$,

$\kappa = \{\text{alphabet of MRA element positions}\}$,

$w_u(di, n)$ is the complex uniform array based optimal combiner weight

corresponding to the element at position di at time nT ,

$w_m(di, n)$ is the complex MRA based optimal combiner weight

corresponding to the element at position di at time nT ,

and $v_i(n)$ is the AWGN at the i^{th} element, at time nT ,

$v_i(n), v_j(n)$ are uncorrelated $i \neq j$.

The summations in (4.13) and (4.14) are over the sets \mathfrak{v} and κ corresponding to the array spacings of a uniform array and a MRA respectively. For example, for four element arrays;

$$\mathfrak{v} = \left\{ -\frac{3}{2}, -\frac{1}{2}, \frac{1}{2}, \frac{3}{2} \right\}$$

$$\kappa = \{-3, -2, 1, 3\}$$

The arrays represented by the sets \mathfrak{v} and κ are centered about $x = 0$, with each sensor of the array located a distance d times the corresponding element i in the set, from the origin.

The weights which maximize the SNR at the output of the combiner, (assuming that the noise power is the same at each element) are [14]

$$w(di, n) = \tilde{z}(di, n) \quad (4.15)$$

Hence, the SNR at the output of the uniform array based combiner is

$$\begin{aligned} SNR_u &= \frac{\left[\sum_{i \in \nu} |\tilde{z}(di, n)|^2 \right]^2}{\sigma_v^2 \left[\sum_{i \in \nu} |\tilde{z}(di, n)|^2 \right]} \\ &= \frac{\sum_{i \in \nu} |\tilde{z}(di, n)|^2}{\sigma_v^2} \end{aligned} \quad (4.16)$$

where

σ_v^2 is the variance of each of the noise components, $v_i(n)$.

Similarly, the SNR at the output of the MRA based combiner is

$$SNR_m = \frac{\sum_{i \in \kappa} |\tilde{z}(di, n)|^2}{\sigma_v^2} \quad (4.17)$$

Substituting (4.12) into (4.16) and (4.17) gives

$$SNR_u = \frac{M(A_1^2 + A_2^2) + \sum_{i \in \nu} 2A_1A_2 \cos(kdi(\sin(\alpha_1) - \sin(\alpha_2)) + \phi_1 - \phi_2)}{\sigma_v^2} \quad (4.18)$$

$$SNR_m = \frac{M(A_1^2 + A_2^2) + \sum_{i \in \kappa} 2A_1A_2\cos(kdi(\sin(\alpha_1) - \sin(\alpha_2)) + \phi_1 - \phi_2)}{\sigma_v^2} \quad (4.19)$$

The cosine summations in (4.18) and (4.19) may be simplified as follows: considering the summation over the elements in the uniform array found in (4.17) first, the spatially variable component ξ_u , is

$$\xi_u \triangleq \sum_{i \in \nu} 2A_1A_2\cos(kdi(\sin(\alpha_1) - \sin(\alpha_2)) + \psi) \quad (4.20)$$

where

$$\psi \triangleq \phi_1 - \phi_2$$

This may then be rewritten, using a trigonometric identity and taking terms not involved in the summation outside:

$$\xi_u = 2A_1A_2\cos(\psi) \sum_{i \in \nu} \cos(kdi(\sin(\alpha_1) - \sin(\alpha_2))) \quad (4.21)$$

Comparing (4.21) with (2.12) it is seen that (4.21) may be rewritten in terms of Φ_u so long as $\sin(\alpha)$, employed in Chapter 2, is replaced with $\sin(\alpha_1) - \sin(\alpha_2)$. Hence,

$$\xi_u = 2A_1A_2\cos(\psi)(M\Phi_u(\alpha_1, \alpha_2)) \quad (4.22)$$

and substituting into (4.18), the SNR at the output of the uniform array based optimal combiner is

$$SNR_u = \frac{M(A_1^2 + A_2^2) + 2A_1A_2\cos(\psi)(M\Phi_u(\alpha_1, \alpha_2))}{\sigma_v^2} \quad (4.23)$$

In a similar fashion, the relationship for SNR_m as a function of its array pattern can be derived, again after replacing $\sin(\alpha)$ employed in chapter 2 with $\sin(\alpha_1) - \sin(\alpha_2)$, can be derived. The resultant formulation is

$$SNR_m = \frac{M(A_1^2 + A_2^2) + 2A_1A_2\cos(\psi)(M\Phi_m(\alpha_1, \alpha_2))}{\sigma_v^2} \quad (4.24)$$

The probability of error per bit for QPSK signals was given by (4.7). The bit error probabilities for the uniform array and MRA based systems for the multipath case, under the assumption that ψ , α_1 , and α_2 are known, are

$$P_{bu}(e | \psi, \alpha_1, \alpha_2) = Q \left[\sqrt{SNR_u} \right] \quad (4.25)$$

$$P_{bm}(e | \psi, \alpha_1, \alpha_2) = Q \left[\sqrt{SNR_m} \right] \quad (4.26)$$

From an examination of (4.23) and (4.24) it is apparent that the SNR at the output of both the uniform and MRA based combiners in the two ray multipath environment is the sum of a fixed term, $M(A_1^2 + A_2^2)$, which represents the average power, and a term which varies over space, $2A_1A_2\cos(\psi)(M\Phi_m(\alpha_1, \alpha_2))$. It is the spatially varying component which is of greatest interest. Ideally, for a communications system, the spatially varying component should be minimized in order to minimize the overall probability of error. This is desirable because the

random phase introduced by the $\cos(\psi)$ function in (4.23) and (4.24) makes it impossible to determine beforehand whether the spatially varying term will result in increased SNR, from constructive interference, or decreased SNR, due to destructive interference.

The assertion that ψ is a random variable is based on the assumption that only a small relative change in the path lengths of the two rays is necessary to cause a large change in the phases of the signals. By increasing the length of the path followed by one of the rays by $\frac{\lambda}{2}$ (where λ is the wavelength of the carrier, and is generally small with respect to the transmission distance) the random phase term associated with that ray, ϕ_i , is increased by 180 degrees. Thus, if the distance from the transmitter to the receiver is a large number of wavelengths, as is necessary in any case for the plane wave approximation to hold true, the assumption that ϕ_i is random is valid. Given that ϕ_i is uniformly distributed in the interval from $-\pi$ to π and independent of $\phi_j, i \neq j$, it follows that ψ is also uniformly distributed in the interval $-\pi$ to π .

Since the properties of the unadapted array patterns were examined in some detail in Chapter 2, it is possible to apply those results to obtain a better understanding of the implications of (4.23) and (4.24).

Remembering that the main lobe of the pattern produced by the MRA is much narrower than that of the corresponding uniform array, it can be seen that when

$\sin(\alpha_1) - \sin(\alpha_2)$ is small, corresponding to a small value of $\sin(\alpha)$ and hence small angles in the unadapted array pattern, the MRA based system will have a smaller variation in SNR over space than the uniform array based system. Thus when the multiple paths are close together the MRA based system would be preferred. However, when the multiple paths are located at some large angular distance from one another, corresponding to a large value of $\sin(\alpha_1) - \sin(\alpha_2)$ in the multipath case, or a large value of $\sin(\alpha)$ for the unadapted array pattern, the uniform array based system will show a smaller variation in the possible range of SNR's.

A specific case is now examined in more detail. Under the two ray multipath model, the worst case occurs when two correlated equal amplitude signals are used, thus allowing for complete spatial nulls, points in space where the two signals cancel each other out completely. This specific case will be used to show that the performance of the MRA based system is superior under worst case conditions for small angular separation of the multiple paths. For convenience, it will be assumed that one of the signals, designated the Line Of Sight (LOS) signal, and representing the direct path, arrives at an angle perpendicular to the array axis. The second signal, the multipath signal, will arrive at an angle α with respect to broadside.

Two adaptive combiners, each containing 4 elements, one based on the uniform array geometry, the other based on the MRA geometry, are employed. The noise variance is chosen to be unity, or 0 dB, for this experiment, while each

of the two multipath QPSK signals is 3 dB. Using (4.25) and (4.26), an upper bound on the probability of error (assuming the channel is not bandlimited) is determined for various values of α . These results are given in Table 4.2 as "theoretical".

To confirm that the performance of the systems under these multipath conditions follows that expected from the calculations, the following simulations were carried out using the system shown in figure 4.12. The desired signal was convolved with two separate channels, one for each of the two rays in the multipath model, with the delay of the multipath channel chosen to introduce a phase shift producing the worst possible SNR at the output of the combiner given the specified angles of arrival. Both channels were identical otherwise, and again were modelled as 256 point Hamming window functions providing a lowpass characteristic. Simulations were then undertaken for various angular separations of the signals. The LMS adaptive combiner shown in figure 4.4 was used to process the signals from a fourth order MRA and a four element uniform array. This LMS combiner again employs the recursions given by (4.6), (4.7) and (4.8). Additive Gaussian noise of 0 dB, a μ of 0.0005 and data samples of 22000 bits were again employed.

Because the spatial correlation matrix is no longer Toeplitz, and hence no longer corresponds to the case of plane waves, the directivity patterns no longer give a good indication of the degree to which a signal arriving from a given angle

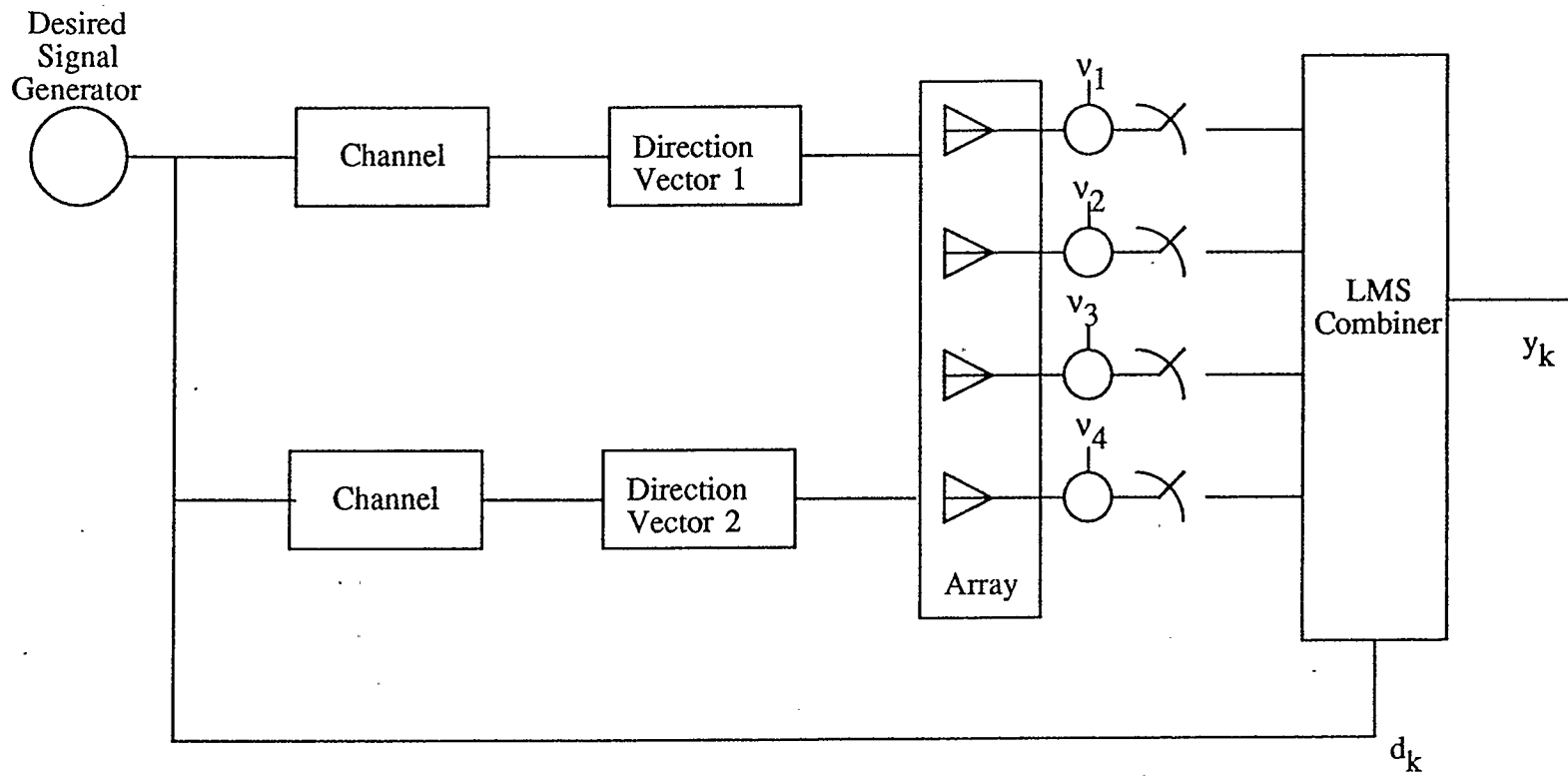


Figure 4.12 - Two ray multipath simulation.

will be rejected [16]. For this reason, no directivity patterns are included in this section.

The probability of error figures for these simulations and, for comparison, the probability of error figures developed theoretically are shown in Table 4.2.

Table 4.2. Error Probabilities for Equal Strength Multipath Signals with Various Angular Separations and Worst Case Phase. $\sigma_v = 1.0$.

Multipath Angular Separation	Simulated $P_b(e)$		Theoretical $P_b(e)$	
	MRA	Uniform	MRA	Uniform
Angle (degrees)				
No Multipath	0.0274	0.0264	0.0228	0.0228
10	0.0102	0.1024	0.0094	0.1172
12	0.0037	0.0960	0.0040	0.0796
14	0.0043	0.0509	0.0046	0.0592
16	0.0088	0.0370	0.0095	0.0347

The preceding results show clearly that under these circumstances, the MRA based array considerably outperforms the equi-spaced array system. Also, note that there is relatively good agreement between the theoretically determined estimates of error probability and those determined through simulation.

It is desired to obtain an estimate of the average error probabilities for these systems. To do this, several assumptions are necessary. We will take ψ , α_1 and α_2 to be independent uniformly distributed random variables. The unconditioned bit

error probability of either the uniform array or the MRA based system may then be found as:

$$P_b(e) = \frac{1}{2\pi} \int_{-\pi}^{\pi} \frac{1}{2\pi} \int_{-\pi}^{\pi} \frac{1}{\pi} \int_0^{\pi} Q \left[\sqrt{SNR} \right] d\psi d\alpha_1 d\alpha_2 \quad (4.27)$$

where

SNR is given in (4.23) for the uniform array

and in (4.24) for the MRA based system.

The inclusion of the Q function within the integrand makes a closed form evaluation of this integral impossible. However, numerical techniques can be used to solve this integral. Equation (4.27) is used to determine the total error probability for 4 element adaptive combiners based on the uniform and MRA geometries operating in a multipath environment where the two rays are of equal strength and differ only in relative phase. Various SNR's at the input of the array are employed and the results are shown in figure 4.13.

The results show a definite plateau effect, past which increasing the SNR at the input has little effect on the error probability. This occurs as a result of the deep fading which is possible because of the simplistic two ray model with equal strength rays and has been reported by Stein in [29]. For low values of input SNR the error probability for both systems approaches 0.5. As the input SNR increases, the low variance in SNR provided by the uniform array for large values of

Log $P_b(e)$

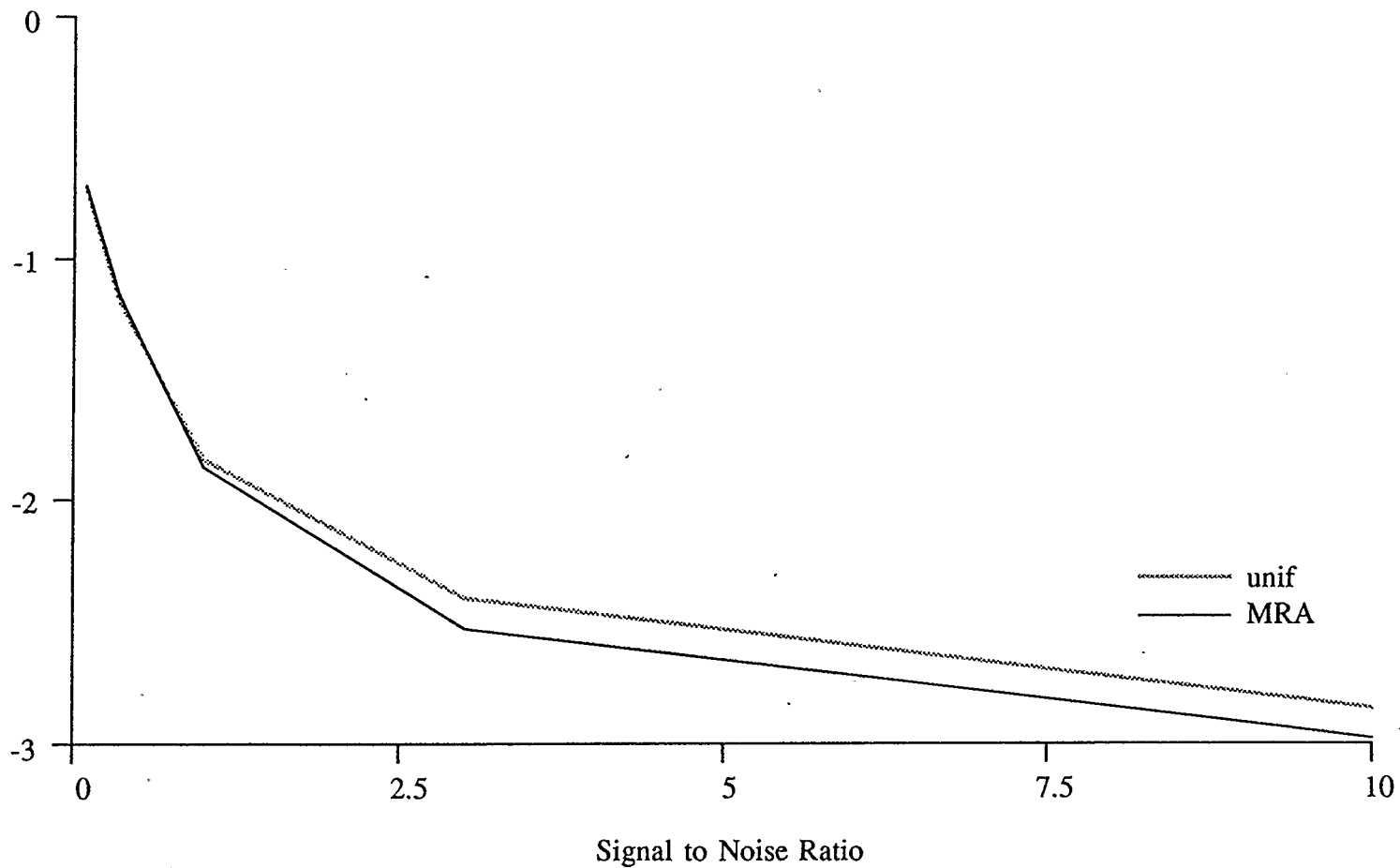


Figure 4.13 - Bit error probabilities for converged 4 element uniform and minimum redundancy adaptive arrays receiving QPSK signals in a two ray multipath environment with equal amplitude rays.

$\sin(\alpha_1) - \sin(\alpha_2)$ causes this array to show a more significant decrease in probability of error. However, as the SNR is increased still further, most of the errors occur when $\sin(\alpha_1) - \sin(\alpha_2)$ is small, allowing for large destructive interference. In this region, the MRA based system performs best. Note that for usable error probabilities, that is, low error probabilities, the MRA based system outperforms the uniform system.

The preceding results were obtained under the assumption that α_1 and α_2 are independent uniformly distributed random variables. In practice, we would expect that α_1 and α_2 would be somewhat correlated, with a tendency towards small values of $\alpha_1 - \alpha_2$. This in turn implies that $\sin(\alpha_1) - \sin(\alpha_2)$ will be biased in favour of small values. As a result the margin of superiority that the MRA based system achieves would, in terms of the unconditioned bit error probability, be greater than that previously indicated.

4.6. Conclusion

It has been shown both through theoretical calculations and by a simulation study that uncorrelated interferences which are within the main lobe of the uniform array tend to be rejected more readily by the MRA because of its narrower main lobe. In a communications system, this translates directly into lower error probabilities. In the multipath case, the two ray multipath model was used to show that the MRA based system outperforms the uniform based system when the

multiple paths are separated by small angles. Again, simulations seemed to confirm this. Calculations undertaken to determine the unconditioned bit error probability indicated that for 4 element arrays operating in an arduous multipath environment, the MRA based system was superior for usable error probabilities.

CHAPTER 5

SUMMARY AND SUGGESTIONS FOR FURTHER RESEARCH

In this thesis, the use of the Minimum Redundancy Array in conjunction with a narrowband adaptive beamformer has been examined. It has been shown that the narrow main lobe of the array pattern formed by the MRA, when used in conjunction with an adaptive beamformer to reduce the effect of interference entering through the sidelobes, allows for better spatial resolution than that obtained using a similar system based on a uniform array. The SNIR obtained using an adaptive beamformer based on a MRA was found, both through theoretical calculations, and through simulations employing a fourth order MRA and a four element uniform array, to be significantly superior to that achieved with a system based on a uniform array for the case when an interfering signal was located in close angular proximity to the look direction. The SNIR achieved by the MRA based system was, however, slightly worse when the interference was located in the sidelobes, at a large angular distance from the look direction.

The minimum spatial redundancy concept was also applied to the choice of adaptive elements in a thinned adaptive array. In comparison to the common method of selecting adaptive elements by simply spreading them uniformly throughout the array, it was seen that choosing the adaptive elements based on a

minimum spatial redundancy criterion in a thinned adaptive array improved the converged SNIR performance of the system for uncorrelated interferences located within the main lobe of the conventional subarray. There was no significant difference in the performance for interferences located in the sidelobes. This performance increase was accomplished without changing the complexity of the system, the length of the array, or any other feature which would tend to reduce the desirability of adopting this technique. A simulation was undertaken using 37 element arrays, with 10 adaptive elements spaced uniformly in one and in a minimum redundancy configuration in the other. The results of the simulation study conformed to the predictions of the previous calculations.

An adaptive LMS combiner, working on the assumption that the desired signal was a known sequence, was simulated in conjunction with both a 4 element uniform array and a four element MRA. The results of the simulations indicated that the MRA based system achieved superior performance, in terms of worst case bit error probability, when an uncorrelated interference was located in close angular proximity to the desired signal. The uniform array based system performed better when the uncorrelated interference was located at a large angular distance from the desired signal. The two ray multipath model was then used to show, both theoretically and through simulation, that for correlated signals located in close angular proximity to one another, the MRA based system achieves superior worst case bit error probabilities. When the two rays of the multipath model were widely

separated, it was seen that the uniform array based system achieved superior performance. It was also shown that in the two ray multipath environment, with equal amplitude rays arriving from independent, uniformly distributed random directions, with random phase, the unconditioned bit error probability of a 4 element MRA based system is lower for usable SNR than that obtained by a 4 element uniform array based system.

An obvious extension of the work in this thesis is to consider the use of MRA's in conjunction with a broadband beamforming structure. By employing information about the signal gathered over several sampling periods, a broadband beamformer can be formed. Broadband beamforming systems have been used to receive frequency hopped, spread spectrum signals. The use of adaptive arrays with spread spectrum signals of this type is especially appealing, as it is a relatively easy matter to allow the beamformer to adapt in a signal free environment (by employing a notch filter which tracks the frequency hopping to remove the signal from the beamformer input)[17]. It would be interesting to discover if the advantages found using MRA based narrowband adaptive systems also extend to the broadband case.

The work in chapter one, dealing with the use of an MRA in conjunction with an adaptive beamformer with the look direction constrained, could be extended to deal with the situation in which the interference is correlated with the desired signal. One method which is currently employed to avoid signal cancellation under

these conditions in uniform array based structures is the Duvall beamformer [17], which adds the signal component in adjacent sensor elements with opposite phase to allow the beamforming to take place in a signal free environment. However, because of the unique structure of the MRA, the Duvall beamforming technique cannot be directly applied to an array based on a MRA. An extension of the Duvall beamformer for the case where sensor elements are not equi-spaced would form a valuable contribution. It is worthy of note that the Duvall technique can be directly applied to thinned suboptimal arrays, even if the adaptive elements are chosen using a minimum spatial redundancy criterion, as the overall array structure used is that of a uniform array, allowing the cancellation of signal components from adjacent signal elements.

While the MRA appears to have significant advantages over the uniformly spaced array in certain circumstances, it is not known how sensitive the adaptive MRA structure is to sensor element perturbations. A comparison of the relative sensitivities of the uniform array and MRA based adaptive beamformers would be of interest.

In order to more closely approximate real world conditions, a more in depth computer simulation could be undertaken. A more sophisticated computer simulation could employ signals and interferences which are spread over a region, rather than originating from a discrete spatial source. In a similar vein, near field (not plane wave) interferences and signals could be employed. This would be

especially useful to simulate reflections off objects which are located close to the receiving array.

Finally, no amount of simulation can replace building and testing a system based on a MRA. This becomes especially important when considering the multipath case, where different multipath models will produce very different results. Because of the high cost and technical complexities associated with RF equipment, it may be desirable to conduct experiments based on an array of acoustic sensors initially (assuming that a suitable RF array is not available to the researcher). The adaptive beamforming techniques employed are general and hence, the type of signal considered, whether it be acoustic, electromagnetic, or some other form, is unimportant.

REFERENCES

- [1] B.D. Van Veen and K.M. Buckley, "Beamforming: A Versatile Approach to Spatial Filtering," *IEEE ASSP Magazine*, April 1988, pp. 4-24.
- [2] N.L. Owsley, "Sonar Array Processing" in *Array Signal Processing*, S.Haykin ed., Prentice-Hall, Englewood Cliffs, New Jersey, 1985.
- [3] A.B. Baggeroer, "Sonar Signal Processing" in *Applications of Digital Signal Processing*, A.V. Oppenheim, ed., Prentice-Hall, Englewood Cliffs, New Jersey, 1978.
- [4] P.M. Schultheiss, "Some Lessons from Array Processing Theory," in *Aspects of Signal Processing*, G. Tacconi, ed., Proceedings of the NATO Advanced Study Institute, Portovenere, La Spezia, Italy. D. Reidel Publishing Co., Boston, Mass., 1976.
- [5] J.W.R. Griffiths and J.E. Hudson, "An Introduction to Adaptive Processing in a Passive Sonar System" in *Aspects of Signal Processing*, G. Tacconi, ed., Proceedings of the NATO Advanced Study Institute, Portovenere, La Spezia, Italy. D. Reidel Publishing Co., Boston, Mass., 1976.
- [6] J.H. Justice, "Array Processing in Exploration Seismology" in *Array Signal Processing*, S.Haykin ed., Prentice-Hall, Englewood Cliffs, New Jersey, 1985.
- [7] A.C. Kak, "Tomographic Imaging with Diffracting and Nondiffracting Sources" in *Array Signal Processing*, S.Haykin ed., Prentice-Hall, Englewood Cliffs, New Jersey, 1985.
- [8] J.A. Arzac, "Nouveau reseau pour l'observation radioastronomique de la brillance sur le Soleil a 9350 Mc/s.," *Academie des Sciences*, pp. 942-946, Seance du 28 Fevrier, 1955.

REFERENCES (Continued)

- [9] J.L. Yen, "Image Reconstruction in Synthesis Radio Telescopes" in *Array Signal Processing*, S.Haykin ed., Prentice-Hall, Englewood Cliffs, New Jersey, 1985.
- [10] W.N. Christiansen and J.A. Hogbom, *Radio Telescopes*, 2nd Ed., Cambridge University Press, Cambridge, New York, 1985.
- [11] S. Haykin, "Radar Array Processing for Angle of Arrival Estimation" in *Array Signal Processing*, S.Haykin ed., Prentice-Hall, Englewood Cliffs, New Jersey, 1985.
- [12] A.A. Oliner and G.H. Knittel, *Phased Array Radar* Artech House, Inc., Dedham Mass., 1972.
- [13] R.T. Compton, R.J. Huff, W.G. Swarner and A.A. Ksienki, "Adaptive Arrays for Communications Systems," *IEEE Trans.*, vol. AP-24, 1976, pp. 599-607.
- [14] W.C. Jakes Jr., "A Comparison of Specific Space Diversity Techniques for Reduction of Fast Fading in UHF Mobile Radio Systems," *IEEE Trans. on Vehicular Technology*, vol. VT-20, No. 4, Nov. 1971, pp. 81-91.
- [15] Alan T. Moffet, "Minimum-Redundancy Linear Arrays," *IEEE Transactions on AP*, Vol. AP-16, No. 2, March 1968, pp 172-175.
- [16] J.E. Hudson, *Adaptive Array Principles*, Peter Peregrinus, Ltd., London, 1981.
- [17] B. Widrow and S. Stearns, *Adaptive Signal Processing*, Prentice-Hall, Englewood Cliffs, New Jersey, 1985.
- [18] W.F. Gabriel, "Adaptive Arrays - an Introduction" *Proc. IEEE*, vol. 64, 1976, pp. 239-272.

REFERENCES (Continued)

- [19] O.L. Frost, "An Algorithm for Linearly Constrained Adaptive Array Processing," *Proc. IEEE*, Vol. 60, Aug. 1972, pp. 926-935.
- [20] N.L. Owsley, "A Recent Trend in Adaptive Spatial Processing for Sensor Arrays: Constrained Adaptation," J.W.R. Griffiths, P.L. Stocklin, and C. Van Schooneveld, eds. *Aspects of Signal Processing*, Proceedings of the NATO Advanced Study Institute on signal processing and underwater acoustics, Loughborough, UK, 1972 (Academic Press, 1973).
- [21] *Array Signal Processing*, S.Haykin ed., Prentice-Hall, Englewood Cliffs, New Jersey, 1985.
- [22] S.U. Pillai, Y. Bar-Ness, and F. Haber, "A New Approach to Array Geometry for Improved Spatial Spectrum Estimation," *Proc. IEEE*, Vol. 73, No. 10, Oct. 1985, pp. 1522-1524.
- [23] L.J. Griffiths, "A Comparison of Multidimensional Wiener and Maximum Likelihood Filters for Antenna Arrays," *Proc. IEEE (Letters)*, vol. 55, Nov. 1967, pp. 2045-2047.
- [24] L.J. Griffiths and C.W. Jim, "An Alternative Approach to Linearly Constrained Adaptive Beamforming," *IEEE Trans on A.P.*, vol. AP-30, Jan. 1982, pp. 27-34.
- [25] R.T. Compton, "The Power Inversion Array," *IEEE Trans. on A.P.*, vol AP-30, Jan. 1982, pp. 27-34.
- [26] S. Benedetto, E. Biglieri, and V. Castellani, *Digital Transmission Theory*, Prentice-Hall, Englewood Cliffs, New Jersey, 1987.
- [27] R.W. Lucky, "Techniques for Adaptive Equalization of Digital Communication Systems," *Bell Syst. Tech. J.*, vol. 46, Mar. 1967, pp. 255-286.

REFERENCES (Continued)

- [28] A.B. Carlson, *Communication Systems*, 3rd Ed. McGraw-Hill, New York, N.Y., 1986.
- [29] S. Stein, "Fading channel issues in systems engineering," *IEEE Journal Selected Areas Commun.*, vol. SAC-5, No. 2, Feb. 1987, pp. 68-89.